



PROJECT EXO



Hochschule für Angewandte
Wissenschaften Hamburg
Hamburg University of Applied Sciences

Presented by: Over The Pond

**2019-2020 AIAA SENIOR CAPSTONE PROJECT
HIGH CAPACITY SHORT RANGE COMMERCIAL TRANSPORT AIRCRAFT**

OVER THE POND DESIGN TEAM



Matthew Bednarz
Aerodynamics
AIAA-901688

Matthew Bednarz



Valentin Krebs
CAD
AIAA-1108692

V. Krebs



David Shane
Systems
AIAA-762093

David Shane



Jonathan Dronfield
CAD
AIAA-1108964

Jonathan Dronfield



Nick Mazzella
Cost & Business Analyst
AIAA-1108695

Nick Mazzella



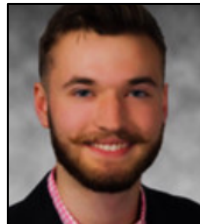
Richard Zwetlich
Cabin
AIAA-1108778

Richard Zwetlich



Ryan Fisher
*Chief Engineer/ Certification
& Compliance*
AIAA-643536

Ryan Fisher



Patrick Rodgers
Propulsion
AIAA-738647

Patrick Rodgers



Murray Kim
Structures
AIAA-1069753

Murray Kim



Amanda Butynes
*Project Manager/ Stability &
Control*
AIAA-1108688

Amanda Butynes



Pradeep Raj, Ph.D.
Virginia Tech Advisor



Jutta Abulawi, Ph.D.
Hamburg Advisor

Contents

List of Figures	iii
List of Tables	v
Executive Summary	1
1 RFP Analysis	3
1.1 Customer Requirements	3
1.2 Market Analysis	3
1.3 Comparator Aircraft Identification	5
1.4 FAA Requirements	6
1.5 Mission Profile	7
1.6 Concept of Operation	8
1.7 Key Design Drivers	9
1.8 Measures of Merit	9
1.8.1 Measures of Merit Sensitivity Analysis	10
1.9 Key Technologies	11
2 Conceptual Design	12
2.1 Initial Concepts	12
2.2 Feasible Designs	13
2.3 Preferred System Concept	15
3 Aerodynamics	19
3.1 Airfoil Selection	19
3.2 Wing Planform Sizing	21
3.3 High Lift Devices	23
3.4 Aerodynamic Characteristics	25
4 Performance	27
4.1 Takeoff/Landing	27
4.2 Payload Range	29
4.3 V-N Diagram	30
5 Structural Design	31
5.1 Material Selection	31
5.2 Material Up-cycling	33
5.3 Spar Analysis	34
5.4 Fuselage Analysis	35
5.5 Landing Gear	37
5.5.1 Landing Gear Placement	37
5.5.2 Landing Gear Loads and Tire Selection	37
6 Weight Summary	38
7 Stability and Control	40
7.1 Horizontal Stabilizer	40
7.2 Vertical Stabilizer	42
7.3 Control Surfaces	44
7.3.1 Ailerons	44

7.3.2	Rudder	45
7.3.3	Elevators	46
7.4	Static and Dynamic Stability	47
8	Propulsion System	50
8.1	Engine Selection	50
8.2	Boundary Layer Ingestion	52
8.2.1	Boundary Layer Ingestion Performance Benefits and Risk Mitigation	52
8.2.2	CFD Boundary Layer Ingestion Validation	54
8.3	Noise Estimation	57
9	Cabin	57
9.1	Cockpit Layout	58
9.2	Passenger Layout	58
9.3	Boarding Simulation	61
9.4	Cargo	62
9.5	Optional Features	64
10	Systems	65
10.1	Electric/Hydraulic system	66
10.2	Fuel system	69
10.3	Avionics	70
11	Project Planning and Management	72
11.1	Project Timeline	72
11.2	Risk Resolution Plan	73
11.2.1	Risk A: Engine Failure	74
11.2.2	Risk B: Single Pilot Ready Capability	75
11.2.3	Risk C: Hidden Component Failures	76
11.2.4	Risk D: Engine Maintenance	77
12	Cost Estimate and Business Case Analysis	78
12.1	Development Costs	78
12.2	Fly Away Cost of Each Member of Family	79
12.3	Estimate of Price	80
12.4	Estimate Direct Operating Cost for 700 nm reference mission	81
12.5	Manufacturing Plan	81
13	Aircraft Emissions	82
13.1	CO ₂ Emissions during Manufacturing	82
13.2	CO ₂ Emissions	83
13.2.1	In-service	83
13.2.2	Lifecycle	84
14	Aircraft Drawings	85
	References	86
	Appendix	89

List of Figures

1	Final three view of Exo	2
2	Airport (BOS) gate availability breakdown.[8]	4
3	Comparison chart showing available comparator aircraft on the market	5
4	Mission profile for design and reference missions	8
5	Cost per available seat mile trade study	10
6	Cycles per day trade study	11
7	Iterative code for weight sizing	12
8	Preliminary aircraft designs	13
9	Preferred system concept	16
10	Wing thrust loading plot showing Exo and comparators	17
11	Isometric view of final PSC design Exo	17
12	Centerline diagram of Exo with OML features highlighted	18
13	Performance curves of 5 final airfoil candidates	20
14	Geometry of Rae (NPL) 5213 [12]	21
15	Exo wing planform	22
16	Exo control surface and HLD distribution along the wing	24
17	Triple slotted flap and leading edge slat positioning in wing [13]	24
18	Exo drag polars of cruise and takeoff flight	25
19	Exo lift distribution compared to ideal elliptical shapes	26
20	Takeoff balanced field length	27
21	Payload range diagram	29
22	V-N diagram	30
23	Percentage of materials used on Exo by weight	31
24	Aircraft material breakdown showing location of innovative materials	32
25	MATLAB and Solidworks wing displacement analysis	35
26	Internal structure of the fuselage	35
27	Longitudinal position of landing gear	37
28	Horizontal stabilizer scissor plot showing controllable and stable center of gravity movement	41
29	Aircraft experiencing deep stall [11]	42
30	Root locus plot showing negative real parts for both cruise and takeoff	48
31	Dynamically stable Exo response to step perturbations	49
32	Trent UltraFan. Photo courtesy of Rolls-Royce.	50
33	Trent UltraFan thrust variation with altitude	51
34	Historical trend of SFC Variation with respect to design thrust [28]	52
35	BLI2DTF rig installed in NASA Glenn wind tunnel [30]	53
36	Preliminary fan stage map showing the approximate achievement in stability margin [30]	54
37	3D view of streamlines flowing near engine inlet in the BLI region	56
38	Scalar velocity field and velocity profiles of engine	56
39	Exo's cockpit, cabin and cargo	57
40	Cockpit layout	58
41	Cabin layout	59
42	Exo cross-section (front view)	60
43	Seat pitch and cross aisle width	61
44	Boarding simulation time after 5 minutes	62
45	Boarding simulation passenger density after 15 minutes	62
46	Cargo floor with 14 cargo containers	63
47	Side view of cargo doors	63
48	Systems layout (side)	65
49	Systems layout	65

50	Electric/Hydraulic system diagram	67
51	Fuel system diagram	69
52	Fatal aircraft accidents [37]	72
53	Project timeline	73
54	Outline of risks and scale	74
55	Engine failure risk mitigation	75
56	Single pilot capable risk mitigation	76
57	Hidden component failure risk mitigation	76
58	Engine maintenance risk	77
59	Production cost breakdown	79
60	Break even analysis	80
61	Texas aerospace industry workforce concentration map	82
62	Dimensioned 3-view diagram of Exo	85

List of Tables

1	Compliance matrix shows that aircraft meets all customers needs and key regulatory FAA requirements	2
2	Requirements imposed by customer in RFP.	3
3	Compliance matrix shows comparator aircraft are not compliant	6
4	Measures of merit identified to show how target values compare to A321neo and Boeing 777. *Normalized to 400 passenger.	9
5	Viable innovative technologies with the corresponding advantages and TRL	11
6	Qualitative down selection criterion	14
7	Quantitative down selection criterion	15
8	Parameters used for constraint plot	16
9	Exo airfoil decision matrix (normalized and weighted scores)	20
10	Key aerodynamic performance values	23
11	Parasite drag breakdown	26
12	Takeoff and landing parameter values	27
13	Materials used on aircraft and their corresponding properties	33
14	Weight and CG Verification.	39
15	Final horizontal stabilizer parameters.	40
16	Historical horizontal stabilizer parameters [11]	40
17	Final stable and controllable vertical tail features.	43
18	Historical vertical tail volume ratios [11]	43
19	Control surface requirements	44
20	Final compliant aileron parameters	45
21	Final compliant rudder parameters	46
22	Final compliant elevator parameters	47
23	Cruise flight characteristics showing compliance with level 1 flying qualities	47
24	Static stability characteristics	47
25	Trent UltraFan parameters.	50
26	Key parameters in CFD simulation	55
27	Noise levels of exo and comparator aircraft	57
28	Seat abreast decision matrix	59
29	Optional features	64
30	Potential cost savings while using Airbus ATTOL system	71
31	Development, testing, and evaluation costs	78
32	Direct operating costs	81
33	Comparator CO ₂ Emissions.	83
34	Example decision matrix for material selection.	89
35	Engine Decision Matrix with Top Five Engines Considered.	89

Abbreviations

AD	Air and Defense
ADG	Aircraft Design Group
AHMS	Aircraft Health Monitoring System
AIAA	American Institute of Aeronautics and Astronautics
APU	Auxiliary Power Unit
AR	Aspect Ratio
ATTOL	Autonomous Taxi, Takeoff, and Landing
BLI	Boundary Layer Ingestion
BLI2DTF	Boundary Layer Ingesting Inlet/Distortion-Tolerant Fan
CASM	Cost per Available Seat Mile
CFD	Computational Fluid Dynamics
CFR	Code of Federal Regulations
CG	Center of Gravity
DTE	Development, Testing, and Evaluation
EHA	Electrohydrostatic Actuators
EIS	Entry into Service
FAA	Federal Aviation Administration
FAR	Federal Aviation Regulation
GDP	Gross Domestic Product
IFE	In-Flight Entertainment
IFR	Instrument Flight Rules
MEA	More Electric Aircraft
OML	Outer Mold Line
PCN	Pavement Classification Number
PMC	Polymer Matrix Composites
QI	Quasi-Isentropic
RAT	Ram Air Turbine
RFP	Request for Proposal
SFC	Specific Fuel Consumption
TRL	Technology Readiness Level
UD	Unidirectional
ULD	Unit Load Devices
VFR	Visual Flight Rules

Executive Summary

Over the Pond, a collaborative enterprise of Virginia Tech and Hamburg students, is pleased to offer Project Exo as the best solution to the AIAA's request for proposal is for a high capacity, short range, transport aircraft. The RFP calls for an aircraft that will reduce congestion at airports in a cost effective manner. The aircraft is to have a reference mission of 700nm and a design range of 3,500nm with capacity for 400 passengers in a dual class configuration. Commercial aircraft currently on the market are designed for high capacity, long range missions, or low capacity, short range missions, neither of which solve the congestion problem without an increased operating cost. Over the Pond provides the best solution to meet the customer's needs with an operating cost for the 700 nm reference mission of 12.3¢ per available seat mile that is 20% less than that of the Boeing 777-300. The proposed design, Exo, shown in Figure 1, uses composite materials to reduce weight of the wide-body fuselage. Exo leverages boundary layer ingestion (BLI) propulsion system to reduce power required by 8%, and Rolls Royce's UltraFan engine which is 20% more fuel efficient than other geared turbofan engines on the market. Implemented in the cockpit is a single pilot capable, dual pilot equipped system, allowing for operation at reduced costs; autonomous taxi, takeoff, and landing (ATTOL) is installed to support single pilot capability. Exo also uses aircraft health monitoring system (AHMS), supported by AI, implemented in parallel with standard avionics equipment to reduce aircraft downtime, decrease maintenance costs, and increase reliability. By using more electric aircraft (MEA), Exo reduces fuel consumption and increases operational efficiency using components such as EHA and no-bleed architecture. The cabin of Exo features a comfortable and innovative three aisle layout, giving 83.5% of passengers a window or aisle seat, and allowing for a 27 minute boarding time, almost 50% faster than the A321neo. This decrease board time, a cruise speed of Mach 0.82 and less than 25 minutes on the runway leads to 9 cycles per day, giving capability for more revenue flow to the buyer and reducing airport congestion. Figure 1 displays Exo along with relevant aircraft specifications. Over the Pond proposes to produce 10 aircraft per month which will take 42 months to break even with a 15% profit on every aircraft sold thereafter. The majority of costs incurred are due to air-frame engineering, manufacturing, engine acquisition, material and equipment purchase. Exo meets or exceeds all RFP requirements including regulatory requirements per FAA 14 CFR Part 25, as seen in Table 1.

Aircraft Specification	
Max Takeoff Weight	381,300 lbs
Fuel Weight	112,700 lbs
Payload Weight	94,300 lbs
AR	9.5
L/D Max	14.1
x_{CG} Wet	125 ft
x_{CG} Dry	123.6 ft
Wing Area	2480 ft ²
MAC	16.15 ft
Cruise Mach	0.82
Clmax	2.5

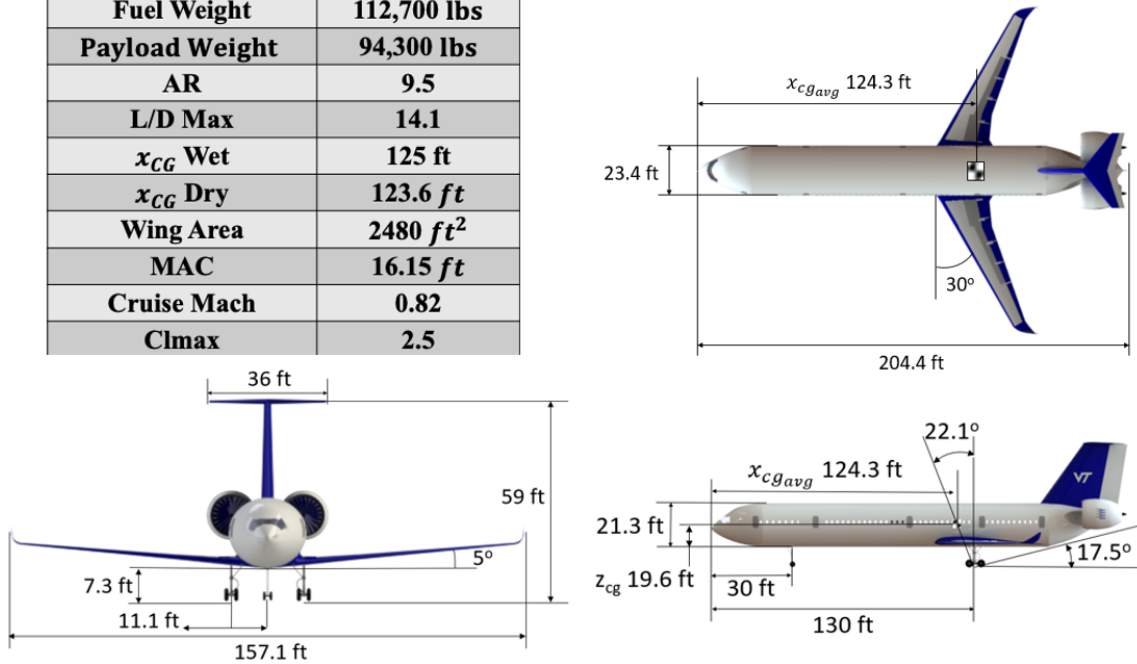


Figure 1: Final three view of Exo

Table 1: Compliance matrix shows that aircraft meets all customers needs and key regulatory FAA requirements

Compliance Matrix		
Item	Requirement	Exo
Entry into service	2029	2029
VFR and IFR capable with autopilot	-	Yes
Crew – (Tradeable)	2 pilots, 8 attendants	1 pilot, 8 attendants
Flight in known icing conditions	-	Yes
Dual class configuration	50 Business, 350 Economy	50 Business, 350 Economy
Design Range	3,500 nm	3,500 nm
Maximum takeoff length w/ 35' obstacle	9,000 ft	7,195 ft
Maximum landing field length	9,000 ft	5,404 ft
Cabin pressurization at cruise – (Tradeable)	8,000 ft	7,000ft
Design mission approach speed – (Tradeable)	145 KCAS	138KCAS
Maximum noise level	103 EPNdB	94 EPNdB
Exhaust emissions	SN < 30	8.5
CFR Part 25	-	Yes

1 RFP Analysis

This section highlights the outcomes of a thorough analysis of the AIAA's RFP for a high-capacity, short range commercial aircraft.

1.1 Customer Requirements

The request for proposal details aircraft requirements, in two categories: general requirements and mission requirements. The general requirements stipulate that the aircraft must be capable of taking off from asphalt or concrete runways, VFR and IFR flight with an autopilot, and flying in known icing conditions. Additionally, the aircraft must meet FAA 14 CFR Part 25 certification requirements, and the engine/propulsion system assumptions must be documented. All general requirements are mandatory.

The mission requirements are listed in Table 2. The RFP requests a 400 passenger capacity cabin with 50 business class seats having a 36" pitch and 21" width seats and 350 economy class seats with 32" pitch and 18" width seats. Each passenger will be allotted 5 cubic feet of storage for baggage in the cargo hold. All galleys, lavatories, and exits must meet 14 CFR Part 25. The weight of each pilot, flight attendant, and passenger is assumed to be 200 *lbs*, with an

Table 2: Requirements imposed by customer in RFP.

Item	Requirement
Entry into service	2029
Dual class configuration	50 Business, 350 Economy
Design Range	3500 nm
Crew - <i>Tradeable</i>	2 pilot, 8 attendants
VFR and IFR capable with autopilot	Yes
Flight in known icing conditions	Yes
Maximum takeoff length w/ 35' obstacle	9,000 ft
Maximum landing field length	9,000 ft
Cabin pressurization at cruise - <i>Tradeable</i>	8,000 ft
Design mission approach speed - <i>Tradeable</i>	145 KCAS
Maximum noise level	108 EPNdB
Exhaust emissions	SN < 30
CFR Part 25	Yes

assumed 30 *lbs* of baggage per occupant. Of the mission requirements, the number of crew, the approach speed, and the cabin pressurization are tradeable. Varying these parameters allows for opportunity to improve passenger comfort and reduce operating cost. All other mission requirements are mandatory. The price of fuel is assumed to be \$3.00 per gallon, with a \$3.00 per gallon carbon tax.

1.2 Market Analysis

To better understand the customer's need, a market analysis of passenger traffic growth and currently active commercial aircraft was performed. Due to the increased accessibility of air travel, many of the

world’s major commercial airports are experiencing congestion. This congestion has lead to significant delays, lack of flight availability, and loss of potential profit for airlines. While busy airports in mature markets such as the US and Europe currently experience delays, the economic growth of countries like China and India will soon worsen congestion worldwide [1]. These countries have some of the largest populations and most highly trafficked air routes predicted to become more popular though through 2029 [2]. One of such routes is Mumbai to Delhi which is the fifth busiest air route globally by the annual number of passengers as of 2018 and the third busiest air route by a number of flights globally as of 2019 [2] [3]. In the United States, the route from Chicago to New York is one of the fifty busiest air routes globally by the annual number of passengers as of 2018, and it is the busiest air route in the United States by the number of flights scheduled as of 2015 [4]. Additional popular routes include New York to Orlando, Chicago to Illinois, and Sydney to Melbourne. All of these highly demanded air routes are about 700 nm and could greatly benefit from utilizing a high capacity, short-range aircraft to reduce the total number of flights scheduled and overall airport congestion.

An important component to consider in understanding congestion at these airports is gate size. As seen in Figure 2 from MIT [8], meeting the Group 4 requirements would allow for docking at eighteen gates at Boston Logan International Airport - doubling the nine for larger Group 5 aircraft [8].

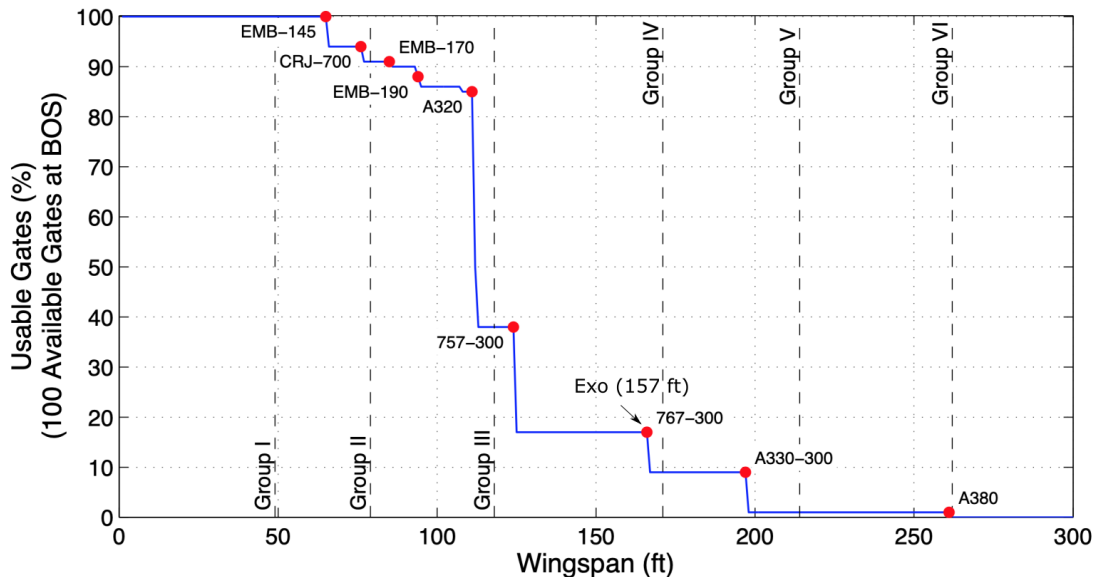


Figure 2: Airport (BOS) gate availability breakdown.[8]

Being capable of docking at these gates directly reduces congestion by eliminating wait times

for large gates and increases the number of cycles per day due to gate availability. Currently, there are aircraft physically capable of performing the short-range, high capacity mission such as the A380, B747-800, A330neo, and A350neo families. These, however, are designed for significantly longer range missions thereby not economically viable for shorter distances. The competitive aircraft for this payload and range are listed in Figure 3. All of these aircraft are grouped in either the long range - high capacity or short range - low capacity quadrant pointed out in the diagram. As long range, high capacity aircraft are commonly designed for fewer pressurisation cycles whereas low capacity, short range aircraft do not fit the required number of passengers, there is a void of capable aircraft in the high capacity, short-range quadrant.

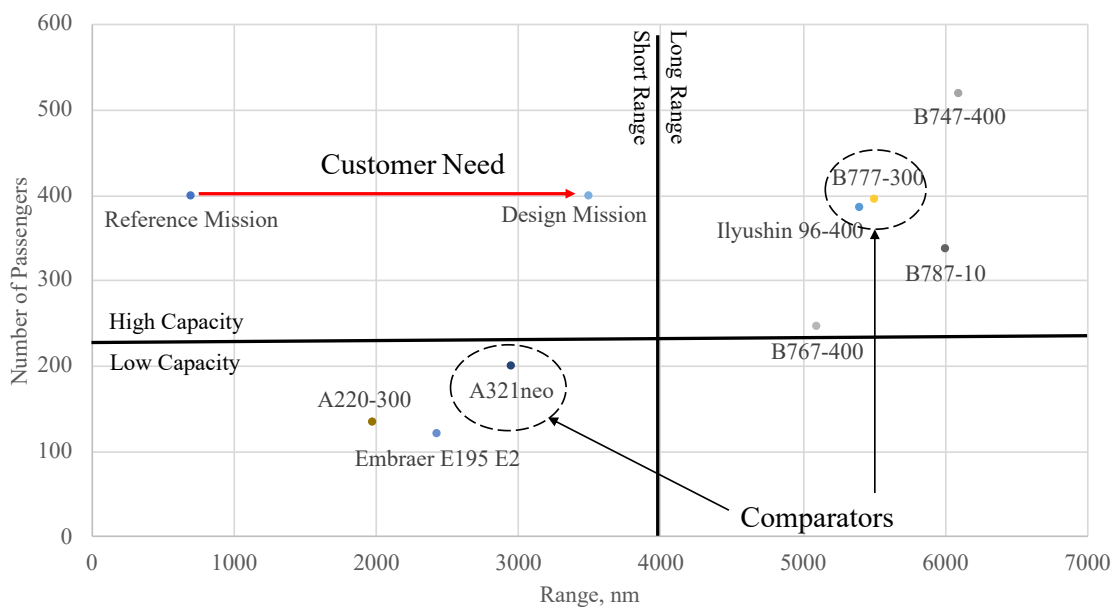


Figure 3: Comparison chart showing available comparator aircraft on the market

It is clear that there is a growing need for a short-range, high capacity aircraft to satisfy the demand for air travel. Current aircraft, however, are not able to satisfy the need without increasing congestion.

1.3 Comparator Aircraft Identification

The two closest comparators to meet the customer's needs are the Boeing 777-300 and the Airbus A321neo. The Boeing 777-300 meets the customer's passenger capacity requirement, but cannot operate cost effectively on short range missions due to excess empty weight, Group 5 ADG wingspan, and low pressure cycle lifetime [7]. Furthermore, it does not meet the RFP's takeoff length requirement. Next, the A321neo

does not meet the customer's capacity requirement, however does operate cost effectively on short range missions. Two A321neo aircraft are required to transport 400 passengers for the 700 nm mission, which can be replaced by one aircraft that could need RFP requirements. Adding more low capacity aircraft to meet demand on the same route will further exacerbate the airport congestion problem. Table 3 summarizes how the two comparator aircraft do not meet the RFP requirements.

Table 3: Compliance matrix shows comparator aircraft are not compliant

Compliance Matrix			
Item	Requirement	Boeing 777	A321neo
Entry into service	2029	Yes	Yes
VFR and IFR capable with autopilot	-	Yes	Yes
Crew - <i>Tradeable</i>	2 pilots, 8 attendants	Yes	Yes
Flight in known icing conditions	-	Yes	Yes
Dual class configuration	50 Business, 350 Economy	Yes	No
Design Range	3,500 nm	No	Yes
Maximum takeoff length w/ 35' obstacle	9,000 ft	No	Yes
Maximum landing field length	9,000 ft	No	Yes
Cabin pressurization at cruise - <i>Tradable</i>	8,000 ft	Yes	Yes
Design mission approach speed - <i>Tradable</i>	145 KCAS	Yes	Yes
Maximum noise level	103 EPNdB	Yes	Yes
Exhaust emissions	SN < 30	Yes	Yes
CFR Part 25	-	Yes	Yes

1.4 FAA Requirements

Partnered with the customer requirements, the FAA provides a set of requirements in the form of airworthiness standards. Many of the requirements are stated in 14 CFR Part 25 Airworthiness Standards for Transport Category Airplanes and other sections including CFR Part 34 (Fuel Venting and Exhaust Emissions Requirements), CFR part 91 (equipment) and CFR part 36 (Noise standards).

The requirements can be classified under one of four categories: main functions, auxiliary functions, performance, and safety. The main functions relate to general operation of the aircraft, including minimum number of flight crew and necessary flight fuel reserves. Auxiliary functions are similar to main

functions, however not as overarching, and focus more on subsystems like fuel tank design and actuator design. The performance airworthiness standards focus on aircraft operation in extreme cases relating to maximum positive maneuvering, maximum dive speed, and aircraft controllability during these maneuvers. Lastly, the remaining regulations focus on the safety of occupants, establishing constraints such as minimum aisle size, number of emergency exits, and CG limitations for passenger comfort during flight operation. Significant FAA requirements, which the customer has mentioned in the RFP, include: maximum allowable noise, smoke number, fuel reserve, and minimum number of flight crew. The maximum allowable noise for any Stage 2 aircraft, per 14 CFR Part 36.103, is 108 EPNdB for aircraft weighing 600,000 *lbs* or more, and a reduction of 5 EPNdB for every halving of this maximum weight. The smoke number, which is a quantification of the particulate emissions from the aircraft, must be less than 30 per 14 CFR Part 34.21. The minimum aisle width is 20 *in* for the 400 passenger aircraft. The minimum number of flight crew on board, established by 14 CFR Part 91.533, is two attendants for a capacity over 100 passengers, and one attendant for every additional 50 passengers after the first 100. Finally, CFR 91.205 defines avionics of the system required for visual and assisted flight. These important requirements constrain the design of the aircraft and must be met.

1.5 Mission Profile

Figure 4 shows the mission profile compliant with all the mission and customer requirements. The aircraft starts at point *A* with its takeoff sequence where it will first taxi out, wait in queue, and takeoff. Next, phase *B* shows the aircraft will begin its stepped ascent at 2,500 *ft/min* to the cruise altitude of 35,000 *ft*. Next, during phase *C*, the aircraft will cruise at Mach 0.82 for the remaining design mission of 3,500 *nm*. The aircraft will then begin its descent at 1,000 *ft/min* as shown in phase *D*. When approaching the destination, the aircraft will begin its landing sequence at point *E*, but in the case of a diversion to a nearby airport, the aircraft will follow route *D1* to 20,000 *ft*. In pursuit of another airport, the route will continue on *D2* for the required 200 *nm*. Next, it will begin phase *D3* for its initial descent followed by *D4* where it will perform a 30-minute hold around the desired airport. Finally, the aircraft will conclude its mission with phase *E* where it will land at an approach speed of 138 *kts*, wait in queue and taxi in to de-board its passengers.

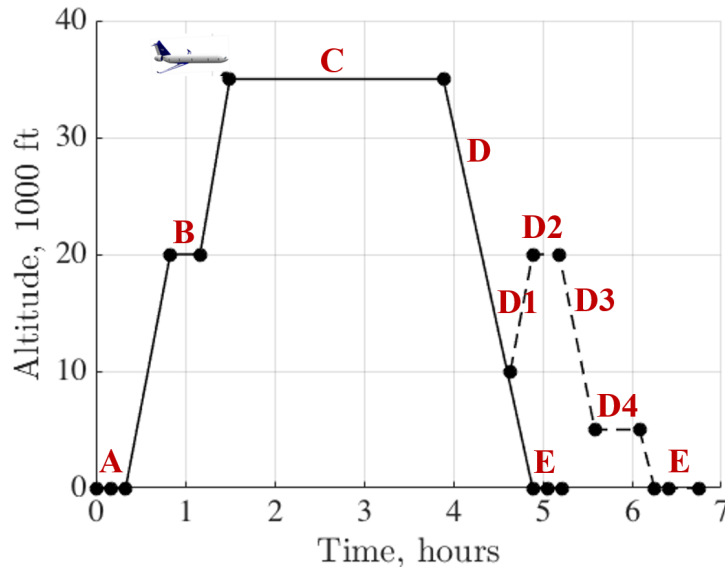


Figure 4: Mission profile for design and reference missions

1.6 Concept of Operation

To get a deeper understanding of the problem, these requirements were examined to determine a typical end-user scenario for a commercial transport flight. The purpose was to facilitate consideration of end-user needs for the new design. A typical scenario is as follows. A family of five traveling from Chicago, IL to New York City, NY on a standard commercial airliner.

There are several features here that the passengers are looking for. First, in-flight entertainment and communication. While the reference mission is only about two hours long, passengers will be more inclined to book again if they have a relaxing and efficient trip. Providing a Wi-Fi enabled cabin and powered seat outlets in every chair would be desirable as this will allow passengers to have full usage of their handheld devices for both work and leisure during the course of the flight. The next feature passengers enjoy is the ability to bring and store luggage on the aircraft instead of under the seat. The aircraft will need to be equipped with ample overhead compartments and cargo hold under the cabin. The seats are also staggered to allow people to fit luggage in at the same time. Finally, the passengers want the option to be able to relax and nap during the flight, so aircraft windows should be equipped with the ability to be dimmed during flight. These extra features will create an enjoyable experience for the passengers encouraging passengers to fly with the airline again.

1.7 Key Design Drivers

A set of design drivers were derived from the RFP before the conceptual design phase to ensure the customer's and end user's needs were at the forefront of the design. A high capacity design, given a spacious interior, allows for more passengers on one flight and a reduced boarding time, directly reducing airport congestion and ramp wait times. A short range design will allow for cost effective and fuel efficient travel between major airports by reducing aircraft empty weight, directly reducing fuel expenditure. A reduced operating cost is also put at the forefront of all design decisions to provide the best solution to the customer for reducing congestion, but in a cost effective way unlike comparator aircraft.

1.8 Measures of Merit

The following set of measures of merit were identified to set Exo apart from the comparators: operating cost, unit cost, boarding time, and number of cycles per day. Operating cost was measured using the cost for available seat mile (CASM), a common metric in the airline industry. By keeping operating costs low and increasing the number of seats available, profit is increased for the airline. The unit cost is targeted to be more than 70% than that of the Boeing 777 and 4% lower than two A321neo. The target boarding time should be approximately 50% less than that of the A321neo, allowing for more than a 30% increase in cycles per day relative to both comparators.

Table 4: Measures of merit identified to show how target values compare to A321neo and Boeing 777. *Normalized to 400 passenger.

Category	A321neo*	Boeing 777-300	Target
Operating Cost(CASM, US ¢)	19.9 (61%)	14.8 (20%)	12.5
Unit Cost (US \$, millions)	230 (4%)	380 (72%)	220
Estimated Board Time(minutes)	40 (48%)	45 (68%)	30
Cycles per Day	7	7	9 (28%)

1.8.1 Measures of Merit Sensitivity Analysis

Trade studies were conducted to analyze the sensitivity of different measures of merit to key parameters. More specifically, a sensitivity analysis for CASM and cycles per day were conducted. In Figure 5, fuel burn and number of flight crew were identified as the most sensitive to CASM. Therefore, eliminating the need of two pilots and reducing the fuel burn will significantly reduce the target CASM by as much as 10%. This analysis helped identify autonomous technologies which allow for a single pilot capable/dual-pilot equipped cockpit featured in Exo and also helped prioritize a propulsion system with a low specific fuel consumption. Further, as shown in Figure 6, note that changing the cruise altitude has little to no affect on cycles per day. However, there must be an emphasis on cruise Mach number, runway time, and board time to achieve 9 cycles per day consistently. Exo has flexibility to fly greater than Mach 0.82, board in less than 29 minutes, and remain on the runway for less than 22 minutes and still achieve 9 cycles per day.

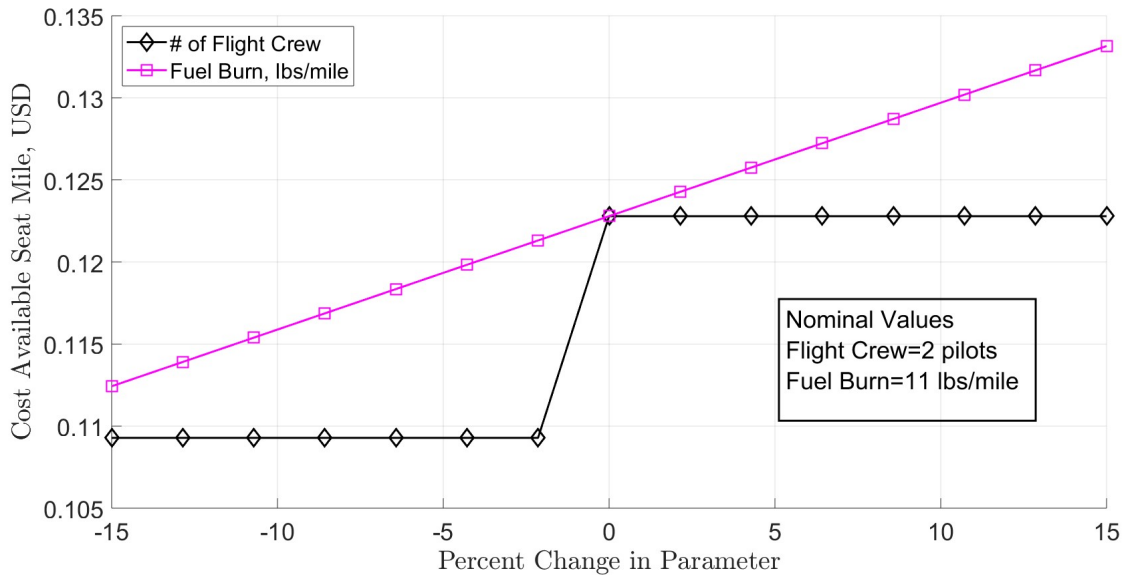


Figure 5: Cost per available seat mile trade study

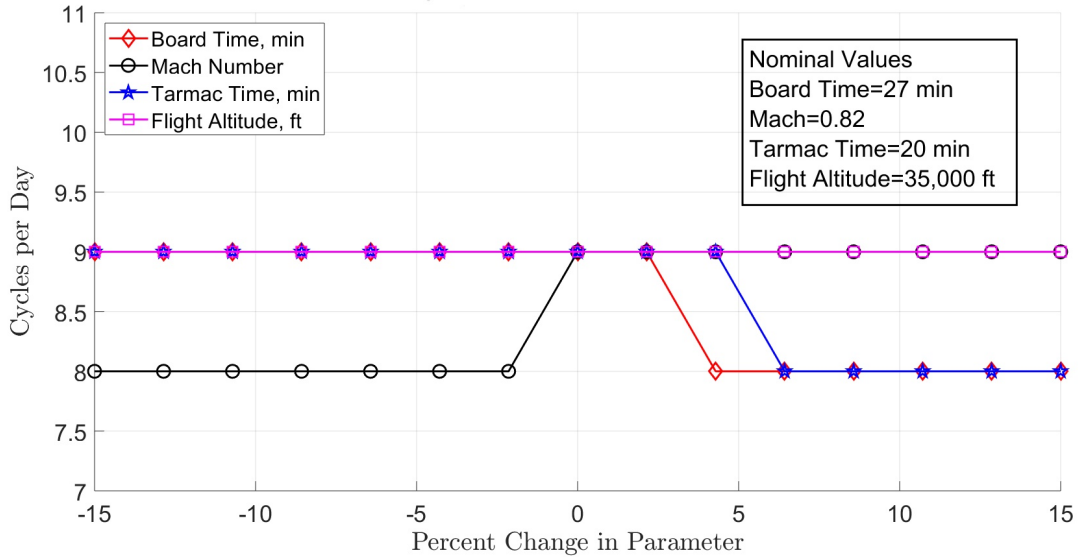


Figure 6: Cycles per day trade study

1.9 Key Technologies

To meet the design challenges, many innovative technologies were investigated. To ensure entry into service (EIS) date of 2029 is met, only technologies that are at TRL of 7 or higher in 2020, per the 2023 technology freeze date, were considered. For example, the hybrid-electric propulsion was evaluated and found not to be a mature technology by 2023.

Table 5: Viable innovative technologies with the corresponding advantages and TRL

Technology	Advantage	TRL (2020)
More Electric Aircraft (MEA)	Maintainability ↑ Weight ↓ Operational Cost ↓ Service Life ↑	9
Composite Materials	Structural weight ↓	9
Cabin 4.0	Operating Cost ↓	9
Geared Turbofan Engines	Fuel Consumption ↓ Engine Noise ↓ Emissions ↓	8
Boundary Layer Ingestion Propulsion	Cruise Efficiency ↑	8
Autopilot (ATTOL) / One Pilot Capable	Operating Cost ↓	8

Table 5 shows six key technologies that are most advantageous. The first of which is MEA systems architecture. MEA systems improve maintainability, reduce weight, operational cost, and improve service life by eliminating bleed-air extraction from the engines/APU and leverages all-electric ECS, electric de-icing, electric starting, and simplifies the hydraulic system with power-by-wire EHA actuation. Innovative materials reduce structural weight. Using Cabin 4.0 reduces operating cost with optional features such as WiFi. Geared turbofan engines impressively reduces fuel consumption, engine noise, and emissions. Boundary layer ingestion reduces drag and improves propulsive efficiency by re-energizing the boundary layer on the aft of the fuselage, ultimately reducing operating costs. Finally, an advanced avionics suite provides a single pilot capable cockpit with an autopilot capable of autonomous taxi, takeoff, and landing. Such capabilities cut the cost of pilots in half from traditional aircraft.

2 Conceptual Design

2.1 Initial Concepts

To meet the requirements in Section 1, each member of the team individually created a design that showcased ingenuity, feasibility, and creativity using hand sketches or models in OpenVSP. Each design was evaluated based on performance and key parameters such as max gross takeoff weight, total fuel weight, required empty weight, thrust-to-weight ratio, and wing loading. Engine selection was conducted based on takeoff thrust required, performance characteristics, and various other initial parameters. Several key parameters had to be estimated from historical data, namely the maximum L/D, cruise Mach number, AR, and drag coefficients. Figure 7 shows the iterative process, performed in MATLAB, used to find the takeoff, empty and fuel weights.

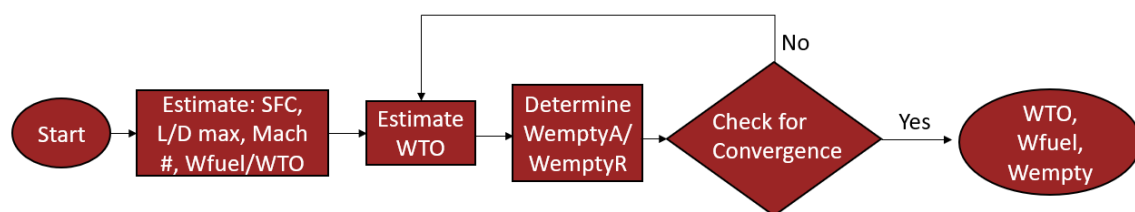


Figure 7: Iterative code for weight sizing

Wing loading and thrust loading plots for each design were generated using Sadraey's [11] equations. Next, designs were down-selected or merged to refine system concept options. This resulted in four

aircraft designs: wide-body fuselage, conventional configuration, blended wing, and Turbo-prop shown in Figure 8.

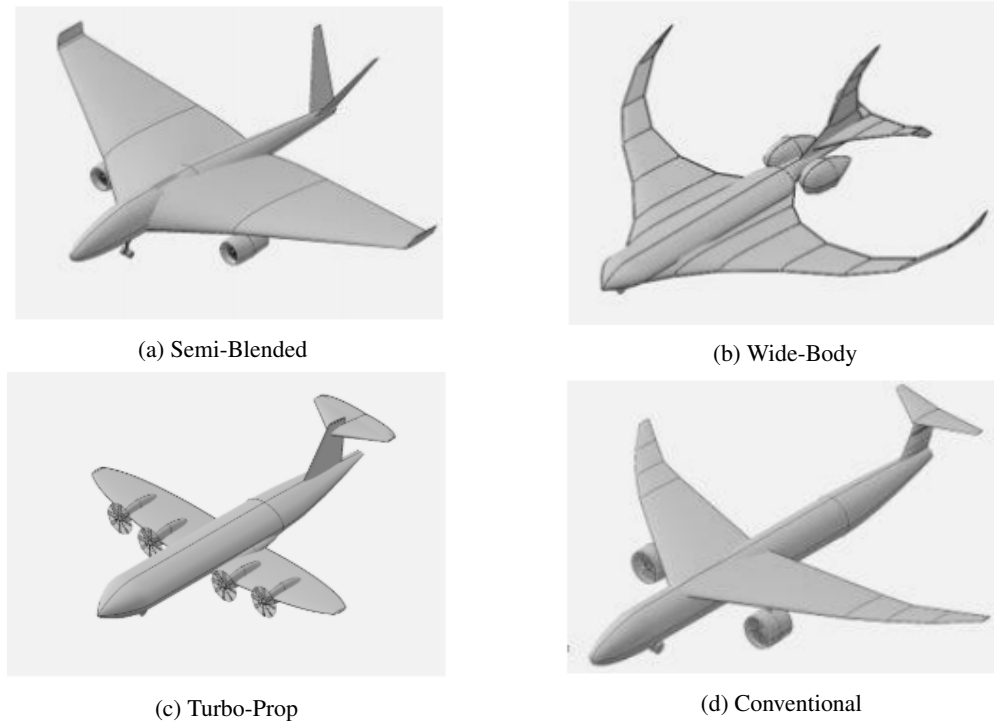


Figure 8: Preliminary aircraft designs

These designs were then ranked and weighted based on the following: cost of operation (25%), unit cost (20%), infrastructure accommodation (12.5%), boarding time (12.5%), safety (10%), maintenance (10%), design feasibility (5%) and passenger comfort (5%). These weights were determined based on the mission requirements, design drivers, and measures of merit. The conventional designs dominated categories such as design feasibility and infrastructure accommodation. The semi-blended and wide-body designs had innovative seating arrangements creating faster boarding and increased passenger comfort. The wide-body also leveraged aft mounted engines enabling the usage of boundary layer ingestion (BLI).

2.2 Feasible Designs

In order to decide between the remaining designs, qualitative and quantitative analyses were used to determine which features were the most beneficial in solving the congestion problem and meeting the customer's needs.

Each design was evaluated on a number of qualitative design parameters. Table 6 identifies the critical features that were evaluated and each design's relative rating, with green upward arrows indicating a positive rating, red down arrow signifying a negative rating and a dash meaning neutral.

Table 6: Qualitative down selection criterion

	Conventional	Wide Body	Semi-Blended
Manufacturability	↑	↓	↓
Emergency	-	↑	↓
Cabin Noise	-	↑	-
Public Perception	↑	-	↓
Passenger Comfort	-	↑	↓

The semi-blended and wide body designs were both given a negative rating for manufacturability as the designs called for innovative geometric features such as the blended wing or the highly curved wings. The conventional design features simpler structural and manufacturing aspects, thus giving it a positive rating. In addition to manufacturing, the designs were evaluated on the ability to perform emergency procedures. The safety rating of each design was based on the expected ability of passengers to reach the emergency doors in under 90 seconds, as well as the ability of the aircraft to utilize standard emergency exits. In this category the wide body design received a positive rating as passengers would have more space. The semi-blended received a negative rating because the size of the wings would prohibit the standard placement of emergency exits. The final three components are based on similar concerns, as the noise in the cabin, the passenger comfort, and the public perception. All of these components are based on the end user's experience and reactions to the design. The semi-blended design received overall negative ratings as atypical designs are viewed as less familiar and therefore less comfortable, as well as the fact that passengers seated in the wings would experience severe rotation as the aircraft performed banked turns. The wide body and conventional design each received neutral or positive ratings as the conventional shape and cabin layouts providing passengers with a familiar and comfortable experience. In addition to the qualitative analysis, a quantitative study was completed. This study focused primarily on the ability of each of the feasible design's performance in the measures of merit, found in Table 7.

Table 7: Quantitative down selection criterion

Measures of Merit	Conventional	Wide Body	Semi-Blended
Operating Cost (CASM, US ¢)	11.8	11.6	12.4
Unit Cost (US \$, millions)	240	220	300
Estimated Board Time (minutes)	30	25	35
Cycles Per Day	8	9	8

The operating cost was calculated as the CASM, and all three of the designs were relatively similar in the predicted cost. The best design, however, was the wide body design with a CASM of 11.6 cents. For unit cost, each of the designs had estimated unit cost derived from the total weight vs cost chart in Nikolai [9], Based on this, the least expensive unit cost of the designs was the wide body, while the most expensive was the semi-blended design. The last two measures of merit for down selection were the estimated boarding time, and cycles per day. As the designs each flies at the same speed, the total cycles per day is effected directly by the estimated boarding time of each design. The boarding time was estimated by taking into account the cabin layout and location of entry points. Taking account of all of the qualitative and quantitative considerations, the final choice of the preferred concept was the wide body. This design scored the best in both areas of assessment.

2.3 Preferred System Concept

The preferred concept featured a low wing and wide body design, with rear mounted engines that utilize BLI and a T-tail. The fuselage has a wide body design in order to utilize a three aisle cabin layout, which allows for faster boarding. Additionally, the wings are low mounted as this allows for increased ground effect during takeoff and landing. Additionally, the design weighed approximately 430,000 *lbs*, of which 136,000 *lbs* was fuel.



Figure 9: Preferred system concept

Table 8: Parameters used for constraint plot

Parameter	Value
CLmax	2.63
CLmaxLDG	2.89
Stall speed	112.5
Oswald Efficiency	0.736
Aspect Ratio	9.5
Zero Lift Drag	0.029
Cruise Lift Coefficient	0.3
Takeoff Flap Lift Coefficient	0.7
L/D max	14.1
Mach Cruise	0.82

A preliminary thrust and wing loading plot was created to determine the expected thrust and wing area that would be required for the preferred system design. Based on the initial takeoff weight of 430,000 *lbs* and the aerodynamic parameters defined in Table 8, the plot in Figure 10 was created to determine the most accurate value of thrust and wing loading. The result was a wing loading of $170 \frac{lbs}{ft^2}$ and a thrust loading of $0.35 \frac{lbs}{lbs}$, which determined the wing size and the required thrust to be 2500 *lbs* and 150,000 *lbs* respectively.

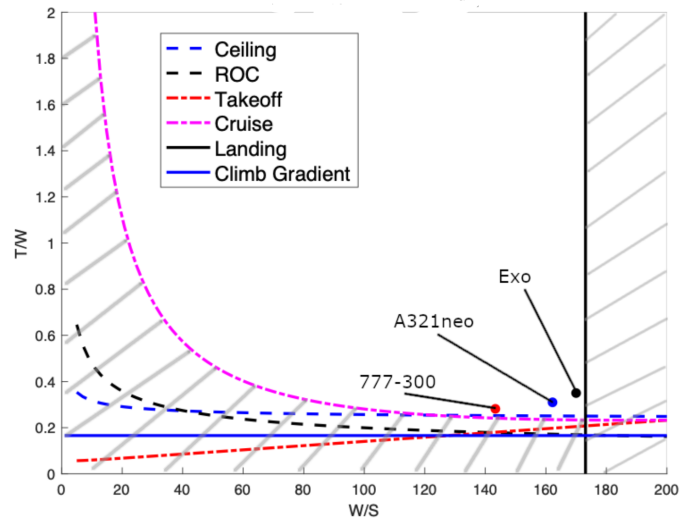
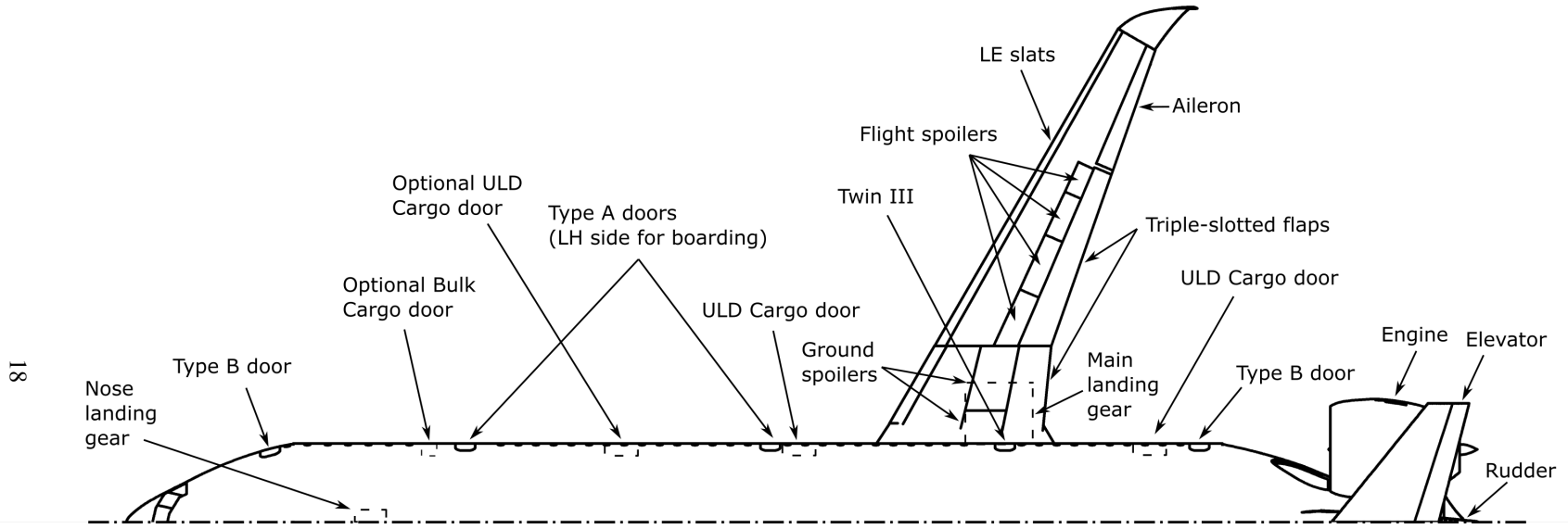


Figure 10: Wing thrust loading plot showing Exo and comparators

Shown in Figure 11 and 12 is the final version of the PSC, named "Exo". The sections following highlight the preliminary design process used to reach this point. Figure 11 shows an isometric view of Exo and Figure 12 shows a centerline diagram highlighting the locations of control surfaces, doors, hatches, engine placement for BLI, and other OML details.



Figure 11: Isometric view of final PSC design Exo



18

Figure 12: Centerline diagram of Exo with OML features highlighted

3 Aerodynamics

3.1 Airfoil Selection

The RAE (NPL) 5213 supercritical airfoil has been selected for Exo, to improve fuel efficiency as well as overall aircraft performance by reducing wave drag while cruising at Mach 0.82. Standard NACA 4 or 5 digit airfoils were not considered because large shocks occur as air accelerates over the airfoil, causing large amount of wave drag. Regarding the airfoil selection process, the following parameters were first identified: coefficients of lift required to complete the reference mission, maximum takeoff gross weight, cruise and stall speed estimations. The required coefficients of lift were calculated to be 0.61 during cruise flight and 2.12 during takeoff with high lift devices deployed to meet the maximum required takeoff distance and for operation during cruise conditions.

Approximately 15-20 airfoils were initially picked, but a 2-D XFOIL and XFLR5 analysis of behavior during cruise and takeoff flight was conducted to reduce the number of possible candidates. This analysis was used to compare the coefficient of lift values with the target values previously discussed. The data collected from XFOIL and XFLR5 was then verified with Dr. William H. Mason's transonic airfoil analysis software, TSFOIL, which was originally created at NASA Ames [10]. This software provides a finite difference solution to transonic small disturbance equations. This is crucial since Exo's cruise flight speed is Mach 0.82, where the flow will reach transonic levels, as it accelerates around the surface of the airfoil.

The five airfoils that most closely matched the required coefficient of lift at cruise and takeoff angles of attack are shown in Table 9. Using XFOIL and XFLR5 to generate data for the airfoils, the plots in Figure 13 were formulated. These plots display the performance characteristics of each of the final airfoil candidates. The decision matrix shown below in Table 9 displays the scoring criterion based on Sadraey's suggested factors [11]. The scores assigned to each airfoil were created based on a normalized value and weighting found by using comparing the desired value to, as well as theoretical equations. The values displayed for each respective airfoil were normalized and then multiplied by the weight of each merit. The total score for each airfoil is based on the sum of the criterion results, where the the RAE (NPL) 5213 was selected for Exo.

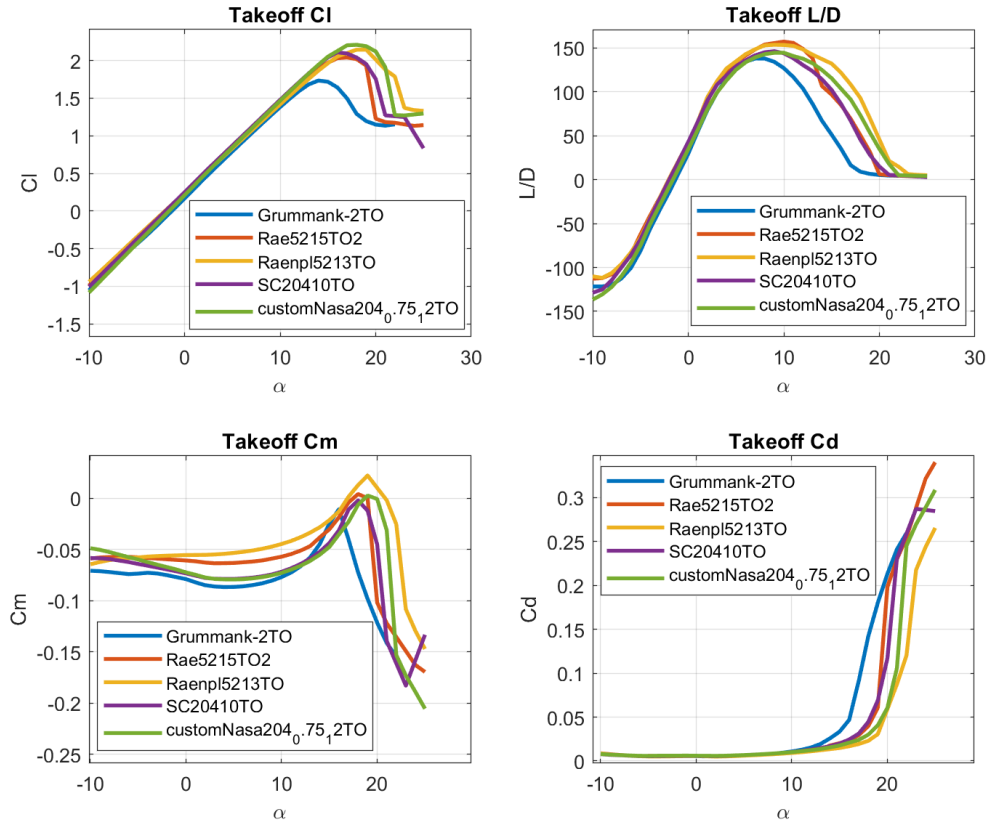


Figure 13: Performance curves of 5 final airfoil candidates

Table 9: Exo airfoil decision matrix (normalized and weighted scores)

Merit	Weight (%)	Rae 5215	Grumman K-2	Rae (NPL) 5213	Custom Nasa204	Nasa SC2-0410
Cruise L/D	30	30.0	29.6	29.1	26.4	29.0
Stall Quality	20	12.0	20.0	16.0	12.0	12.0
C_{d_0}	15	11.0	15.0	10.3	14.2	10.2
C_{m_0}	15	14.2	10.2	15.0	13.2	12.4
Alpha stall	20	17.9	14.7	20.0	18.9	16.8
Total Score	100	85.1	89.6	90.3	84.7	80.4

Based on wing performance characteristics, such as cruise lift/drag, stall quality, stall angle of attack, and zero lift drag and moment coefficients, the RAE (NPL) 5213 proved to be the best option for Exo. This airfoil was chosen due to its ability to reduce wave drag during transonic cruise from a drag divergence Mach number of 0.8496. An image of the airfoil, highlighting its supercritical shape as shown in Figure 14. Analyzing the XFOIL and XFLR5 results, at both cruise and takeoff, the RAE (NPL) 5213

produced one of the highest lift/drag ratios and a zero lift pitch moment value closest to zero. This airfoil also stalls at the highest angle of attack, approximately 19 degrees, of every airfoil tested, giving the aircraft great stall resistant characteristics during takeoff and any other flight maneuvers to comply with CFR Part 25 Subpart B requirements for performance, stall, controllability, and stability.

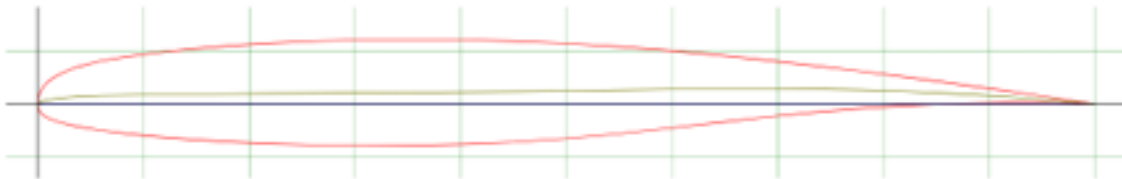


Figure 14: Geometry of Rae (NPL) 5213 [12]

3.2 Wing Planform Sizing

The overall wing planform configuration is displayed in Figure 15, where the center spar connecting the two wings intersects the fuselage. The highly curved winglets reduce drag by mitigating the large wingtip vortices created during high cruise speeds. The low mounted wings incur more ground effect during takeoff and landing, therefore generating more lift and less drag than a high wing aircraft. In case of an emergency landing, the low mounted wings assist in buoyancy in a ditching scenario, and act as an exit path in any emergency evacuation to assure the safety of the passengers and crew on board. The total span of the wing is 157.11 *ft* to meet the Group 4 airport requirement of 172 *ft*. This gives Exo the capability to operate at airports that larger comparator aircraft cannot. To be able to takeoff and land within the required distance stated in the request for proposal and produce enough lift to carry the required number of passengers, the overall area of the wing is calculated to be 2,480 *ft*². By accommodating the aerodynamic shape of the wing and the maximum Group 4 span requirement, the root and tip chord of the wing is 31.7 *ft* and 4.96 *ft* respectively, resulting in a mean aerodynamic chord length of 16.15 *ft* and an aspect ratio of 9.46. To meet the 35 *ft* height requirement during takeoff, the takeoff angle of attack has been set to 12° to produce enough lift during takeoff with the high lifting devices, as well as to consider a factor of safety for wing stall in various weather and altitude conditions.

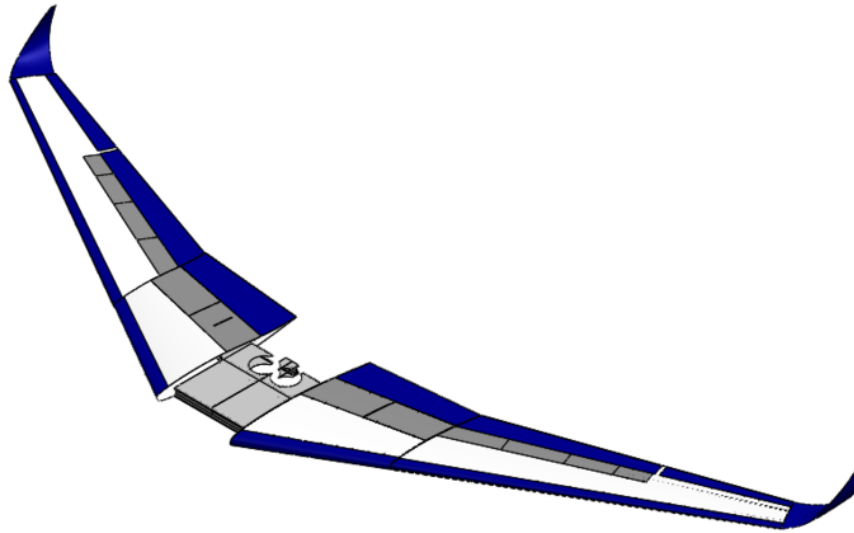


Figure 15: Exo wing planform

To increase aircraft longitudinal stability, a dihedral was set to 5° based on historical data of comparator aircraft of similar maximum takeoff weight, such as the Boeing 767 and Airbus A321neo. The wing incidence angle is set to 2° in order to obtain the required coefficient of lift value during cruise necessary to maintain steady, level flight. This thereby increases the fuel economy during steady level cruise, as the fuselage can be near level, reducing drag. In addition, a level fuselage alleviates workload for the flight crew and creates a more comfortable cabin for passengers. The wing features a twist ranging from 0° to -2° located at 25% of the chord and -5° at the winglet to obtain a nearly elliptical load distribution during cruise conditions and a wing tip that does not stall before the root; this is important to ensure aileron effectiveness. To further decrease wave drag during cruise flight, a constant 30° leading edge sweep along the wing will help avoid Mach divergence and any shocks that will form along the wing while cruising at Mach 0.82.

An in-depth aerodynamic analysis using NASA's OpenVSP program determined the coefficient of lift and drag of a 3-D model of Exo at both cruise and takeoff conditions for a wide range of angles of attack. A deeper discussion of the OpenVSP process is discussed in Section 3.4, Aerodynamic Characteristics and Performance Metrics. With this analysis, estimates of Exo's coefficient of lift, drag, and moment, along with a variety of other aerodynamic characteristics were determined. These characteristics are shown in Table 10, where the coefficient of lift of Exo at a cruise speed of Mach 0.82 and an angle of attack of 2° is approximated to be 0.560 and a coefficient of drag of approximately 0.048. By incorporating the high lifting

devices into the OpenVSP analysis, the takeoff coefficient of lift and drag are approximated to be 1.818 and 0.103, respectively.

Table 10: Key aerodynamic performance values

Feature	Value	Feature	Value
C_L @ cruise flight	0.560	α_{stall}	19 °
C_D @ cruise flight	0.048	Drag Divergence Mach Number (M_{DD})	0.8496
C_L @ takeoff flight	1.82	Critical Mach Number	0.7419
C_D @ takeoff flight	0.103	Wave Drag Coefficient	0.000744
Wing C/4 Location	130 ft	$C_{D_{l=0}}$	0.0327
Wing Area	2480 ft ²	L/D_{max}	14.1
Mean Aerodynamic Chord	16.15 ft	$C_{L_{max}}$	2.504

To increase stability, the wing was placed such that Exo achieved a static margin of 25% with fuel and 14% with dry reserve required by the FAA; where the static margin is the distance between the center of gravity and the neutral point, expressed as a percentage of the MAC of the wing. This results in the wing's neutral point being placed around 127ft from the tip of the nose, while the center of gravity is placed 125ft from the tip of the nose. This allows for adequate CG travel while fuel burns during flight to maintain longitudinal stability.

3.3 High Lift Devices

Exo's wing features a triple slotted Fowler flap and leading edge slat, extending from the fuselage out to 65% of the wingspan, leaving 30% span for ailerons and the remaining 5% for the winglet, as depicted in Figure 16. The triple slotted flap is 25% of the overall chord in length and is stowed within the wing when not in use, as shown in Figure 17. The triple slotted flaps were chosen to achieve the highest coefficient of lift during takeoff and to implement a system that is used by many aircraft today which is simple to integrate due to its high technology readiness level.

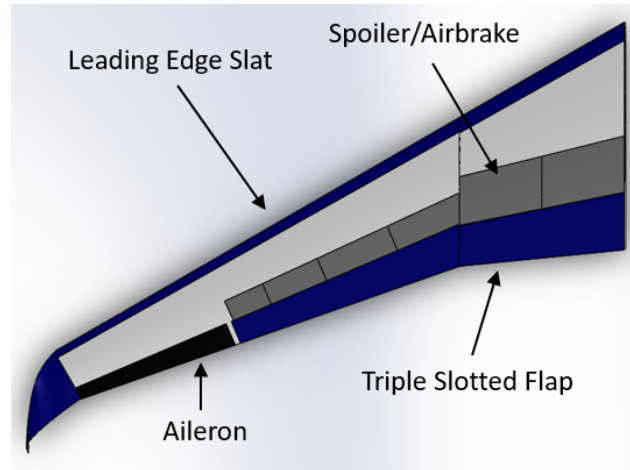


Figure 16: Exo control surface and HLD distribution along the wing

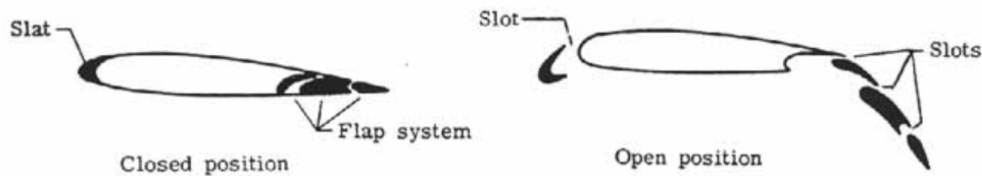


Figure 17: Triple slotted flap and leading edge slat positioning in wing [13]

The wing also incorporates a Yehudi flap near the root of the wing to increase the wing root chord. This allows for the build height for the root to increase for the same relative thickness. This will assist the wing in maintaining structural integrity because it is at this location where the wing experiences the most stress. While landing, Exo will deploy spoilers located in front of the flaps to greatly increase the drag, therefore reducing the landing distance dramatically. By incorporating these high lifting devices, the coefficient of lift has increased by approximately 26%, which directly relates to a decrease in takeoff distance by approximately 22.5% and landing distance by approximately 18%.

The approach speed of Exo during landing was determined to be 138 *kts* which is less than the design mission requirement of 145 *kts* as stated in the RFP and complies with CFR Part 25 Subpart B § 25.125 landing regulations. Airbrakes and spoilers will be deployed during landing to further reduce the landing distance. The high lifting devices and spoilers give Exo the ability to land and takeoff at smaller airports, that which the comparator aircraft such as the Boeing 767 can not access. This is exceptionally helpful in the case of an emergency landing, where Exo can land at smaller airports that maybe closer to the incident location.

3.4 Aerodynamic Characteristics

After creating the wing and aircraft in NASA's 3-D modeling program, OpenVSP, several implicit inviscid flow computations for the aircraft were performed at both cruise and takeoff conditions. Key aerodynamic performance characteristics were determined at each stage in the design process using OpenVSP's VSPAero software. OpenVSP was also used to determine the parasite drag of the aircraft, which was added to the induced drag values obtained by the VSPAero analysis, along with the wave drag which was previously calculated. The aerodynamic performance values of Exo were plotted to produce drag polars for cruise and takeoff conditions, as well as the wing lift distribution at cruise and takeoff angles of attack shown in Figures 18 and 19, respectively. The takeoff drag polar ranges in angles of attack from -13° to 15° in iterations of 1° . While the cruise polar ranges from -5° to 5° in iterations of 0.2° . These figures are critical to determining the performance and behavior of the aircraft at off-design conditions, as well as, to check the structural integrity of the ribs and spars of the wing under typical and extreme accelerations. The data collected from the VSPAero analysis was also used to assist in estimating the required center of gravity position relative to the aircraft's aerodynamic center, ensuring that it was within the 10-30% allowable tolerance to account for turbulence and crosswind effects for full and empty fuel flight. These estimates assisted the stability and sub-systems in assuring correct placement of critical control surfaces and sub-systems layout. All VSPAero computations were validated by extrapolating the use of TSFOIL from Dr. William Mason [10].

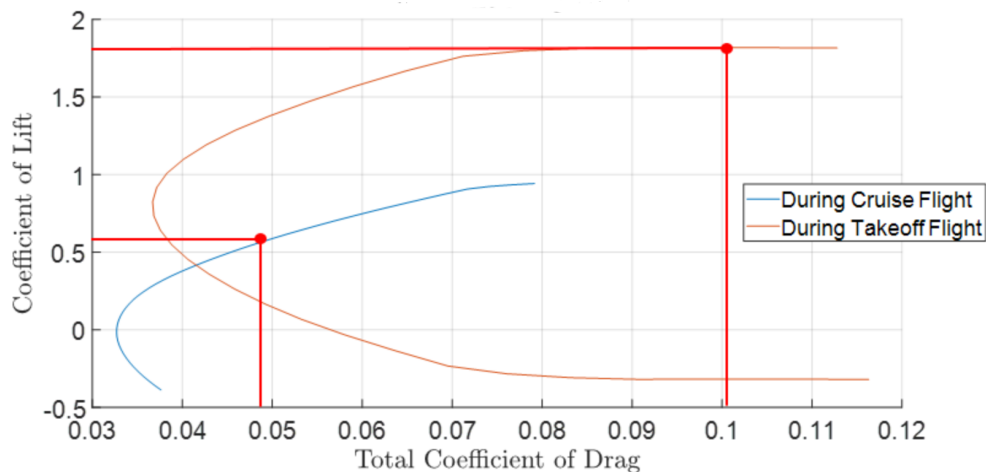


Figure 18: Exo drag polars of cruise and takeoff flight

From Figure 18, the cruise and takeoff lift and drag values can be obtained for any angle of attack.

This information is critical for takeoff because the aircraft will undergo the entire range of angles of attack from 0° to 12° in order to climb to the designed cruise altitude. For cruise flight, the drag polar shows how drag varies with a change in payload or fuel (changes required lift coefficient), and hence reflecting the required thrust needed to operate. Parasite drag build-up for aircraft components can be found in Table 11. Note that C_{d0} is reduced to 0.2065 after landing gear are retracted during cruise configuration.

Table 11: Parasite drag breakdown

Component	Cd0	Percentage %
Fuselage	0.0120	55.9
Vertical Stabilizer	0.0013	6.3
Horizontal Stabilizer	0.0010	4.7
Landing Gear	0.0085	39.4
Wing	0.0066	30.9
Engine	0.0017	7.8
Total	0.0215	100

The lift distribution shown in Figure 19 is specific for the cruise angle of attack of 2° and takeoff angle of attack of 12° . Plotted along with the lift distribution curves are the respective elliptical shape that represents the ideal lift distribution along the wing. Both curves are not perfectly elliptical, however they both approach the ideal case, therefore justifying the wing planform shape. The estimated Oswald efficiency is 0.85 for cruise conditions. The increase of lift at the root of the airfoil during takeoff is a result of the Yehudi flap providing additional lift during takeoff as a result of the increased root chord length.

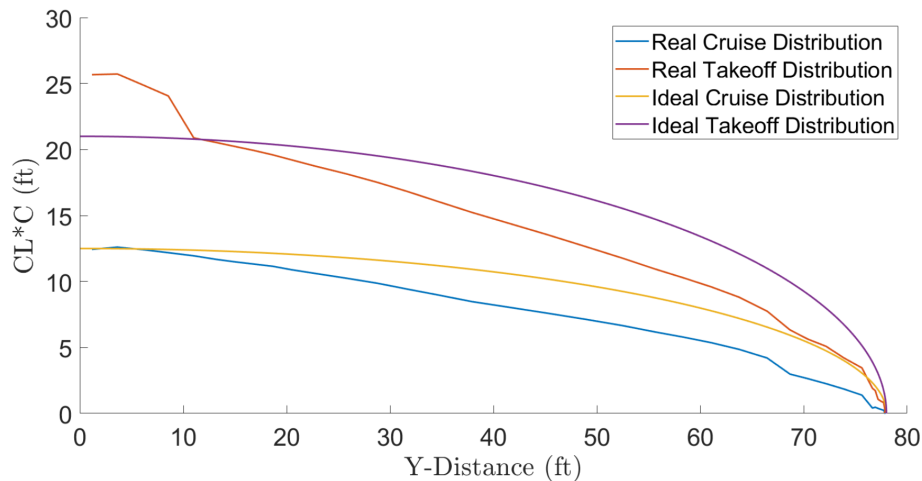


Figure 19: Exo lift distribution compared to ideal elliptical shapes

4 Performance

4.1 Takeoff/Landing

The design must be capable of taking off and landing in under 9,000 *ft*, balanced field length with dry pavement, and with a 35 *ft* barrier located at the end of the runway. Exo meets this requirement by achieving takeoff in 7,200 *ft* and by landing in 5,400 *ft* at sea level. These values were calculated by breaking the takeoff and landing sequences into stages, and by using the data found in table 12.

Table 12: Takeoff and landing parameter values

Take off Parameters	Value
Take off Weight (lbs)	415,700
Wing Area (ft ²)	2,480
Cl Cruise	0.67
Cl Max	2.5
Take off Velocity (ft/s)	307
Cl Groundrun	2
Cd Takeoff	0.085
Thrust (lbs)	161,700
Climb Angle (deg)	20
Landing Parameters	
Cd Landing	0.088
Cl Landing	2.12
Approach Angle (deg)	3
Stall Velocity (ft/s)	260
Landing Speed (ft/s)	300
Landing Weight (lbs)	280,100

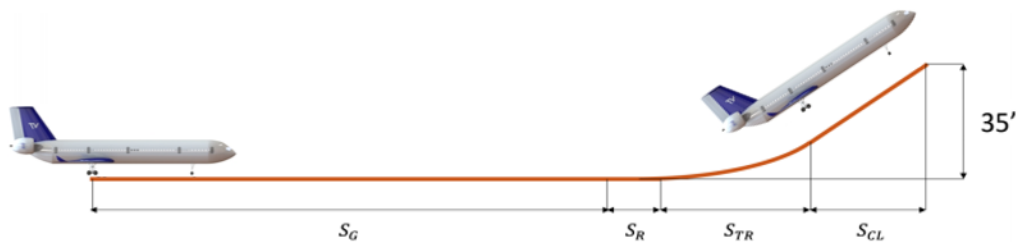


Figure 20: Takeoff balanced field length

For takeoff, four key stages were identified as shown in Figure 20. The first of these stages is the ground run stage. In this stage, the distance is defined as the runway length it takes for the aircraft to accelerate to the design takeoff velocity from rest (Equation 1), where a is the acceleration of the aircraft. Next, the rotation distance is the distance in which the aircraft, while still on the ground, is rotated to the angle of attack such that $C_L = 0.8C_{Lmax}$. For FAA-commercial aircraft the time it takes to achieve this is established during flight testing, and estimated with Equation 2. After the rotation distance is the transition distance, S_{TR} . In the transition distance the aircraft flies a constant velocity arc of radius R . Given the climb angle, θ_{CL} , S_{TR} can be approximated with Equation 3. Finally, the climb distance (S_{CL}) is the distance it takes to climb and get over a specified obstacle height, h_{TR} (Equation 4). In Exo's case, the object is 35 ft as specified in the RFP.

$$S_G = \int_0^{V_{TO}} \frac{V}{a} dV \quad (1)$$

$$S_R = 2 * V_{TO} \quad (2)$$

$$S_{TR} = R \sin(\theta_{CL}) \quad (3)$$

$$S_{CL} = \frac{50 - h_{TR}}{\tan \theta_{CL}} \quad (4)$$

As for landing analysis, the distance is the horizontal distance required to clear a 50 ft obstacle, free roll, and then brake to complete stop. The landing distance is broken into three sections: air distance, free roll distance, and braking distance.

The air distance, S_A , is defined in Equation 5, where θ_{app} is the approach glide slope. The free roll distance, S_{FR} , is the distance covered while the pilot reduces the power to idle, retracts the flaps, deploys the spoilers, and applies the brakes. Free roll is assumed to be three seconds and defined in Equation 6. Finally, let a =deceleration. Then braking distance, S_B is defined in Equation 7.

$$S_A = \frac{50}{\tan \theta_{app}} \quad (5)$$

$$S_{FR} = 3V_{TD} \quad (6)$$

$$S_B = \int_{V_{TD}}^0 \frac{V}{a} dV \quad (7)$$

The takeoff and landing analysis outlined above and their associated equations are estimations from established aerospace author, Nicolai [9]. Based on the fuel required for the reference mission, the aircraft has

a takeoff and landing distance of 7,200 *ft* and 5,400 *ft*. This allows Exo to employ more runways thus reducing ground wait times to operate with full loads from high airports or on hot days.

4.2 Payload Range

The payload range diagram containing three important points is shown in Figure 21. The first point is the maximum payload point, at which the design is flying at maximum fuel and maximum payload. At this point, the aircraft should be flying the design range of 3,500 nm, however FAA regulations require 200 nm of extra range as well as 30 minutes of loiter time and 5% additional fuel. Taking this into account, Exo is designed to fly the design range of 3,500 nm with the additional range reaching 4,000 nm to comply with these regulations, and utilizes the full volume of the fuel tanks. The second critical point is the fuel range tradeoff point. This point is defined as the case in which the aircraft is flying with a total payload of only 80% of the maximum payload. This defines a situation in which the aircraft is flying at lower capacity in order to achieve further range or in the case seats are unused due to cancellations or no shows. Based on this point Exo can reach a range of approximately 5,200 nm, allowing it to complete larger missions if needed. The final point on the diagram is the payload range trade off point located at approximately 7,000 nm, and denotes the case in which the design is flying at zero payload and maximum fuel capacity. This point is critical as an aircraft must often make longer flights, as well as maintenance missions in which the aircraft simply needs to get from point A to point B as fast as possible.

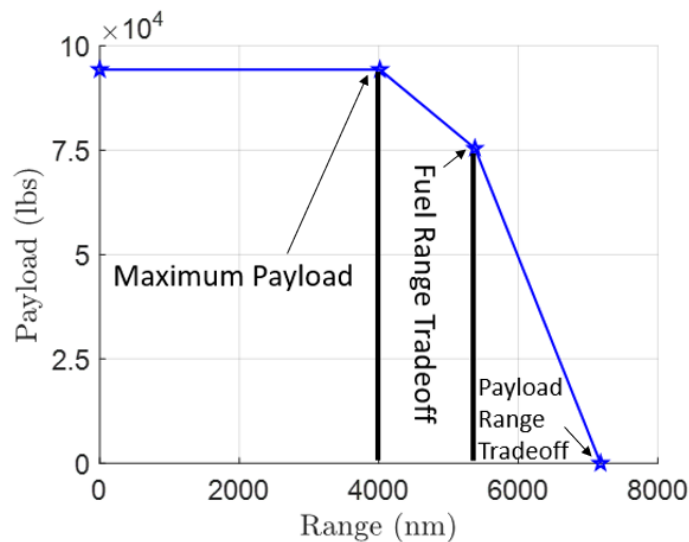


Figure 21: Payload range diagram

4.3 V-N Diagram

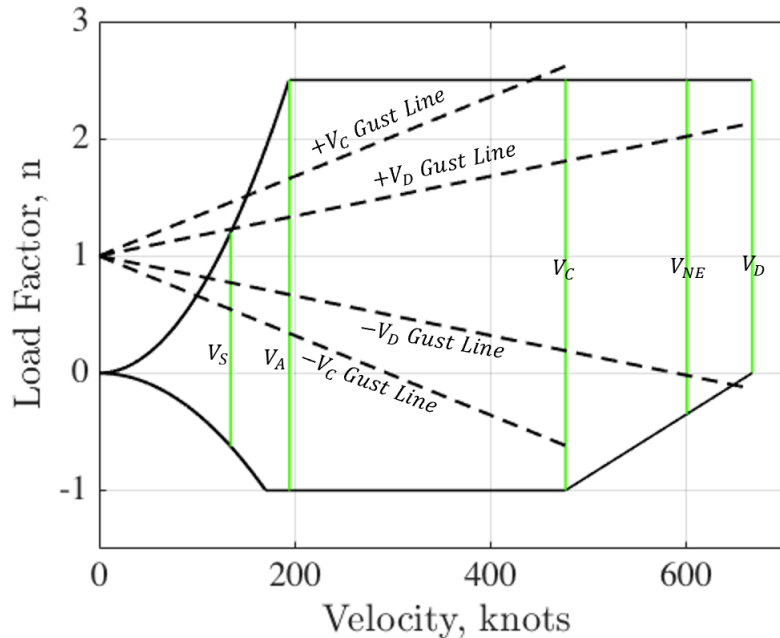


Figure 22: V-N diagram

The flight envelope of Exo can be observed in the V-N diagram of Figure 22, where all the speeds are adjusted for cruise atmospheric conditions. This diagram represents the limits aircraft's maneuvering capability from the lowest to the highest limit. The upper and lower limits of the aircraft is shown by the maximum dive speed, V_D , of 670 *knots* and a stall speed, V_S , of 135 *knots*. V_D represents the maximum speed that can be achieved until permanent structural deformation occurs. To create a buffer, the never exceed speed, V_{NE} , is set to be the maximum operational speed as $0.9V_D$. The stall speed is the absolute lowest speed the aircraft can operate before stall, regardless of the angle of attack. The cruise speed, V_C , is 480 *knots* and the speed at which the aircraft reaches a load factor of 2.5, V_A , is 195 *knots*. Design load factors of 2.5 and -1 are established based on 14 CFR § 25.337. The gust loads, listed as dotted lines, are also compliant with 14 CFR § 25.337.

5 Structural Design

5.1 Material Selection

Multiple mechanical evaluations of various materials were completed, leading to the materials selected. Each study was tailored for identification of materials suitable for specific structural applications, with an emphasis on PMCs and polymer reinforced aluminum alloys compared to conventional materials. Given recent evolution of the uses of PMCs in current aircraft, such as the Boeing 787, a growing competitive market focused upon production and sale of PMCs for aerospace applications is both industrially accessible as well as cost beneficial to Exo's construction. While the use of classical materials, such as specific steel and aluminum alloys, would reduce cost in production, most of the life cycle cost of a commercial aircraft has been identified to be fuel and maintenance. By using lightweight and easily fabricated PMCs as the primary material for this aircraft, the life cycle cost is directly decreased through the reduction of empty weight and, in turn, fuel consumption. The pie chart in Figure 23 shows that Exo is truly a composite based aircraft, with almost 80% of airframe structural material being carbon fiber based.

Materials for the exterior of the aircraft, as well as structural members, were identified through comparative analysis of relevant load cases for specific parts with an emphasis on reduction of weight. Figure 24 shows a breakdown of materials located on the aircraft, many leveraging polymer matrix composites (PMCs). Multiple decision matrices, with an example shown in Table 34 located in the Appendix, were constructed to narrow candidate materials. From these candidate materials, a full-scale material breakdown and weight analysis

were conducted, the results of which may be observed in Figure 23. The utilization of carbon fiber composites in this aircraft presents the possibility of reducing the weight of a part by approximately 25-35%, given a conversion of 7075 Aluminum directly to composites of that nature.

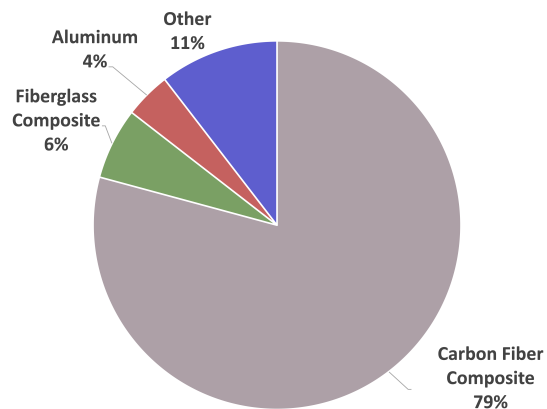


Figure 23: Percentage of materials used on Exo by weight

- Epoxy/HS Carbon Fiber QI lay-up
- LYTEX® 9063 BK-E Fiberglass Reinforced Compound
- PEEK/IM Carbon Fiber, UD prepreg, UD lay-up
- Aluminium 7075 T6 with Carbon Laminate Plating
- Aramid Paper-Phenolic Honeycomb 0.05“

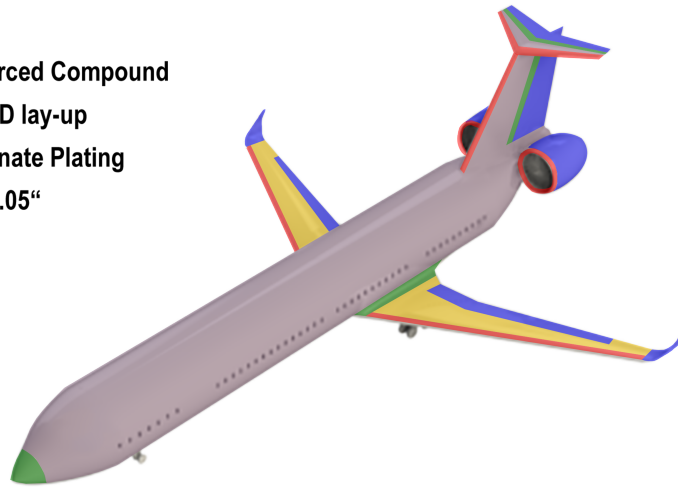


Figure 24: Aircraft material breakdown showing location of innovative materials

It is known that the skin of the aircraft is not under extreme load bearing, as the load is mainly tension from pressurization and shear force from fuselage twist, leading to the main constraint of density for candidate materials. The fuselage skin is composed of QI high strength carbon fiber reinforced epoxy matrix panels, which proved to display a substantial reduction of material density with no loss to service performance when compared to the use of conventional 7075 Aluminum. However, while carbon fiber has exceptionally properties in yield strength and density, one concern for its use on the fuselage is that it is a poor conductor of electricity. This could result in serious damage in the case of a lightning strike. To combat this, the Exo will utilize Dexmet's MicroGrid material [14], which is an aluminum and copper material that is woven with the strands of carbon fiber to increase its electric conductivity without compromising the structural properties of carbon fiber.

The best candidate for the wing skin was identified to be UD high strength carbon fiber reinforced epoxy matrix panels, as this allowed greater longitudinal support of the leading edge than QI layups, as well as maintaining the same degree of weight reduction as the choice for the fuselage skin. For the leading edge of the wing, an Aluminum 7075-T6 with carbon fiber/epoxy reinforcement was chosen, as the load due to stagnation of flow during flight calls for a degree of mechanical performance that the candidate PMCs could not supply. However, the inclusion of the PMC reinforcement was determined to increase the lifetime of the surface finish of the leading edge due to the PMCs high degree of chemical corrosion and physical fatigue resistance. Control surfaces and engine paneling were chosen to be composed of an Aramid Paper/Phenolic Honeycomb with Carbon Fiber Epoxy matrix paneling, which granted the high degree of physical stiffness

that would be required during service, as well as the low density and service temperatures of the various applications. A reinforcement material for control surfaces, fuselage-wing connections, and nose of the aircraft was chosen to be LYTEX BK-E Fiberglass reinforced paneling, which showed a high degree of strength and resistance to deformation for its low density. Table 13 may be observed for a comparison of the physical properties of the materials designated for use.

Table 13: Materials used on aircraft and their corresponding properties

Finalized Materials Candidates	Epoxy/HS Carbon Fiber QI Layup	PEEK/IM Carbon Fiber, UD prepreg, UD Lay-up	LYTEX 9063 BK-E Fiberglass	Aramid Paper-Phenolic Honeycomb	Aluminum 7075-T6 with Carbon Laminate
Density (lb/in ³)	0.0569	0.565	0.667	0.00177	0.0849
Yield Strength (ksi)	79.7	283.5	27.5	0.0032	80
Specific Strength (lb* ² /ft/lb)	1.16e5	4.17e5	3.44e4	150.5	7.86e4
Specific Stiffness (lb* ² /ft/lb)	9.68e6	3.03e7	3.76e6	923	9.72e4
Price (\$/lb)	25.3	17.95	1.62	16.25	165

5.2 Material Up-cycling

Material up-cycling has been considered a viable option for reducing costs and emissions when obtaining required materials for manufacturing the aircraft. Since Exo is made up of nearly 80% carbon fiber composites by weight, up-cycling carbon fiber composites from aircraft being decommissioned provides materials at a reduced cost. For example, the A380, which is currently being discontinued due to its lack of demand, is made of 25% composites by weight and is an ideal aircraft for up-cycling composites. Other materials identified for up-cycling are aluminum alloys, which are 60% of all recyclable material on existing aircraft. Many processes have been implemented by companies to reduce the contamination that commonly occurs from the corrosion resistant compounds. Lastly, thermoplastics using the recycled carbon fiber are great replacements for steel and magnesium, providing stronger and lighter weight electric aircraft components [15].

5.3 Spar Analysis

Once the airfoil and the outer mold of the wing were finalized, the internal skeleton of the wing could be developed. The main objective was to create an internal structure that would meet all the extreme loading standards while keeping the weight at a minimum. The considered loading cases were the +3G vertical load, -1G vertical load, and a full fuel landing case. The +3G and -1G vertical load cases were both analyzed in cruise atmospheric conditions with 70% and 30% fuel burned, respectively. The amount of fuel burned was taken into account in order to reduce the fuel weight that would counteract the vertical gust. The full fuel landing case, although slightly misleading, has 11% fuel burned. This case was studied in the event of an emergency during takeoff after V1 (commit to fly speed) and an immediate plan to return to the airport. Eleven percent of the fuel would be burned during the required 30-minute loiter before the approach. This case is significant because it does not require the aircraft to dump fuel and still conduct a heavy landing. This could prevent fuel dumping in densely populated areas and save money that would otherwise have been wasted on unused fuel. These test cases were chosen based on the flight envelope.

The first step in the wing spar analysis was to divide the wing into 10 span-wise panels. In doing so, the distribution of lift as well as the distribution of the structural and fuel loads were determined. To calculate the distribution of lift, the elliptical and trapezoidal lift equations, that can be expressed as a function of wing station y in the following, were used.

$$L_{trap}(y) = \frac{2L}{b(1+\lambda)} \left[1 - \frac{2y}{b}(1-\lambda) \right] \quad (8)$$

$$L_{ellip}(y) = \frac{4L}{\pi b} \sqrt{1 - \left(\frac{2y}{b}\right)^2} \quad (9)$$

Where L is the total lift, λ is the taper ratio, and b is the total wingspan. By taking the average of the two methods, accurate estimations of the lift load distribution were obtained. The structure and fuel weight of each panel was determined to calculate the lift minus weight load. This gives the net load of each panel, which can be utilized to find the stress, moment, and displacement distribution. This calculation was done through MATLAB.

Once the physical quantities of the internal forces and deformation was determined, it became possible to shape the spar using the material properties. Each wing has two, I-beam spars that stretches the span of the wing and tapers to a percentage of the chord. One I-beam will be at the leading edge of the wing box while the other will be at the trailing edge. The I-beam was determined to be the most favorable

structural shape for its excellent performance in unidirectional bending. The height, width, and thickness of the beam is 5.4%, 4.8%, and 1% of the local chord length, respectively. These numbers yield the minimum weight for the spar while still achieving a factor of safety of 1.6 even in the most extreme case studies. This is even enough to achieve a hypothetical 100% fuel load landing.

In order to validate the MATLAB results, a structural analysis was done through Solidworks. As seen below in Figure 25, the solution of the two methods have an average deviation of 15% for the +3G case and 12% for the -1G case.

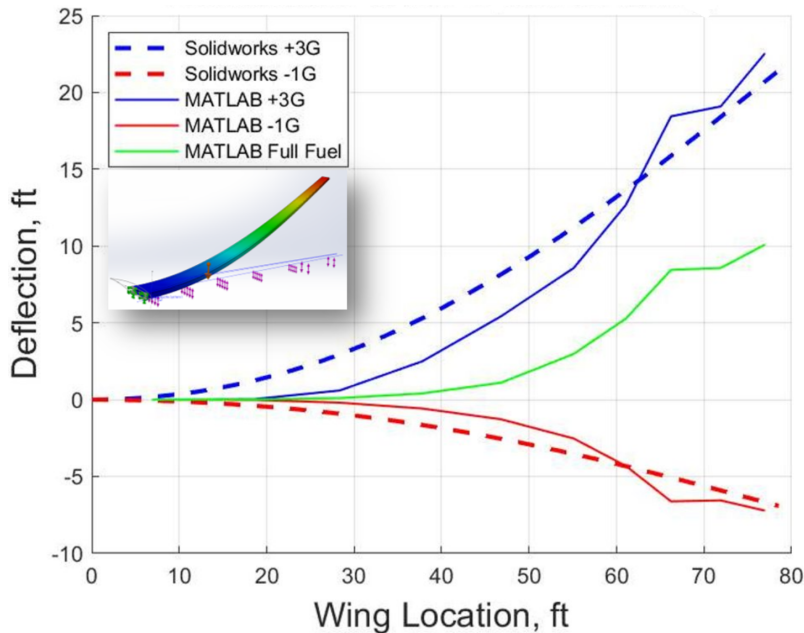


Figure 25: MATLAB and Solidworks wing displacement analysis

5.4 Fuselage Analysis

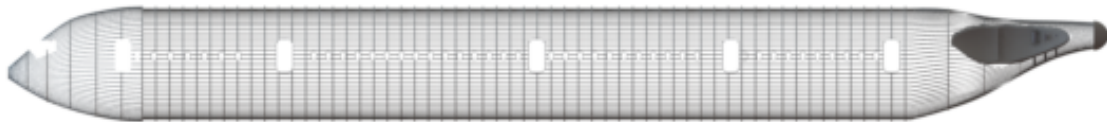


Figure 26: Internal structure of the fuselage

Similarly to the spar analysis, the fuselage structure was developed using the same extreme loading cases. In order to better model these cases for the fuselage, the +3G and -1G cases had an additional load of

internal cabin pressure in cruise atmospheric conditions and the full fuel case was now done at touchdown to better apply the forces that is exerted from the landing gears into the fuselage.

For simplicity, the fuselage was modeled as a free-free beam where all forces deflect relative to the CG. The main and nose landing gear, vertical and horizontal stabilizers, lift minus wing and fuel weight, engines, and cabin loads were all considered as significant point forces along the "beam," resulting in a total moment at the CG. Using the total moment, maximum stress of the fuselage was calculated, σ_{max} , using the following equation:

$$\sigma_{max} = \frac{Mr}{I_{zz_f}} \quad (10)$$

where M is the total moment about the CG, r is the average radius of the fuselage, and I_{zz_f} is the moment of inertia in the horizontal and vertical axis through the centroid of the fuselage. I_{zz_f} is influenced by skin thickness. Although the skin is too thin to provide sufficient structural support for the fuselage, it does yield exceptional performance in hoop stress, σ_θ , that is calculated in the equation:

$$\sigma_\theta = \frac{Pr}{t} \quad (11)$$

where P is the internal pressure of 12 *psi* and t is the skin thickness of 0.05 *in*. Hoop stress support will alleviate some load that would otherwise be exerted on the skeleton. Then, the buckling stress equation of the longeron is used to find the critical stress of a single longeron, $\sigma_{critical}$, as shown in the following:

$$\sigma_{critical} = \frac{\pi^2 EI_{zz_l}}{AL^2} \quad (12)$$

where E is the modulus of elasticity of the material, I_{zz_l} is the moment of inertia in the horizontal and vertical axis through the centroid, A is the cross-sectional area, and L is the length of a longeron. The cross-sectional area was predetermined by the amount of space that was left between the cabin wall and the outer skin. Since I_{zz_f} is a function of the number of longerons, the σ_{max} was set equal to $\sigma_{critical}$ to determine the minimum number of longerons that will be needed. This resulted in 76 longerons that each have a circular cross-section of radius 0.09 *in*. This internal fuselage structure yields a total deflection of less than 2 feet in the full fuel touchdown case and less than 1 foot in the +3G and -1G vertical load cases. Even in the most extreme case, the fuselage achieves a factor safety of 1.75.

5.5 Landing Gear

5.5.1 Landing Gear Placement

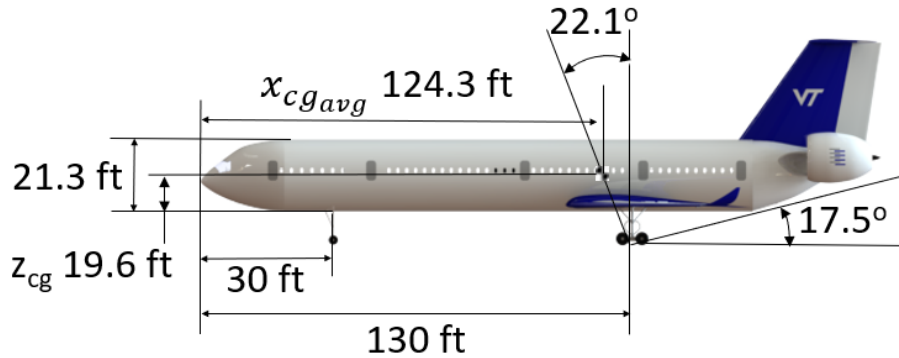


Figure 27: Longitudinal position of landing gear

The position of the landing gear (supplied by Safran Landing Systems) in the longitudinal direction is influenced by the tip-back angle. According to Nicolai, this angle is determined by rotating the aircraft to an angle of attack that would produce 90% of the $C_{L_{max}}$ [9]. Since only 72% of the $C_{L_{max}}$ is necessary for rotate at takeoff and landing, the extra 18% takes into account for pilot overshoot. As shown in Figure 27, 17.5° angle of attack approximately give 90% of the $C_{L_{max}}$.

Placement of landing gear in the lateral direction was driven by the requirement of a minimum radius of $0.54h_{cg}$ from the center of gravity, where h_{cg} is the height from the ground to center of gravity. The lateral direction placement estimate, which is based on derivations by Dr. William Mason [16], evaluates to 9.8 ft. This minimum was sufficiently met as the wing structure and landing gear height forced the gear to be placed at 13.7 ft.

5.5.2 Landing Gear Loads and Tire Selection

Another reason Exo is capable of operating at smaller airports is because it meets most runway requirements that restrict the maximum tire pressure on the pavement. Exo complies with the PCN Y, which allows a maximum tire pressure of 181 psi; this is enough to operate even at most regional airports. To comply with this classification, the main landing gear utilizes a total of 8 wheels, while the nose utilizes 2.

Then the pavement contact area is calculated using the following equation:

$$A_p = 2.3\left(\frac{d}{2} - R_{roll}\right)\sqrt{wd} \quad (13)$$

where d is the diameter, R_{roll} is the rolling radius, and w is the width of the wheel. Dividing the load of each wheel and the pavement contact area determines the maximum wheel pressure.

As a result, the main landing gear uses the Michelin 49x17 461B-2688-TL for a maximum tire pressure of 152 *psi* and the nose landing gear uses the Michelin 36x11 461B-3383-TL for a maximum tire pressure of 108 *psi*, maintaining well below the requirement of PCN Y. Another reason these tires were chosen was for their excellent compliance to operate on both rigid and flexible pavement, allowing for aircraft operation on asphalt or concrete, per the RFP. Also, the nose wheels utilizes chine tread in order to deflect water towards the side and away from the engines.

6 Weight Summary

The weight statement, featured in Table 14, details the respective weights and locations of each component validating the location of the CG. This table displays system, cargo, airframe structure, propulsion and cabin weights. These results yield a wet CG location of 125 *ft* and dry of 123.6 *ft*.

Table 14: Weight and CG Verification.

	CG Location	Wet	125.0
		Dry	123.6
Object	# Objects	Mass (lb)	X Location (ft)
Systems		25,693	142.9
Surface Controls/Pneumatics/Hydraulics	1	4,819	154
Instrument Weight	1	525	10
Electrical Systems	1	3,500	119
Fuel System (Dry)	1	1,001	126
ECS (Air Conditioning)	1	6,157	165
Engine Control	1	79	193
Starting Systems	1	233	193
Battery	2	881	170
Avionics	1	1,840	10
Water/Waste	1	4,392	163
Oxygen (pilots)	1	30	10
APU	1	1,355	201
Cargo		14,834	131.9
LD3	14	181	93
Cargo	410	30	140
Airframe Structure		94,037	119.5
Wing	1	44,821	130
Fuselage	1	32,473	93
Htail	1	1,763	193
Vtail	1	3,549	180
Landing Gear (nose)	1	1,100	40
Landing Gear (main)	1	9,896	130
Propulsion		172,900	140.9
Engine	2	18,640	195
Fuel	1	112,683	126
Cabin		96,262	97.2
Business Seats	50	242	30
Economy Seats: Section 1	138	219	74
Economy Seats: Section 2	120	219	116
Economy Seats: Section 3	94	219	147
Lavatory 1	2	198	13
Lavatory 2	2	198	42
Lavatory 3	2	198	93
Lavatory 4	2	198	158
Galley 1 + Food	2	1,119	44
Galley 1 + Food	2	1,119	160
Potable Water Tank 1	1	507	44
Potable Water Tank 2	1	507	160

7 Stability and Control

7.1 Horizontal Stabilizer

The horizontal stabilizer has to support sufficient center of gravity travel and avoid deep stall due to the T-tail orientation. The final parameters are denoted in Table 15.

Table 15: Final horizontal stabilizer parameters.

Parameter	Horizontal Tail
Airfoil	NACA0010
Incidence	1 °
Dihedral	3 °
Aspect Ratio	3
Root Chord, ft	16
Tip Chord, ft	8
Span, ft	36
Sweep	35 °
Moment Arm, ft	68.7
Volume Ratio	0.887

The first step in sizing the horizontal tail was to consider historical values of aircraft with similar wing sizes shown in Table 16.

Table 16: Historical horizontal stabilizer parameters [11]

Aircraft	Wing Area, ft ²	Horizontal Tail Area/Wing Area	Tail Volume Ratio
Boeing 757-200	1951	0.299	1.15
A300-B4	2799	0.267	1.12
A310	2357	0.292	1.09
TU-154	2169	0.201	0.71

These values show that for an aircraft of this size, typical area and volume ratios are 0.2-0.3 and 0.7-1.15.

Where the horizontal tail volume ratio is as follows,

$$\bar{V}_V = \frac{S_H l_h}{S_W \bar{c}} \quad (14)$$

Given these bounds, Digital DATCOM was used to determine stability derivatives. These values produced the following scissor plot in Figure 28. A scissor plot shows the controllable and stable regions of operation based on the horizontal tail area ratio.

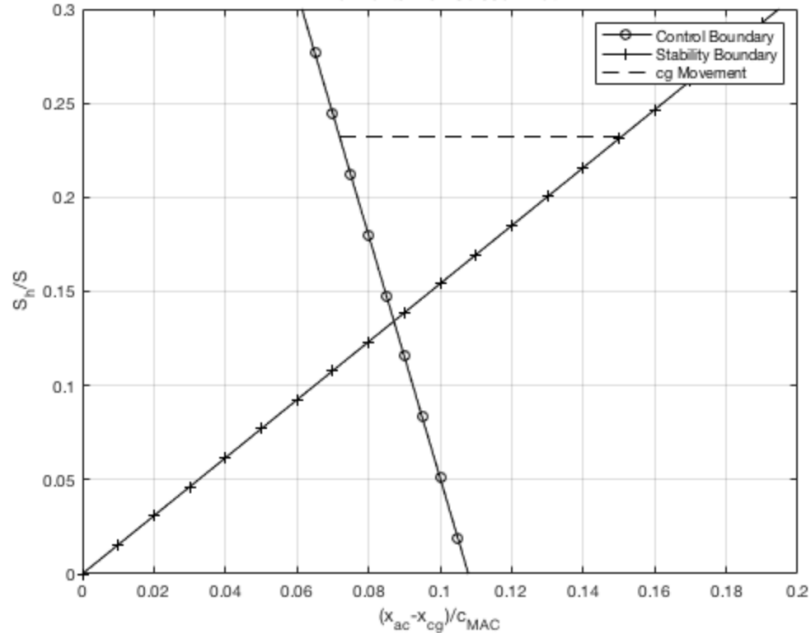


Figure 28: Horizontal stabilizer scissor plot showing controllable and stable center of gravity movement

For commercial aircraft of this size, Roskam[17] suggests a minimum static margin of 10% and operational static margin of 15% to 25%. Given the mean aerodynamic chord of 16.15 *ft*, this requires a 1.61 *ft* shift in center of gravity. These values were calculated using an aerodynamic center at 127.3 *ft*. Using these requirements, the historical data and the scissor plot constraints, a area ratio of 0.23 was selected. The scissor plots shows this ratio allows for a 1.30 *ft* movement in the center of gravity and stable aircraft performance, however, when validated with Digital DATCOM and VSPAero, it was found that the aircraft is stable between static margins of 10% and 30%. While these limits will not be reached in commercial flight, during maintenance missions the aircraft will remain stable with a center of gravity range from 122.9 *ft* to 125.5 *ft*. This allows the aircraft to be stable and controllable in all levels of fuel loading.

This area ratio yields a volume ratio of 0.887. While this is lower than most aircraft this size, T-tails have 30-50% lower downwash slope than the low-tail configuration typically used in commercial airliners [18]. This allows the horizontal stabilizer to have a smaller area without sacrificing effectiveness.

The next parameter to select is the incidence angle of the horizontal tail. The advantage of the T-Tail is that the horizontal stabilizer is out of the wing wake, wing downwash, wing vortices, and engine exit flow at low values of alpha [11]. The biggest concern for this tail is the possibility of deep stall. Deep stall is when the aircraft is at a stall angle much higher than predicted and the horizontal tail is ineffective as shown in Figure 29.

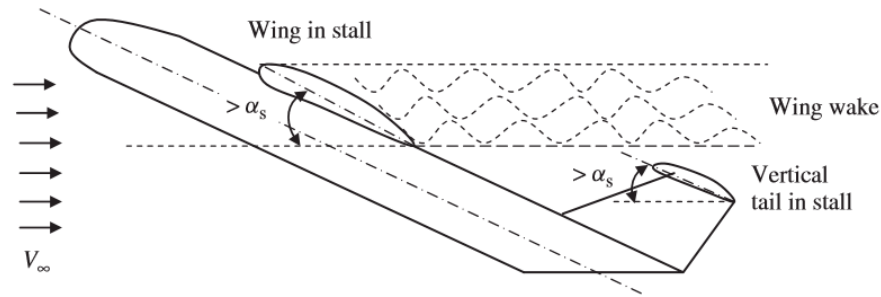


Figure 29: Aircraft experiencing deep stall [11]

To prevent it from occurring, the elevators must be able to fold down at a large angle and the tail must have a stable pitch down at high angles of attack. To satisfy these conditions an incidence angle of 1° was selected. Similar to the incidence angle, most important quality for this selection is stall characteristics. To satisfy these requirements the NACA 0010 was selected which has a stall angle of 22° . Using the equation below, during takeoff, the horizontal tail experiences an angle of attack of 7.72° .

$$\alpha_t = \alpha \left(1 - \frac{\partial \epsilon}{\partial \alpha}\right) - \epsilon_0 - i_t \quad (15)$$

Where $\partial \epsilon / \partial \alpha$ is the derivative of downwash angle, α is the aircraft angle of attack, ϵ_0 is the downwash angle at 0° and i_t is the incidence angle of the tail. Therefore, the stall angle of the airfoil needed to be significantly larger than 7.72° . Since aircraft has a stall angle of 19° , the NACA 0010 works very well as its stall angle is larger. The combination of this airfoil and the incidence angle allows for the best defense against deep stall. These results were iterated through Digital DATCOM, VSPAero and hand calculations to enhance stability and control and reduce the weight of the structure.

7.2 Vertical Stabilizer

The primary function of the vertical stabilizer is to supply the necessary directional stability, trim and control functions as well as support the weight and forces of the T-Tail. The final parameters are listed in Table 17.

Table 17: Final stable and controllable vertical tail features.

Parameter	Vertical Tail
Airfoil	NACA0010
Aspect Ratio	0.95
Root Chord, ft	40
Tip Chord, ft	22
Span, ft	32
Sweep	30 °
Moment Arm, ft	55.7
Volume Ratio	0.127

Similar to the horizontal tail, the first step for sizing this component was to look at historical values to get an understanding of the design space. Table 18 shows that typical aircraft have a vertical tail volume ratio of 0.02-0.12 [11].

Table 18: Historical vertical tail volume ratios [11]

Aircraft	Wing Area, ft^2	Tail Volume Ratio
Boeing 757-200	1951	0.086
A300-B4	2799	0.094
A310	2357	0.098
TU-154	2169	0.055

The tail volume ratio creates a trade-off between vertical tail area and moment arm as seen in the equation below.

$$\bar{V}_v = \frac{l_v S_v}{Sb} \quad (16)$$

Where l_v is the moment arm, S_v is the tail area, S is the wing area and b is the span. The airfoil for this component was chosen based on generating the required lift coefficient with a low drag coefficient and large $C_{L\alpha}$ as the static directional stability derivative is a direct function of the lift slope. Given these requirements, the NACA 0010 was chosen as it is symmetrical in the xz direction, has a low drag coefficient and is thick enough to allow for extra structural support for the T-tail.

In determining the aspect ratio, there were several key considerations. First, a high aspect ratio increases the height of the vertical tail and to fit in Group 4 ADG, the aircraft must be less than 60 ft . A higher aspect ratio also increases the tail mass moment of inertia decreasing lateral and longitudinal stability. These factors must be balanced with directional stability as increasing the aspect ratio increases stability in

this direction. The aspect ratio process coincides with that of the sweep angle. Increasing the sweep angle decreases the height, but weakens the directional stability. Additionally, since the aircraft is flying at a very high subsonic speed. To reduce wave drag, the sweep angle was chosen to be similar to that of the wing [11]. To compromise this features, and maintain stability, parameters such as root chord, tip chord and span were iterated in Digital DATCOM to ensure lateral stability derivatives met stability and control requirements.

7.3 Control Surfaces

The control surfaces were sized with the intent of providing level 1 Cooper-Harper handling qualities and FAR requirements as seen in Table 19 as well as physical constraints of the aircraft.

Table 19: Control surface requirements

Surface	Requirement	Source
Aileron	Perform controlled 20-degree banked in steady flight	14 CFR § 25.147
Rudder	Stable during engine out and 25 knot cross wind landing	14 CFR § 25.147
Elevator	Maintain longitudinal trim and takeoff rotation requirements	14 CFR § 25.161, 14 CFR § 25.145

7.3.1 Ailerons

The primary function of the aileron is to control the roll performance of the aircraft. The major constraints to the design are aileron stall, the location of the wing rear spar and adverse yaw. To avoid aileron stall, flow separation and loss of roll control, the maximum aileron deflection in either direction is 25° [11]. The aileron is also sized to be 25% of the chord to prevent any interference with the rear wing spar. This constraint limits the aileron effectiveness parameter to 0.42 [11]. The remainder of the aileron features were sized according to the adverse yaw induced by a 20-degree banked turn in steady flight. The first step of this process is to define the roll control derivative using the following equation,

$$C_{l\delta A} = \frac{2C_{L\alpha w}\tau}{Sb} \int_{y_i}^{y_o} cy dy \quad (17)$$

Where τ is the aileron effectiveness parameter, y_o is the outer aileron span, y_i is the inner aileron span and c is the chord. The roll control derivative is then used to calculate the roll rate, \dot{P} . The roll rate is then used

to determine how long it takes to perform a 20-degree turn using the following equation,

$$t_2 = \sqrt{\frac{2\phi_{des}}{\dot{P}}} \quad (18)$$

Here, t_2 is the time it takes to perform the turn and ϕ_{des} is the desired bank angle. Using an iterative in-house MATLAB code, the final aileron parameters were finalized to the values in Table 20.

Table 20: Final compliant aileron parameters

c_A/c_W	$\pm \delta_{A_{MAX}}$	Inner Span/Wing Span	Outer Span/Wing Span
0.25	25 °	0.7	0.92

7.3.2 Rudder

The rudder is responsible for directional control. When the rudder is rotated, it creates a yawing moment, lift force and roll moment. The rudder helps in four main events: asymmetric thrust, crosswind landing, a coordinated turn and adverse yaw. The rudder was sized to address all of these behaviors. All scenarios require an sufficient roll control derivative, $C_{N\delta r}$.

$$C_{N\delta r} = -C_{L\alpha V} \bar{V}_v \eta_V \tau_r \frac{b_R}{b_V} \quad (19)$$

Where \bar{V}_v is the vertical tail volume ratio, η_V is the vertical tail efficiency constant and τ_r is the rudder effectiveness constant. The two predominate cases for this aircraft are cross-wind landings and asymmetric thrust. To satisfy the cross-wind landing requirement, the rudder has to be capable of withstanding the aerodynamic side force and yawing moment caused by the wind. In order to support asymmetric thrust, the rudder deflection must satisfy the following,

$$\delta_R = \frac{T_L y_T}{-\bar{q} S b C_{N\delta R}} \quad (20)$$

Where y_T is the y -coordinate of the engine from the center of gravity, T_L is the thrust of one engine and \bar{q} is the dynamic pressure. With the use of Mathematica and MATLAB, the design meets all scenarios with final parameters shown in Table 21.

Table 21: Final compliant rudder parameters

c_A/c_W	$+/- \delta_{RMAX}$	b_R/b_V
0.3	20 °	1

7.3.3 Elevators

The elevator works to maintain longitudinal control and trim. The most critical phase of flight for pitch control is flying at low speeds such as takeoff. Because of this hazard, the elevators have a take-off rotation requirement. For commercial aircraft, the aircraft is allowed 1-3 seconds of rotation time during takeoff and a takeoff pitch angular acceleration of 8-10 $\frac{deg}{s^2}$ [11]. For a factor of safety, the elevator is sized to accelerate at the stall speed instead of the takeoff speed. This requirement dictates the maximum upward deflection, $-\delta_E$, of the aircraft. The horizontal tail must be able to produce the required lift during takeoff. The elevator helps provide this extra lift as seen in the following,

$$C_{Lh} = C_{L\alpha h}(\alpha_h + \tau_e \delta_e) \quad (21)$$

Here, α_h represents the angle of attack for the horizontal tail, τ_e is the elevator effectiveness parameter which is a direct function of the chord of the component and δ_e is the downward deflection of the elevator.

The maximum downward deflection, δ_E , is determined by the longitudinal trim requirement. Longitudinal trim signifies when all forces and moments are in equilibrium. This angle was calculated using the following equation

$$\delta_e = \begin{vmatrix} C_{L\alpha} & C_{L\delta_e} \\ C_{m\alpha} & C_{m\delta_e} \end{vmatrix}^{-1} \begin{vmatrix} C_{L\alpha} & C_{L_1} - C_{L_0} \\ C_{m\alpha} & -Tz_T/(\bar{q}S\bar{c}) - C_{m_0} \end{vmatrix} \quad (22)$$

Here, z_T is the z -coordinate of the engines from the center of gravity and C_{L_1} is the steady state lift coefficient during cruise.

The elevator was also sized to assure maximum deflection of the control surface would not significantly reduce the tail stall angle. All of these requirements are dependant on the physical features of the elevator. With the use of Digital DATCOM and team-made MATLAB scripts, the elevator parameters were finalized as listed in Table 22. The hinges for all control surfaces are located at their respective chord ratios.

Table 22: Final compliant elevator parameters

c_E/c_H	b_E/b_H	$-\delta_{EMAX}$	δ_{EMAX}
0.3	1	-20°	25.4°

7.4 Static and Dynamic Stability

Exo is statically and dynamically stable both in the longitudinal and lateral directions during all stages of flight. The control system is compatible with Level 1 Flying standards according to the Cooper-Harper Pilot Opinion Rating Scale, meaning pilot compensation is not a factor for desired performance. Table 23 shows Exo's compliance with these standards providing the pilot and passengers with a safe and enjoyable flying experience. Here, ζ represents the damping ratio, ω the natural frequency, t_{half} the time to half amplitude and τ is the time constant.

Table 23: Cruise flight characteristics showing compliance with level 1 flying qualities

Mode	Requirement	Exo
Short Period	$0.3 < \zeta_{SP} < 2.0$	0.392
Phugoid	$\zeta_p > 0.04$	0.108
Spiral	$t_{half} > 20$	29.61 seconds
Roll	$\tau_R < 1.4$	0.825
Dutch	$\zeta_D > 0.08$ $\zeta_D \omega_D > 0.15$ $\omega_D > 0.4$	1 1.213 1.213

Table 24: Static stability characteristics

Stability Derivative	Value
$C_{N\beta}$	0.006 /radian
C_{M_0}	0.588
$C_{M\alpha}$	-0.103 /radian
$C_{L\beta}$	-0.24 /radian

In order to be statically stable, there are four stability derivative requirements that must be met. First, the aircraft must have a positive pitching moment at a zero angle of attack to provide balanced flight.

The next three requirements dictate that moments must restore the course of the aircraft in each direction. Laterally, the pitching moment must decrease as the angle of attack increases positively. Directionally, Exo must have a positive yaw moment with respect to sideslip angle to restore the course. Finally, longitudinally, there must be a negative change in lift with respect to sideslip. With the use of Digital DATCOM, Table 24 details the compliant stability derivatives.

As stated previously, Exo performs exceptionally well in dynamic stability as the eigenvalues of the state matrix have negative real parts in both takeoff and cruise as shown in Figure 30. It is important to note that the aircraft is stable during both takeoff and cruise.

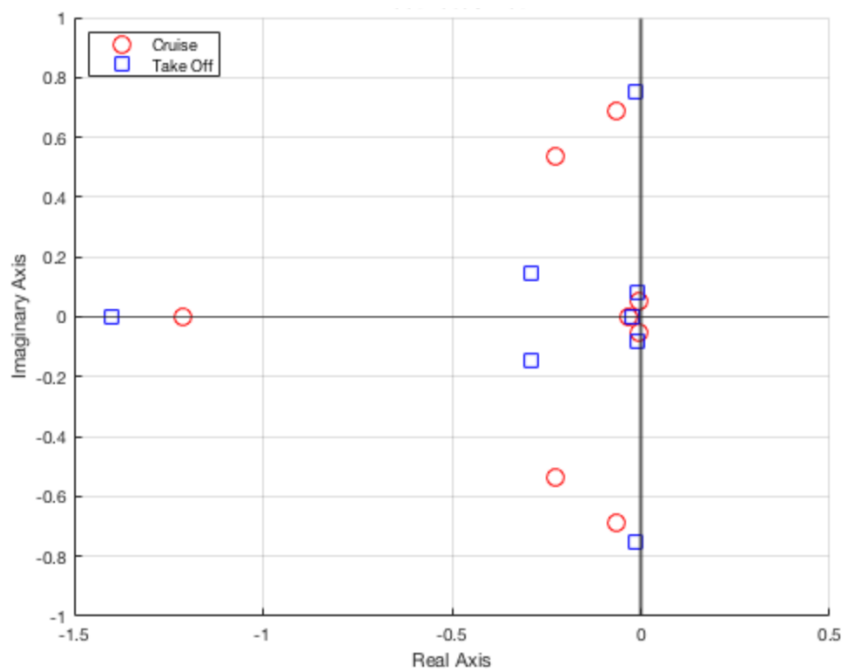
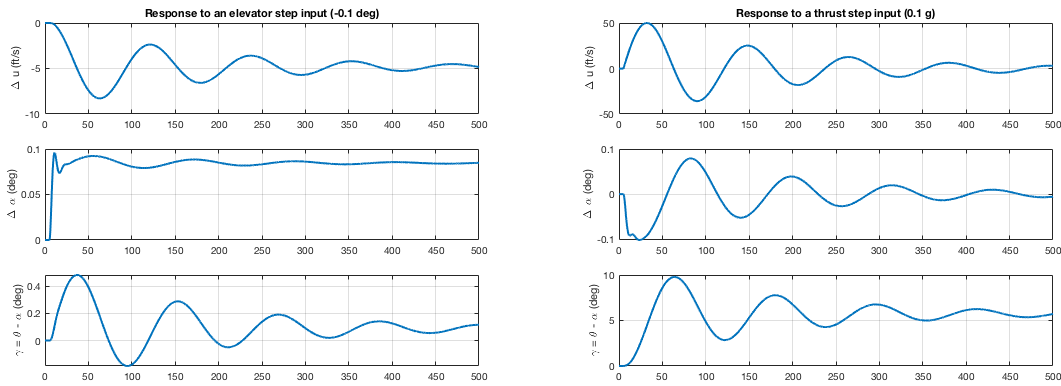
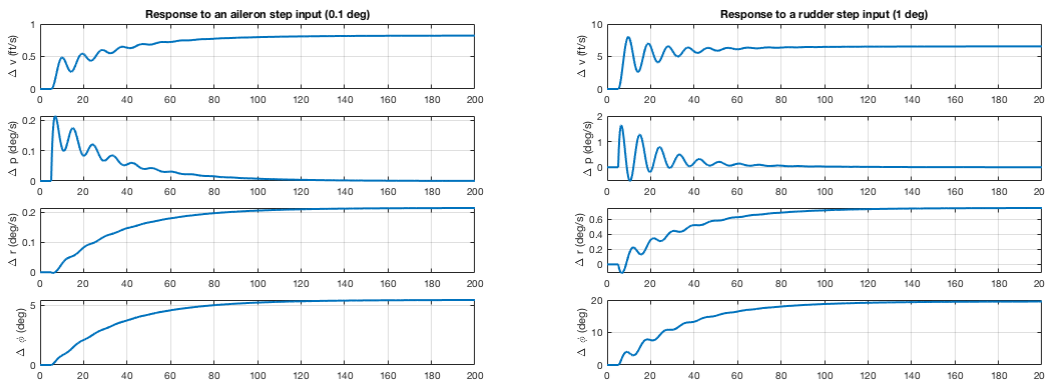


Figure 30: Root locus plot showing negative real parts for both cruise and takeoff

Therefore, when the system is perturbed in the longitudinal and lateral direction, the aircraft converges to equilibrium promptly and efficiently. Figure 31 shows Exo's long-term behavior to adjustments experienced during flight. The high caliber stability and controllability of this aircraft is a result of the properly sized empennage and control surfaces.



(a) Longitudinal linear velocity returns to equilibrium value and angle of attack and pitch angle reach new equilibrium in response to elevator input (b) Longitudinal linear velocity, angle of attack and flight path angle all return to original equilibrium after step thrust input



(c) Lateral linear velocity, roll angle and directional angular velocity converge to new values where longitudinal angular velocity returns to original value after aileron input (d) A rudder step input maintains longitudinal angular velocity, but changes linear velocity, roll angle and directional angular velocity

Figure 31: Dynamically stable Exo response to step perturbations

8 Propulsion System

8.1 Engine Selection

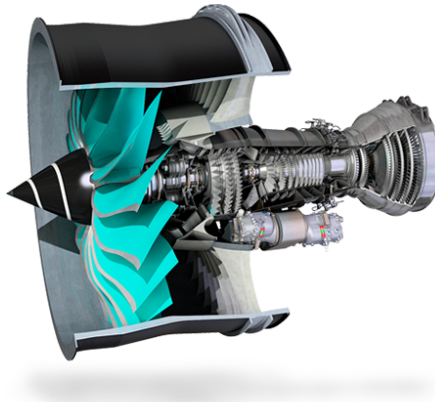


Figure 32: Trent UltraFan. Photo courtesy of Rolls-Royce.

The Exo, is designed to employ the Trent Ultrafan which is shown in Figure 32. The UltraFan best meets the requirements and selection criteria. The ultra-high bypass geared turbofan engine, features approximately 115,000 pounds of thrust, a very low SFC, low noise level, and low emissions. Table 25, lists key parameters of the Trent UltraFan engine. In order to obtain missing or incomplete data, Nicolai's methods for engine scaling were used for various parameters for the UltraFan [9]. Given the known data of the UltraFan [19] and other similar engines such as the Trent XWB-97 [20] [21], estimations can be made for mass flow rate, weight, diameter, length, and thrust. Similarly, the predecessor of the Ultrfan, the XWB-97, gives

estimations on SFC and noise based on Rolls-Royce quotes on UltraFan performance. For example, the UltraFan has a 25% improvement in fuel burn and noise reduction of a large twin-engine aircraft by 15 dB,

Table 25: Trent UltraFan parameters.

Merit	Trent UltraFan
Thrust (lbs)	115,000
Unit Cost (\$, USD)	\$40,700,000
Length (ft)	22.5
Fan Diameter (ft)	11.6
Weight (lbs)	18,600
Emissions (SN)	2.77
SFC (lb/(lb ² hr))	0.357
Noise level (EPNL)	94
Mass Flow Rate (lbs/s)	4470
Bypass Ratio	15
Overall Pressure Ratio	70

making its noise equivalent to a Learjet 45 [22] [23] [24]. Refer to Section 8.3 below for more Noise and Emissions Estimates.

In Figure 33, the Trent UltraFan’s thrust variation with altitude is depicted for two engines. Also on the plot, is the typical cruise drag Exo will encounter (35,000 feet at 2 degrees angle of attack). At 35,000 feet, the UltraFan engines only need to operate at approximately 68% of their design thrust to meet cruise thrust requirements. At 68% design thrust, historically large turbofan engines will see a 5% rise in sfc as seen in Figure 34 [28]. Despite this small increase in SFC, the Trent UltraFan is still more efficient than the other top 4 engines considered by a margin of as little as 38% (see Table 35 in the Appendix for SFC values of the other top 4 engines considered).

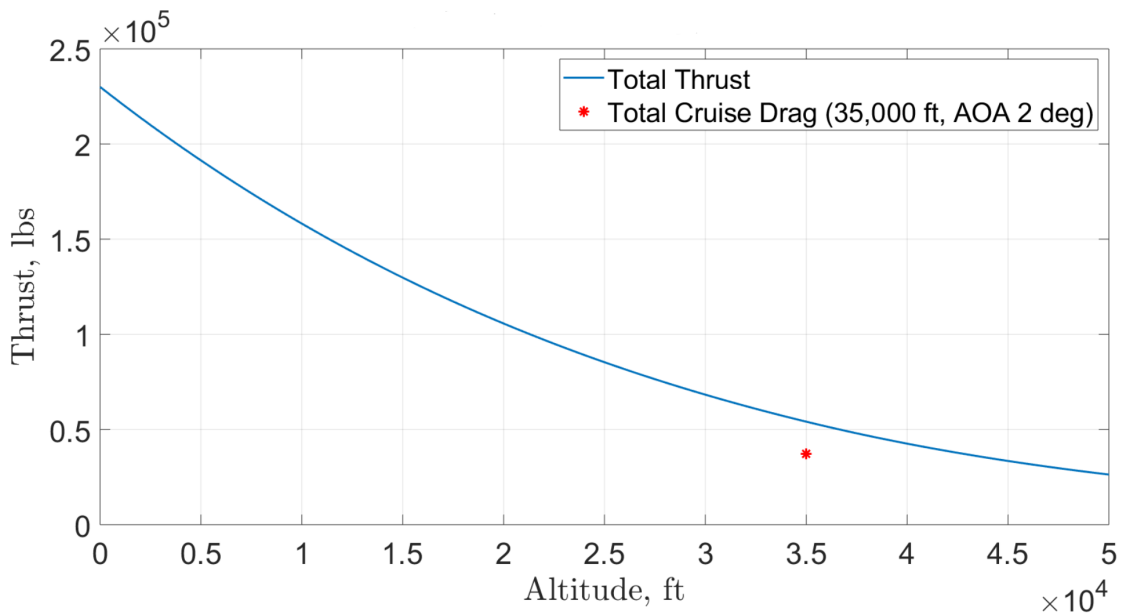


Figure 33: Trent UltraFan thrust variation with altitude

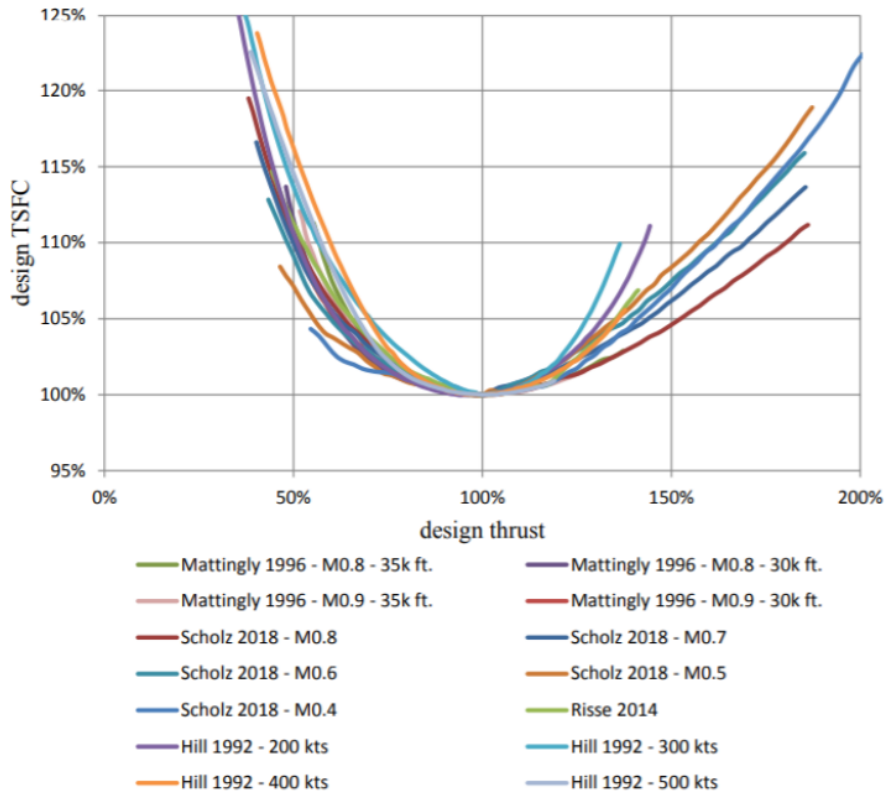


Figure 34: Historical trend of SFC Variation with respect to design thrust [28]

More than 40 different turbofan engines were analyzed and compared using a decision matrix. The criteria for evaluation in the down selection process, ranked by weight are: SFC (35%), weight (25%), unit cost (20%), fan diameter (10%), and emissions (10%). Nicolai’s methods for engine scaling were used for estimation [9]. Note that hybrid-electric propulsion systems were removed from consideration early in the design process due to low TRL levels presented by the hybrid-electric systems. Refer to Table 35 in the Appendix to see the decision matrix with the top five propulsion systems considered.

8.2 Boundary Layer Ingestion

8.2.1 Boundary Layer Ingestion Performance Benefits and Risk Mitigation

BLI is a propulsion concept in which a large fraction of the vehicle boundary layer is ingested by the propulsion system and reaccelerated instead of turning into wake. Research has shown that BLI increases propulsive efficiency due to decreased jet mixing losses, a decrease in nacelle and pylon wetted area losses, decrease in wake mixing losses due to wake ingestion, decrease fan efficiency due to inlet distortion, and

changes in airframe performance because of propulsor-airframe interaction [29].

BLI can provide decreases in fuel burn through reducing the propulsor power requirement [29] [5]. In a study of the D8 "Double-Bubble" aircraft computational and experimental results of BLI yielded an 8.7% reduction in propulsor mechanical flow power, with 60% of the benefit coming from reduced jet dissipation and 40% coming from the reduced airframe dissipation [29]. The research determined it was found that increasing the ingestion fraction, or the percentage of the boundary layer that is ingested, monotonically decreases the required mechanical flow power. Additionally, through a parametric analysis, it was found that increasing the nozzle area to increase the propulsor mass flow and propulsive efficiency yields an even larger power savings with BLI (10.3% reduction in power requirement) [29]. Through using a larger diameter engine, like the Trent UltraFan, Exo can expect such performance benefits. Ultimately, these power requirement savings lead to decreases in engine fuel burn and conversely cost savings for the customer.

A key issue surrounding BLI is the inlet distortion and how it affects the engine performance and mechanics. Research suggests inlet distortion representative of BLI leads to decreases in fan efficiency of 0.5-5% depending on fan design and the type of distortion [29]. However, the stagnation pressure distortion attenuation through the propulsor is a difference more than an order of magnitude lower than the 5-7% BLI benefit achieved. Thus, propulsor distortion attenuation has little effect on the BLI benefit [29]. Another key issue is that there may be additional mechanical loads on the fan when implementing BLI. The non-uniformity of the flow may excite cyclic stresses within the fan system. This risk can be mitigated by mixing the flow before it reaches the engine face or developing a fan capable of operating in a non-uniform environment [5].

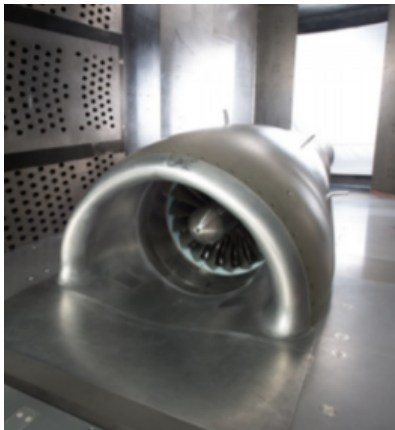


Figure 35: BLI2DTF rig installed in NASA Glenn wind tunnel [30]

Exo leverages the BLI2DTF effort sponsored by the NASA Advanced Air Transport Technology Project, shown in Figure 35. This BLI2DTF demonstrated the ability to perform in a highly non-uniform distorted inlet flow field caused by BLI. The fan provided acceptable performance while meeting the mechanical challenges inherent in this type of system through managing high incidence angle fluctuations and high total pressure distortion levels [30]. This distortion tolerant fan was designed, fabricated, and successfully tested at NASA Glenn, showing a significant stability margin for the application as seen in Figure 36.

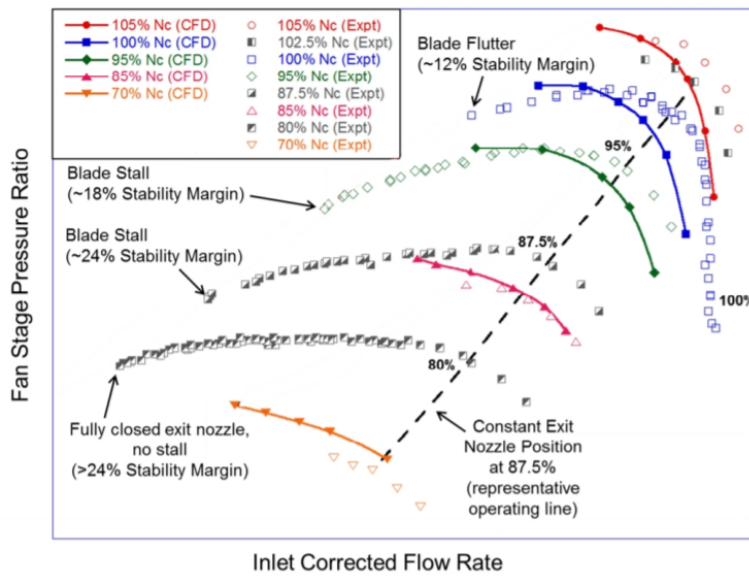


Figure 36: Preliminary fan stage map showing the approximate achievement in stability margin [30]

8.2.2 CFD Boundary Layer Ingestion Validation

To validate the use of BLI on Exo, a Reynolds Average Navier Stokes based CFD model was implemented to ensure feasibility of the propulsion concept. The center of the UltraFan inlet is 11 *ft* outboard and 5.4 *ft* vertically with respect to the mid-planes of the fuselage. The inlet is located 182.5 *ft* aft of the nose. The following assumptions were made for the CFD model: engine inlet velocity boundary condition will not affect flow in front of nozzle, pressure build up from engine nacelle will not largely affect results, and only flow forward of the inlet is valid for analysis. The conditions for the simulations are listed in Table 26.

Table 26: Key parameters in CFD simulation

Parameter	Value
Mach	0.82
T_{∞}	219 K°
P_{∞}	23.79KPa
Turbulence Model	K-Omega SST
Transition Model	Gamma
Time	Implicit Unsteady
Flow	Coupled Flow
Gas Model	Van der Waals
Angle of Attack	0°

The residuals associated with the K-Omega SST model converged showing sufficient convergence with each time-step, leveraging inner iterations for the solution. A mesh refinement study was completed showing minimal variation in results with mesh perturbations. Another analysis using Spalart Allmaras, a one-equation turbulence model, was run (under comparable assumptions) and showed similar results to the K-Omega SST model; this solution is not shown here.

Figure 37 shows streamlines of the flow at the empennage where BLI engines are located. Due to the nature of an implicit unsteady computation and its variation over time, the result is shown at a specific point in time. There is some distortion visible in the streamlines, hence the need for the distortion tolerant fan. This distortion is generated due to the adverse pressure gradient occurring on the tapered portion of the fuselage as seen in Figure 38a, which shows the velocity profile at the engine midpoint. This pressure gradient can be eliminated by reducing the abruptness of the taper to the engine inlet. Looking closer at the velocity profile just forward of the engine inlet, visible in Figure 38b, it can be seen that approximately 40% of the ingested air is from the boundary layer produced by the fuselage, with the remaining portion being clean air. An improved empennage tapering would further increase the velocity intake outboard of the empennage. Due to the similarity between the D8 and Exo, it can reasonably be expected to yield similar performance benefits with BLI given Exo ingests the same amount of clean air and boundary layer as the D8. Through use of CFD, it was verified that the engine ingests approximately 40% fuselage boundary layer and 60% clean air. More extensive analysis and testing will be performed in the detailed design phase of the project.

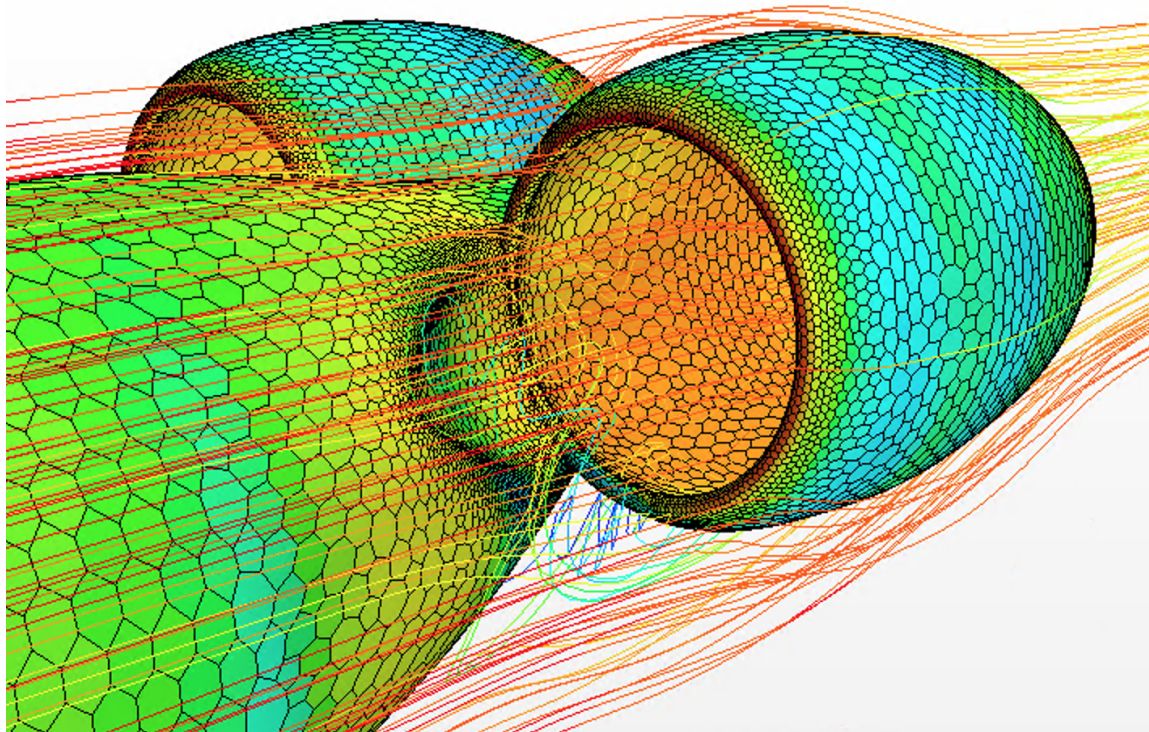
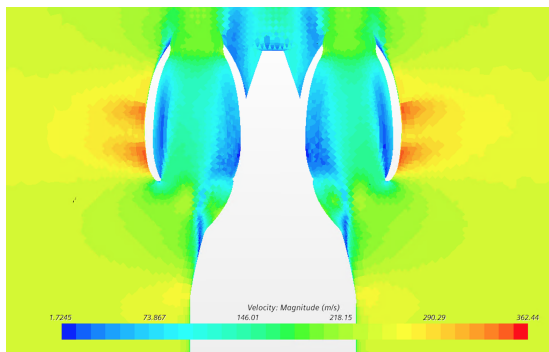
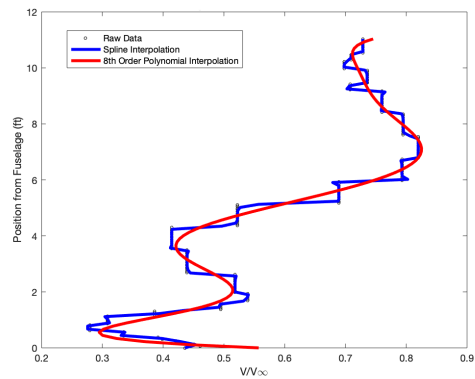


Figure 37: 3D view of streamlines flowing near engine inlet in the BLI region



(a) Scalar velocity field around engine in a 2D plane, showing adverse pressure gradient and near freestream flow entering engine



(b) Velocity profile at probe located in front of engine

Figure 38: Scalar velocity field and velocity profiles of engine

8.3 Noise Estimation

For comparison, Table 27 displays comparator noise levels alongside Exo [24] [25] [26] [27]. Exo comes out to be the quietest aircraft amongst the three, despite being the second heaviest aircraft.

Table 27: Noise levels of exo and comparator aircraft

Aircraft	Mass (lbs)	Lateral EPNL		Flyover EPNL		Approach ENPL	
		Level	Limit	Level	Limit	Level	Limit
Exo	381,273	85.1	99.4	75.5	95.1	93.4	103.0
B777-300	660,000	97.3	101.9	94.4	99.6	99.9	105.0
A321neo	196,200	95.6	97.5	89.1	92.6	96.9	101.1

9 Cabin

Exo has an innovative and efficient cabin shown in Figure 39. New approaches on conventional solutions have led to significant improvements of passenger comfort as well as boarding time, while staying within current regulations to ensure an expedited certification process. A simulated walkthrough is available at: <https://youtu.be/Y8Emx08Axn8>

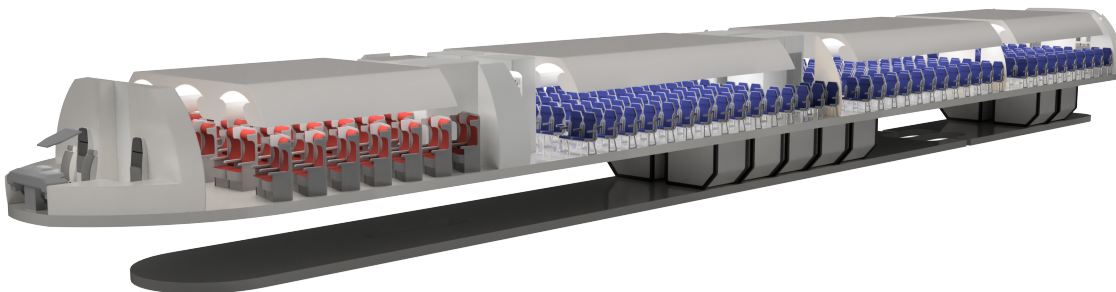


Figure 39: Exo's cockpit, cabin and cargo

9.1 Cockpit Layout

The flight deck of the aircraft, shown in Figure 40, is divided into three panels: the overhead panel, the main panel and the center pedestal. On these panels, all relevant indicators and controls are located in compliance with CFR §25.1301 to §25.1337 and the underlying systems meet the requirements §91.205. The overall layout is similar to current aircraft cockpits like the Airbus A350, which facilitates the transition from other aircraft to Exo. The modern glass cockpit consists of six LCD screens, on which the displayed information can be adapted to the individual needs of the pilot.

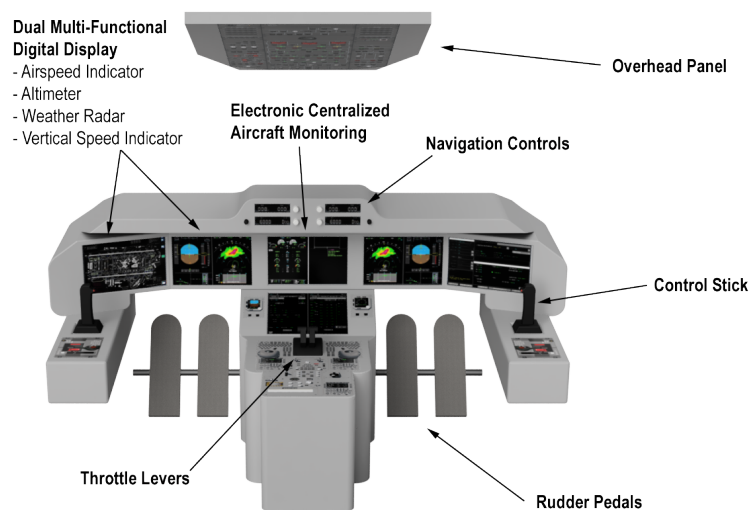


Figure 40: Cockpit layout

9.2 Passenger Layout

To reduce boarding time, we decided to utilize three aisles, displayed in Figure 41. This also increases passenger comfort throughout the flight as 83.5% of the seats are either aisle or window. Also the center aisle can be used by passengers during catering. Exo features a 2-3-3-2 economy and a 2-2-2-2 business class seat abreast configuration. Our state of the art, three aisle cabin layout offers 50 business class seats and 350 economy class seats. These seats are placed in a staggered manner, to reduce the interference between passengers while storing their luggage in the overhead compartments.

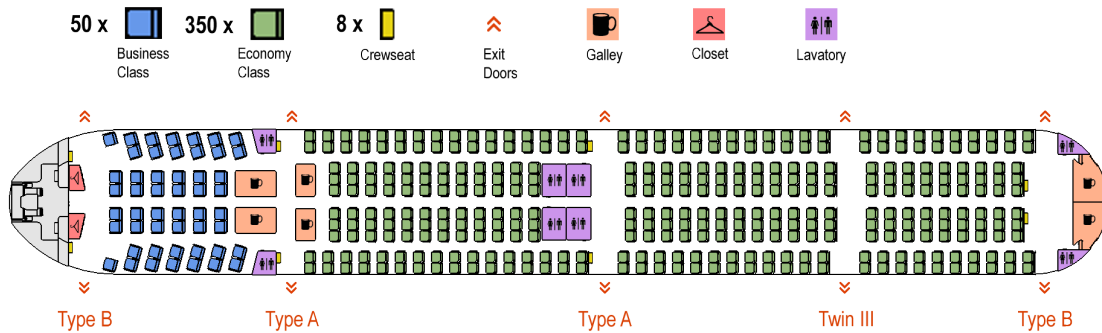


Figure 41: Cabin layout

The decision on the economy abreast was made utilizing the decision matrix shown in Table 28. With the exception of the first row in the business class we adjusted the business abreast according to the resulting cabin width. The boarding and evacuation process play an important role for the turn around time as well as safety regulations and is rated in respect to aisles per passenger per row as well as passengers distance to the door. The ratio of pay floor to total floor area, manufacturing cost and aerodynamic drag are economically relevant. Wider abreast configurations result in a wider but shorter fuselage as the same number of passengers fit in fewer rows and vice versa. The fuselage width and length affect the total floor, cross section and wetted fuselage areas. The 2-3-3-2 configuration turned out to have the smallest floor and wetted fuselage area, while the 2-2-2-2 shows the smallest cross section area. The attractiveness of seating relates to the percentage of seats at windows or aisles, while the overhead compartment volume per seat are driven by the cross section dimensions as well as passengers per row. Both of these effect the passenger comfort.

Table 28: Seat abreast decision matrix

Merit	Weight (%)	2-2-2-2	2-3-3-2	2-4-4-2
Boarding & Evacuation	30	2.7	2.7	2.1
Manufacturing cost	20	1.2	1.8	1
Aerodynamic Drag	20	1.4	1.2	0.8
Attractiveness of Seating	15	1.5	1.35	0.9
Used Floor Ratio	10	0.6	0.9	0.8
Overhead Compartment	5	0.4	0.35	0.2
Total Score	100	7.8	8.3	5.8

The seat width and pitch requirements stated by the RFP and the aisle and cross aisle width stated by the FAA are complied in this configuration. Further details can be seen in Figure 42 and Figure 43. For more privacy, lower cabin noise and to keep the emergency exits free, the seats are located in four sections, separated by section walls or other cabin monuments. The front section accommodates comfortable business class seats equipped with IFE and further amenities. Located in the other three sections are practical economy class seats with foldable tray tables to hold personal electronic devices while in cruise. Furthermore the front wall of each section holds two big flight information screens implemented in the front wall.

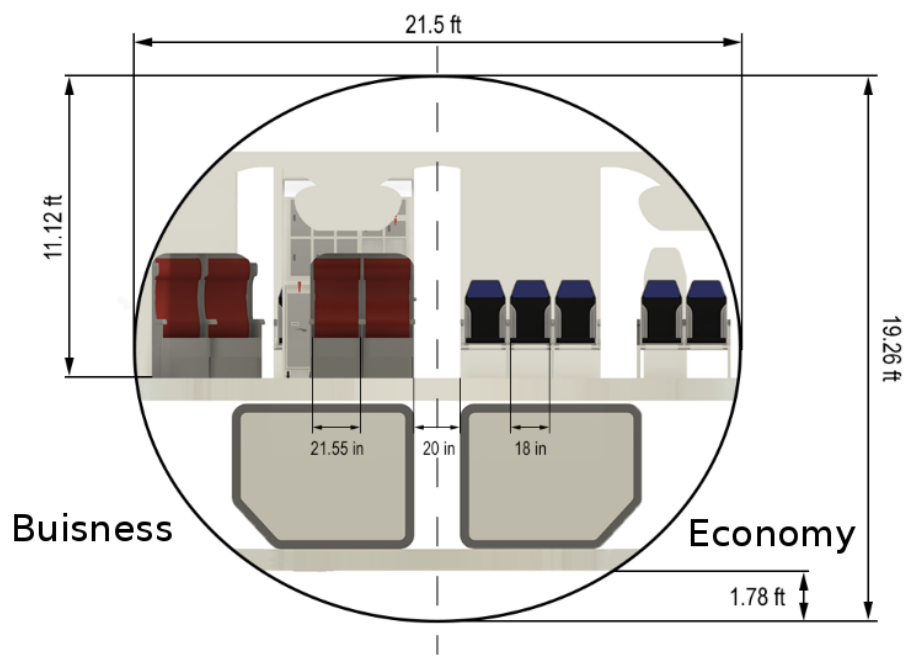


Figure 42: Exo cross-section (front view)

There are a total of ten emergency exits: four Type A doors, four Type B doors, and two Twin III doors. The position of each door is defined by its capacity, the number of passengers sitting between two doors and the maximum distance of 60 *ft* between two doors. Each Type A and B door require the assistance of a crew member in emergency situations, resulting in eight crew seats positioned in proximity to these doors. We meet FAA requirements by providing one crew member per 50 passengers. If additional crew members are required, more crew seats can be fitted in the aft section of the aircraft. With this configuration of doors, the aircraft can be certified for a maximum capacity of 435 passengers, giving it more flexibility for high density layouts of future aircraft family members. The front two doors support double jetways for faster boarding.

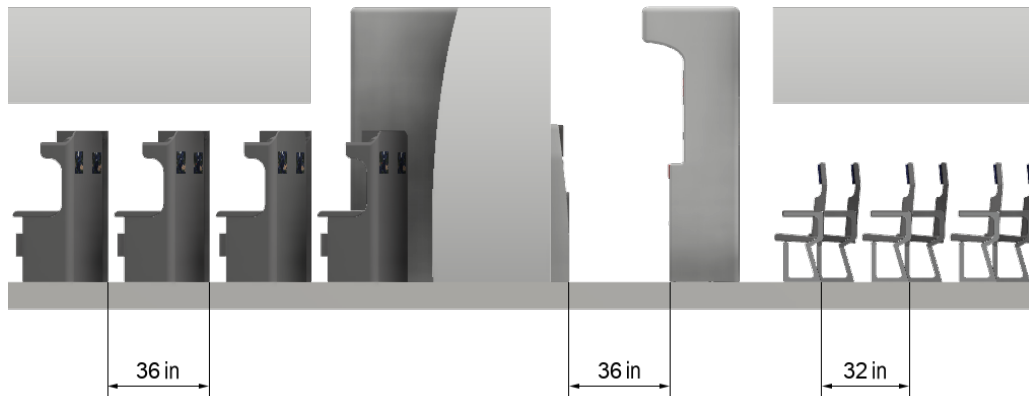


Figure 43: Seat pitch and cross aisle width

The amenities include galleys, lavatories and closets. Empirical values state, that for each 50 passengers one lavatory is required. With a total of 400 passengers, this relates to eight lavatories. Two of these are located behind the business class separating it from the economy class. Another four can be found at the end of the first economy section, the last two are in the rear of the aircraft. The galleys were sized using the PreSTo tool [34]. As a result, total galley space is 141.78 ft^2 . This results in a large galley in the aft section and two mid-sized galleys in the second section for the economy class and two mid-sized galleys in the first section for the business class. Furthermore, two medium closets are located in the front section of the business class to provide extra storage room for coats or other items. All cabin monuments are placed in consideration of the center of gravity of the aircraft to ensure the in-flight stability. The equivalent pressure altitude in cruise is $7,000 \text{ ft}$, reducing the time passengers need to adjust to changing flight phases to account for short haul flight duration.

9.3 Boarding Simulation

To validate the three aisle design, a boarding simulation was created using the program Anylogic. The simulation was based on the following key assumptions: passenger velocity of 4.5 ft/s , 65% of all passengers equipped with luggage, no boarding groups and boarding through the front door only. Further statistical values regarding stowage time, passenger assistance and behavior were obtained from Reference [35]. These values relate to the boarding statistics of all high capacity aircraft, such as Airbus A330-300 and A340-300. Each run of the simulation results to a slightly different boarding time. The average boarding time after 10 runs is approximately 27 minutes. A still frame of the simulation is shown in Figure 44.

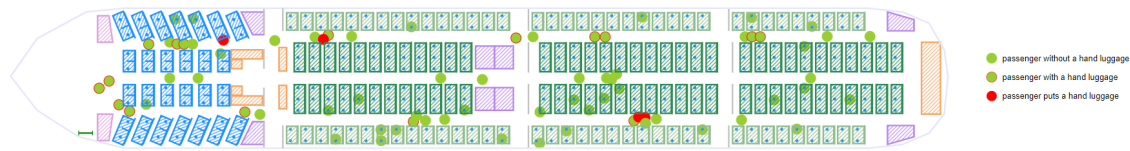


Figure 44: Boarding simulation time after 5 minutes

The density map in Figure 45, showing passengers per unit area, proves that all three aisles are used evenly and that none of them is overly congested. Red areas are expected since there is always a little congestion due to passengers stowing their hand luggage in the overhead compartments. Galley and lavatory areas show low congestion, so do the door zones and cross aisles. This means that the galley is wide enough to ensure a steady passenger flow, which is important in the case of an emergency evacuation. This simulation snapshot in time is taken at approximately 15 minutes into boarding.

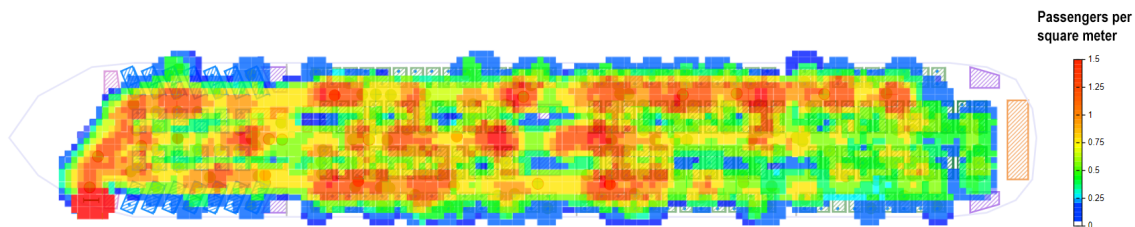


Figure 45: Boarding simulation passenger density after 15 minutes

9.4 Cargo

The aircraft holds 14 LD3 cargo containers in order to carry the required baggage, as shown in Figure 46. If the customer wishes to carry additional payload, Exo can offer up to 8 more LD3 containers as shown in green and an extra 1600ft^3 bulk cargo volume as shown orange. As the turn around time is also limited by the cargo loading time, standardized ULD containers will be used for cargo as these containers can easily be loaded and positioned in the cargo bay. As ULD type, LD3 containers were selected to store the required cargo, as these are the most common on current airplanes and also most fitting dimension without making the required cross section too elliptical. Weight wise only four LD3 containers would be needed, however the volume of the baggage requires a total of 14 LD3 containers. In order to fly the aircraft without much trim drag, the location of the containers are split up into a cargo bay in front and one behind the wing, reducing the resulting moment around CG.

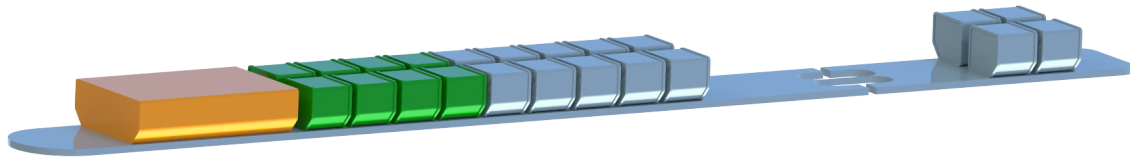


Figure 46: Cargo floor with 14 cargo containers

All containers are stored on the cargo floor located beneath the passenger floor, which also hold a majority of the aircraft’s systems as well as the landing gear when stored in flight. The cargo compartments are also pressurized and comply with 14 CFR §25.857 Class C. The deck of the cargo compartments are equipped with rollers and ball bearings to assist in moving the containers to their position. Loading and unloading is quick and easy through the two cargo doors on the right side of the aircraft displayed in Figure 47. The dimensions of a ULD door is 106 x 67 *in* and for a bulk door 36 x 45 *in*. For even shorter total turn around time one extra ULD door and one bulk freight door can be implemented. All cargo doors can easily be accessed by cargo loaders and dollies without interfering with passenger boarding on the opposite side of the aircraft and in safe distance from the high mounted engines at the tail and the low mounted wings. If the costumer decides on additional cargo and/or cargo doors the weight and balance in Section 6 will change slightly, but CG remains within bounds. Fuel and cargo positioning can be used to trim out the changes of CG.

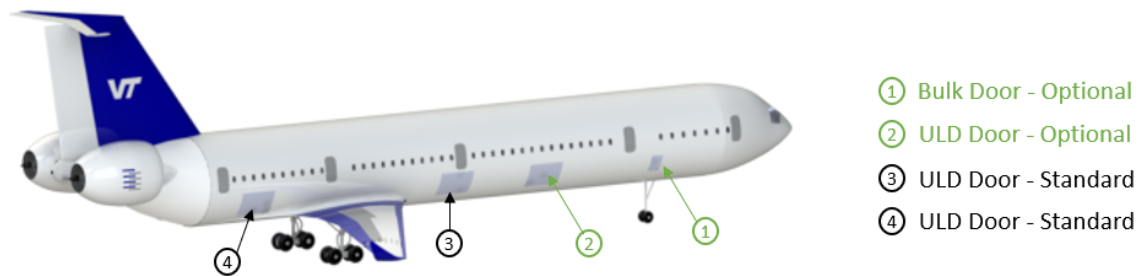


Figure 47: Side view of cargo doors

9.5 Optional Features

Exo offers the best solution for passenger comfort as well as flight performance in a cost efficient way. To fulfill each customer's specific needs, Over the Pond offers a range of options listed in Table 29 with their respective effect on the price and/or weight.

Table 29: Optional features

Feature	Standard	Variants	Difference
Cockpit	Single Pilot Ready	Dual Pilot	+\$150,000 annually
Flight Attendants	7 for Economy, 1 for Business	Up to 9 for Economy and 3 for Business	+\$74,000 annually/ flight attendant
Wi-Fi	Yes	No	-\$100,000 -190 lb
IFE Economy	Flight Information Displays	Per seat monitors	+\$10,000/seat
Lavatories	8	10	+200 lb/Lavatory
Galleys	2 big, 4 small	Up to 3 big, 6 small	+1200 lb/1 big and 2 small
Windows	Standard	Electronically Dimmable	+\$0.40/sq. ft.
Cargo	14 LD3	Extra LD3's and bulk cargo	+180.8 lb/LD3 tare weight

In the operational aspect the customer can select from two variants regarding the pilots and the crew. Due to the state of the art cockpit and Airbus ATTOL technology implemented on Exo, the aircraft is able to be flown by a single pilot. As regulations may still prevent a single pilot aircraft in 2029, the cockpit is also capable of a dual pilot configuration. Furthermore the number of flight attendants is tradable. Exo offers space for eight flight attendants, which is the minimum for the given reference mission according to 14 CFR §121.391 requirements. For customers with different needs, up to 4 additional crew seats can be installed. Regarding passenger comfort, five variants can be selected. Exo implements Wi-Fi on the aircraft as standard, but a customer may choose to forgo it to save cost and weight. For the IFE in the economy class, large display screens with flight information are implemented in the section walls. For an additional charge, monitors can be fitted in each individual seat. The number of galleys and lavatories is determined by empirical values, but can also be adapted to specific needs of the customer. The standard window shades can be replaced by electronically dimmable ones for an enhanced user experience. In the cargo section Exo has 14 LD3 containers as standard to fulfill the mission requirements. The forward cargo bay is enough space to fit eight more containers of this type and also a bulk compartment. To improve accessibility and loading

time, the two standard cargo doors can be extended by a third one of the same dimensions and a smaller bulk door.

10 Systems

Exo’s systems are carefully selected and integrated to give it numerous advantages in cost, efficiency, and reliability over it’s competitors. Figure 48 and 49 schematically show the main systems and their respective locations.

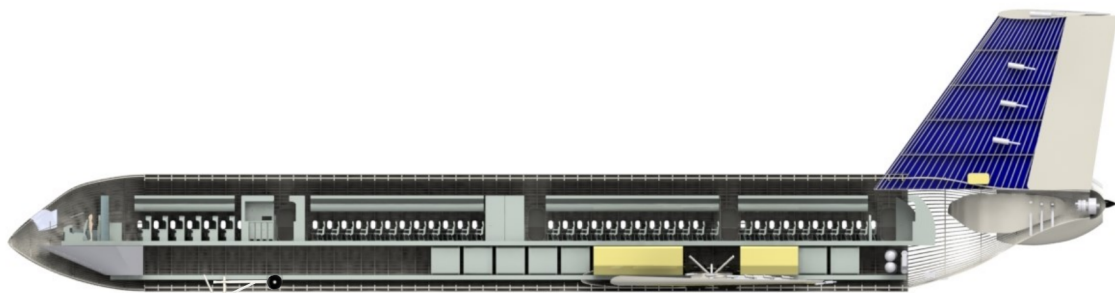


Figure 48: Systems layout (side)

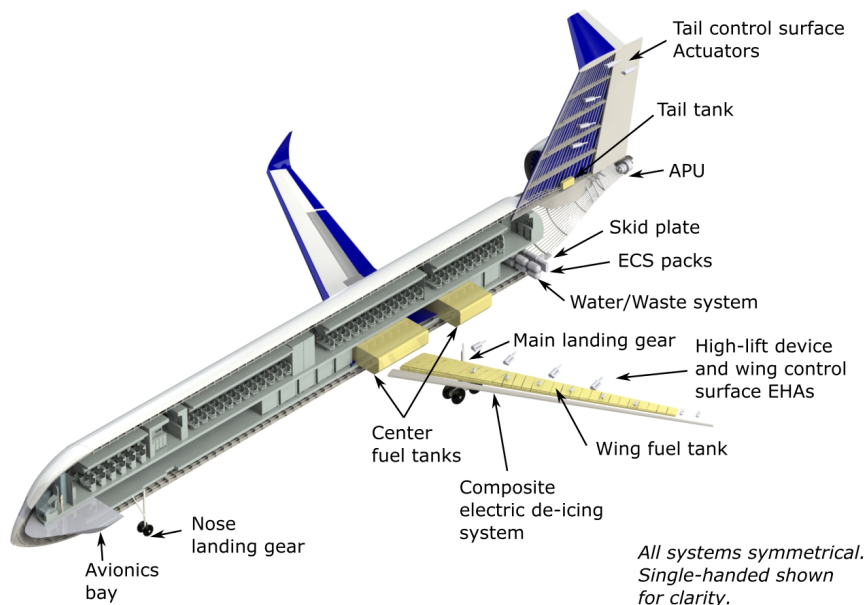


Figure 49: Systems layout

10.1 Electric/Hydraulic system

Exo uses innovative MEA system architecture by using a unified electric power type. This is achieved with electrohydrostatic power-by-wire actuators, a no-bleed architecture using an all-electric environmental control system, engine starting system, and de-icing system.

The advantages over traditional systems architecture are numerous. A no-bleed architecture for the de-icing, environmental control, and starting systems reduces the extracted power required of the engines by 30% compared to traditional systems [6], and removing the need for bleed-air extraction reduces the complexity of the engines and APU thus reducing maintenance cost and improving aircraft reliability. Reduced power required for systems lowers fuel burn and operating cost. Electrohydrostatic actuators in a power-by-wire hydraulic system setup decentralizes the hydraulic system. Isolating the hydraulic lines and fluid to each actuator reduces the likelihood and impact of a hydraulic system component failure. Maintenance costs are reduced in two key ways; first, the location of a failure such as a leak is much simpler to determine. Second, many backup systems required for a traditional centralized hydraulic system are rendered unnecessary. A unified electric power type reduces weight, improves power efficiency, improves system reliability, and reduces maintenance costs.

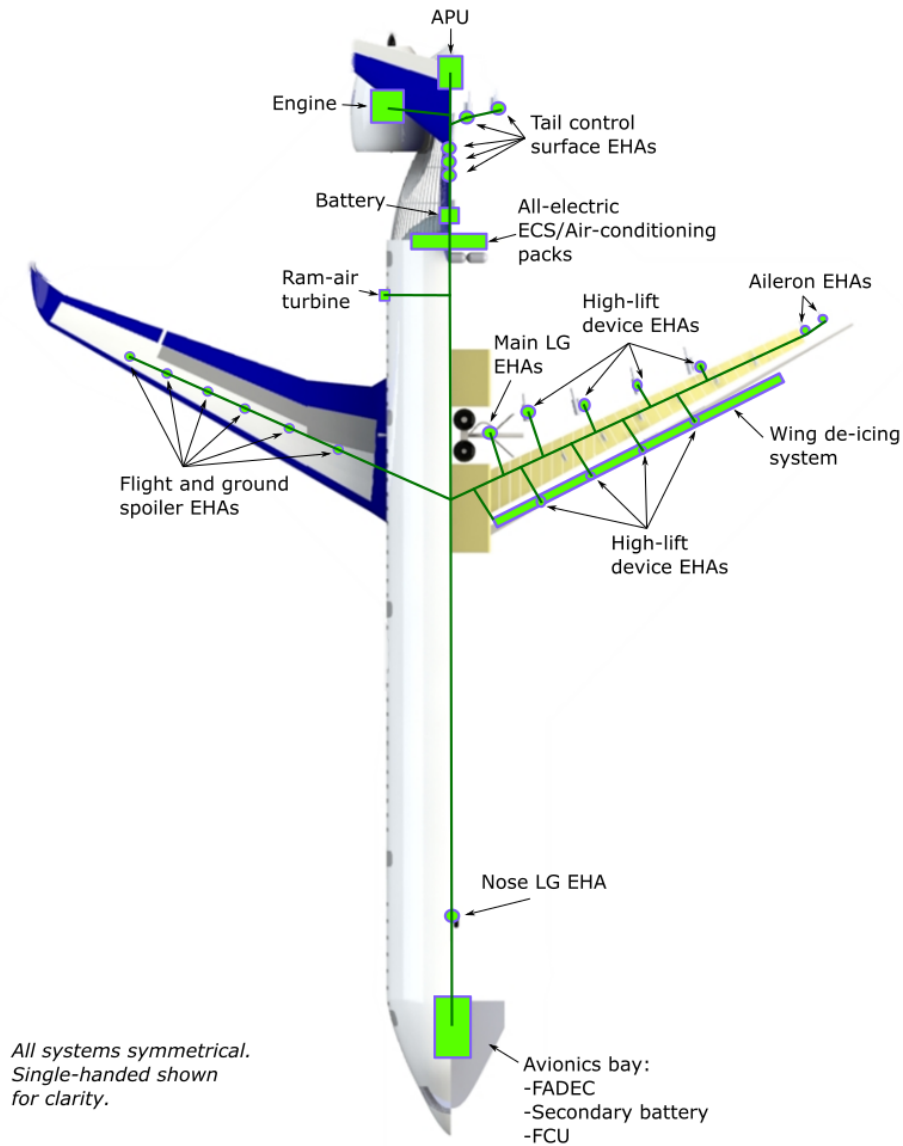


Figure 50: Electric/Hydraulic system diagram

Shown in Figure 50 is a diagram of Exo's electrical and hydraulic system. Due to the power-by-wire integration of the hydraulic system into the electrical system, the two diagrams have been combined. For power sources, each engine is equipped with a generator located on the accessory gearbox of each engine providing 3 phase, 115 VAC, CF 400 Hz power to the aircraft and current may be reversed during starting procedures to start each engine without the need for pneumatic systems. The APU has the same properties

and may be supported by a ground power cart and electrical service link. In an emergency, a RAT can drive critical electrical systems. Wire weight adds up fast in traditional aircraft, and with more electric components to power, wire weight is a heightened concern for Exo. This is why Exo utilizes remote distribution units. This combines power wires further down the aircraft closer to the power consumers and doesn't split wires until the nearest power distribution unit. This significantly reduces wire weight [6] and length of wires to trace in troubleshooting/maintenance. The main battery is located near the tail, with a second backup battery located in the avionics bay. The avionics bay, located in the nose, contains the flight control unit, FADEC, AHMS, and other avionics. Finally, the electric-composite de-icing systems are located in the leading edges of ice-sensitive surfaces and are fully electric powered without the need for complex bleed-air architecture.

10.2 Fuel system

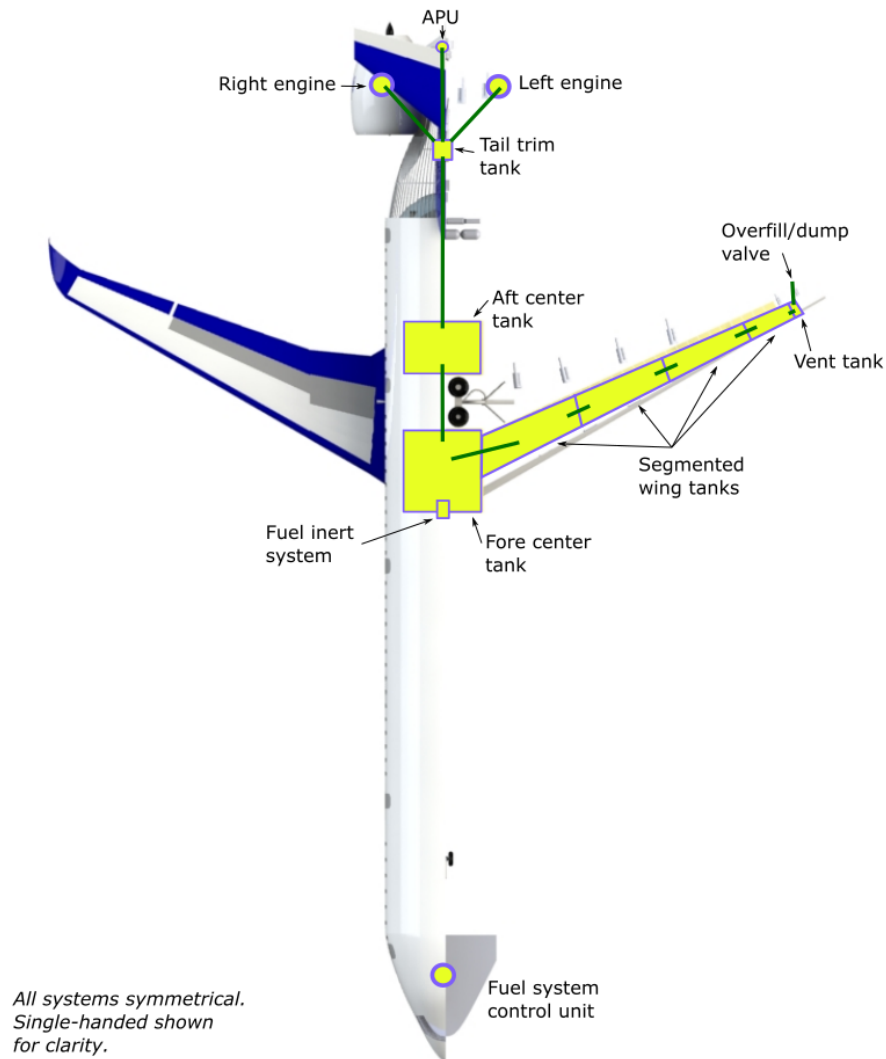


Figure 51: Fuel system diagram

Due to the smaller wing volume inherent with a short range aircraft, 76% of the fuel is stored in the fuselage in center tanks as shown in Figure 51, and the rest in the wing. Due to placement of the large center tanks, CG travel is reduced compared with that of long range aircraft with primarily wing-stowed fuel. This decreased travel in CG reduces trim drag of the aircraft. In addition, by having two center tanks, fuel balance

may also be used to adjust trim in cruise to reduce trim drag of the elevator. A tail tank is provided to assist with trim if necessary. It also functions as a fuel flow stabilization reservoir, eliminating any gas pockets or unsteadiness in fuel flow just before the fuel is fed to the engines or APU. In case of fuel pump failure, the tail tank is mounted in a way (Figure 48) to allow gravity to continue to feed 58 gal of fuel (over a minute of fuel at full burn) to the engines or APU to give the pilot(s) extra time and power to make a safe emergency landing. The most outboard tanks on the wing are CFR § 25.969 compliant vent tanks for overfill protection and gas ventilation as well as accommodating the end-nozzle of the fuel jettison system.

10.3 Avionics

Exo has an advanced avionics suite supporting a single pilot capable cockpit with autonomous taxi, takeoff, and landing capabilities. In addition, Exo is integrated with an aircraft health monitoring system (AHMS) to help predict component failures using machine learning allowing for scheduled necessary preventative maintenance. AHMS takes a prognostic approach to maintenance and system health, allowing for the operator to be notified in real time when a component is at risk to fail (an incident), compared to the conventional diagnostic approach, where warning is provided only upon the incident occurring. By implementing AHMS, the need for hourly service inspections will be reduced, which directly lowers the aircraft maintenance downtime, maintenance costs, and creates a more reliable, safer, and cost-effective aircraft [36].

Exo's autonomous capable autoflight system includes flight control, auto-stabilization, autopilot, auto throttle, and envelope protection, allowing for VFR and IFR capability. This is achieved using navigation and approach aids including: very high frequency omni-range, distance measuring equipment, automatic direction finding, tactical air navigation system, VOR/TACAN, instrument landing system, microwave landing system, and global navigation systems; as well as flight management, performance based navigation, PBN/AMP, RVSM, area navigation (RNAV), LNAV and VNAC guidance, GPS/GNSS approaches, surveillance, GPWS/TAWS, TCAS, ADS-B, navigation, and terrain databases. Supporting sensors include body rates, air data, attitude, and inertial reference sensors.

Exo's communication systems include: high frequency radio transmit/receive, very high frequency radio and aircraft communications and reporting system, ultra high frequency radio, satellite communications including passenger telephone communications, aircraft transponder and air traffic control mode A/C, traffic collision and avoidance system, communications control system. Basic vehicle management is broken

into five categories:

- Functional: primary and secondary power management and distribution
- Fuel System: fuel measurement, refueling, jettison, center of gravity control, and load alleviation
- Landing Gear: extension and retraction, braking, and nose wheel steering
- Wing: anti-ice/de-ice, environmental control system
- Engine Control: FADEC, with AHMS being treated as a separate category

Table 30: Potential cost savings while using Airbus ATTOL system

Flight Hours with One Pilot	Savings
4,865 (1 year)	\$2,140,600
14,595 (3 years)	\$6,421,800
24,325 (5 years)	\$10,703,000
38,920 (8 years)	\$17,125,000

Exo will be single pilot capable/dual-pilot equipped through use of the Airbus ATTOL technology. This TRL 8 demonstration leverages computer vision to enable aircraft to navigate and detect obstacles during taxi, takeoff, approach, and landing. Through using this technology and reducing Exo's need for two pilots to one pilot, Exo is capable of significant reductions in operating costs. Table 30 shows cost savings with respect to flight hours using ATTOL on Exo. After a short 5 years of service, the customer can save over \$10 million. Also, it is important to note that takeoff and landing is the most dangerous portion of flight. Per Figure 52, over 50% of fatal aircraft accidents are due to pilot error [37]. Using the ATTOL technology will not only reduce the operating costs for the customer, but will make the aircraft much safer for the end user.

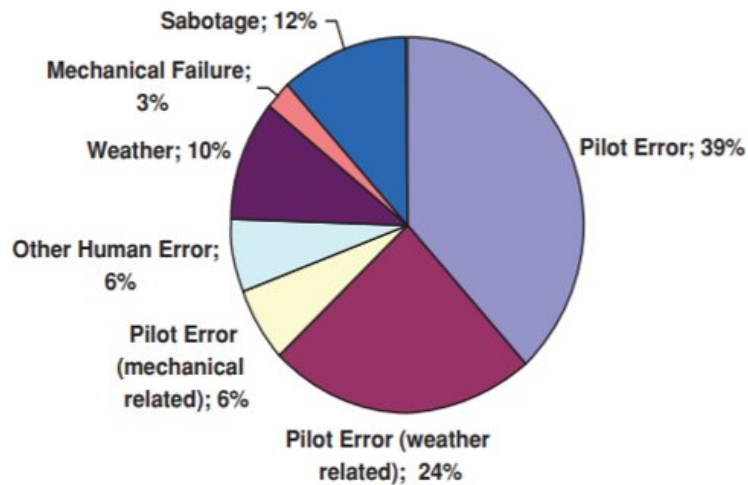


Figure 52: Fatal aircraft accidents [37]

11 Project Planning and Management

11.1 Project Timeline

To complete the project by the required 2029 EIS, the following plan, illustrated in Figure 53, was devised. The submission of this final report concludes the Conceptual Design phase for Project Exo. Next, the project will enter the Detailed Design from May 2020 to May 2023 where the outline of manufacturing procedures, sub-assemblies, construction of manufacturing sites and establish a bill of materials will all be completed. During this time, there is a Technology Freeze date of May 2023. This freeze date allows for six years of technology development and testing to be ready for integration onto the aircraft. The following phase, manufacturing, will last two years and will establish an efficient process for constructing the aircraft. Come May 2025, Exo will have its first flight. Here, the design will be tested, to validate and assess flight performance. Once the testing is complete in May 2027, Over the Pond will begin the two-year certification process to allow Exo to be fully certified and ready for January 2029.

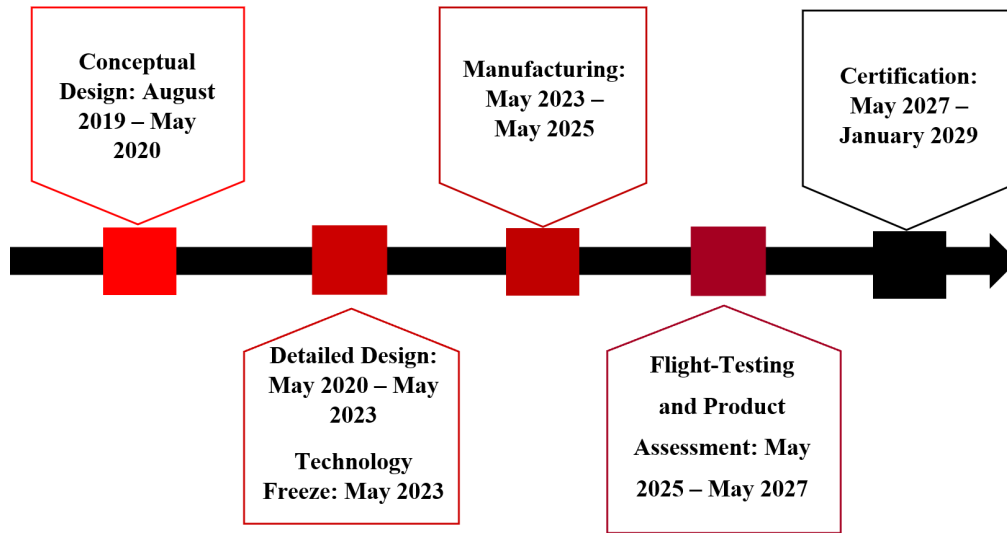


Figure 53: Project timeline

11.2 Risk Resolution Plan

Risk is inherent with any engineering design, however as the complexity of the system increases as in the case of Exo, risk must not simply be identified at any one stage, but rather continually examined and mitigated if. In order to ensure the most effective design, several key risks and mitigation plans were identified. In order to analyze these risks, the likelihood and impact of the risks were compared on a scale of 1-5 where each risk could be placed in its relative category of effective risk. Figure 54 identifies 4 of the major risks and their relative scale, each of which has a mitigation plan.

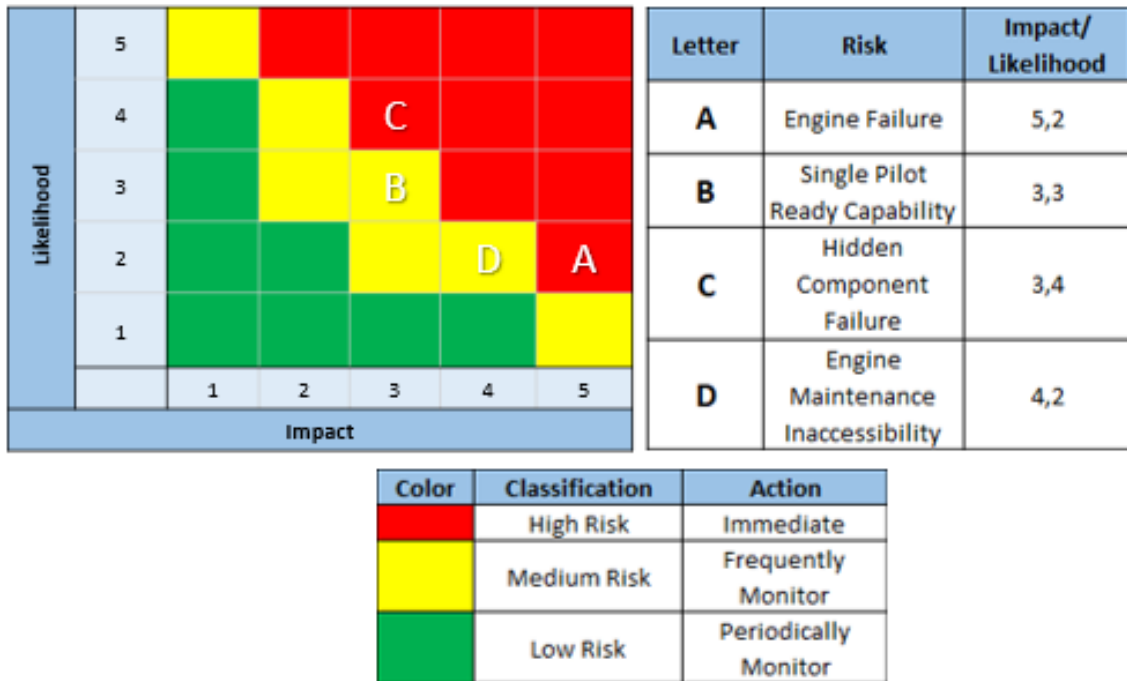


Figure 54: Outline of risks and scale

11.2.1 Risk A: Engine Failure

Exo features rear mounted engines that are connected to the fuselage alongside the vertical tail. As such, the utilization of rear mounted engines is identified as a risk as the engines are located near the empennage and the APU as well as other systems that run through the tail. In the event of a catastrophic failure of an engine the aircraft could suffer damage and would have to perform an immediate emergency landing. As this impact is severe the risk of engine failure is given an impact of 5, while the likelihood is set at a 2 on the scale as the high bypass engines are designed to withstand common failures. However, while the engines are designed to withstand failures, a mitigation plan was created in order to ensure that this risk was completely addressed. The mitigation plan is to implement blade containment technology which would keep any damage to the blades of the engines isolated such that they do not damage the rest of the structure. Additionally, the structure surrounding the engine was designed to be more durable in the case of any damage, while additionally placing the critical systems such as the APU outside of the burst disk area of the engine. By implementing this mitigation plan the risk is reduced to an impact of 3 and a likelihood of 1 (shown in Figure 55), as the engine is less likely to suffer a catastrophic failure, and as the failures are likely to be contained, they would not require immediate emergency procedures.

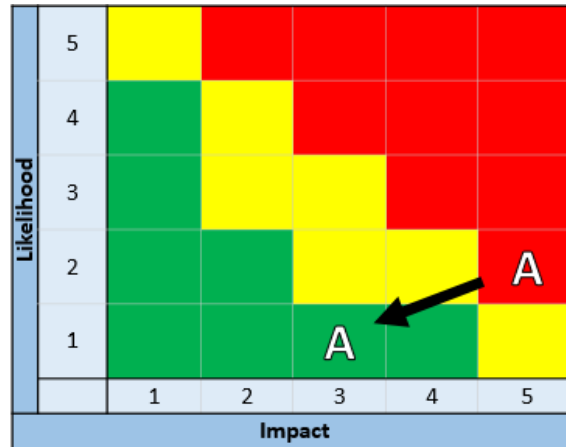


Figure 55: Engine failure risk mitigation

11.2.2 Risk B: Single Pilot Ready Capability

Additionally, the single pilot capability of the aircraft is a risk as the technology is in the process of being validated and certified. If single pilot capable technology is not certified by the technology freeze date of 2023, a delay of manufacturing or entry into service may occur. This risk is moderately likely as the technology certification is not guaranteed by the technology freeze date. Additionally, the impact is moderate as the safety is not a concern merely the date at which the aircraft could fly. Based on this the likelihood and impact are given a rating of 3 on the scale placing the risk in the moderate zone. As shown in Figure 56, this risk can be reduced to a rating of a likelihood of 1 and an impact of 3 by implementing a mitigation plan which calls for designing a cockpit that is outfitted for the standard dual pilot configuration. This would allow Exo to enter service on time regardless of the technology being fully certified. In addition, the design has the added benefit of being able to fly in countries that would not allow single pilot flight of commercial aircraft as individual countries may not allow this in their airspace.

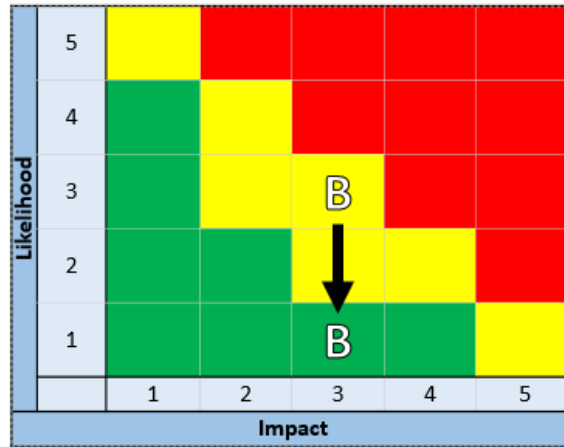


Figure 56: Single pilot capable risk mitigation

11.2.3 Risk C: Hidden Component Failures

Aircraft require maintenance and repairs at regular intervals, and given the complexity of the system, many of the components that could experience failures and require maintenance are hidden or hard to reach. As such, a risk is identified in hidden component failures, which could cause the system to function incorrectly or not at all. Because of the high likelihood that failures could occur within the systems, a likelihood of 4 is given, with an impact of 3, as any such hidden failures are unlikely to cause major problems but would require maintenance at the next possible opportunity to safely fly.

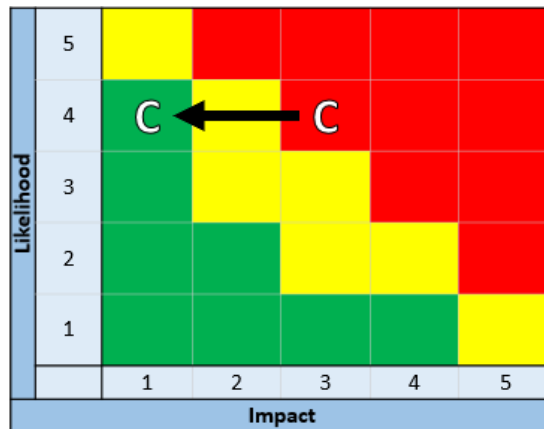


Figure 57: Hidden component failure risk mitigation

This risk can be mitigated through the use of AHMS and other integrated sensors throughout the design that, combined with AI, will predict and monitor the aircraft and all its systems for existing and

potential failures to reduce the impact of these failures before they occur. This reduces the impact of the risk to a 1 on the scale as shown in Figure 57, while the likelihood remains the same as the mitigation plan cannot prevent the failures but merely identifies them ahead of time.

11.2.4 Risk D: Engine Maintenance

An additional risk related to the engine is that of engine maintenance. The fact that the engine is mounted to the rear end of the aircraft can be problematic due to the nature of engines which have a wet and dry side (i.e. a side with fuel systems and a side with electronics). Additionally, engines that are mounted on the tails of aircraft as in Exo are traditionally designed to do so, whereas the Ultra-Fan is designed for use in under-wing mounted positions. As such there are potential issues in both the mounting and the maintenance access to the engines. This risk is evaluated in Figure 58 as an impact of 4 and likelihood of 2. The mitigation plan for this risk is to contact the manufacturer and potentially increase the development costs of Exo in order to ensure that critical components of the engine are accessible and to allow the engine to be securely mounted to the tail section of the aircraft. By doing so Exo is able to mitigate the risk to an impact of 2 while maintaining an impact of 2.

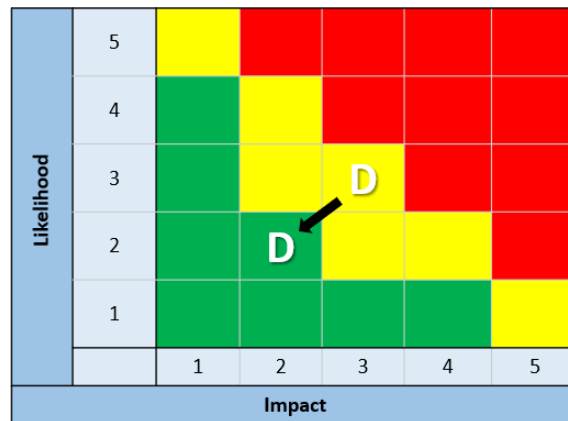


Figure 58: Engine maintenance risk

12 Cost Estimate and Business Case Analysis

All costs that appear in this report have been adjusted for inflation and reflect the value in U.S. dollars in the year 2029 unless explicitly stated otherwise.

12.1 Development Costs

The development, testing and evaluation (DTE) costs of the project incorporate the engineering from design to construction, the process of appropriate certification, and the facility, labor, and equipment costs needed to produce the prototype aircraft. It is important to note here that the DTE costs are calculated by the Rand model which assumes a conventional aircraft unlike Exo's innovative design. The engineering costs involved in developing this aircraft would be slightly higher than a conventional aircraft. It is also reasonable to assume the certification process will take longer to complete, and as a result the costs associated with testing and evaluation will be higher than calculated. The assumed number of development aircraft produced was five. This is a fairly average number of aircraft to produce for testing and certification purposes, where as few as two aircraft may be sufficient. Five was assumed due to the aforementioned certification process being more rigorous for an entirely new aircraft design. These aircraft will be used for structural, performance and systems tests.

Table 31: Development, testing, and evaluation costs

Development, Testing, and Evaluation Costs	
Airframe Engineering Cost	\$3,835,991,000
Development Support	\$983,994,000
Tooling Costs	\$1,765,765,000
Manufacturing Labor	\$1,452,813,000
Material and Equipment	\$463,066,000
Certification Costs	\$234,607,000
Quality Control	\$122,595,000
Total	\$8,858,831,000

The costs associated with the development and production of the aircraft were calculated using the Rand DAPCA IV model. This model was chosen for its use in several texts, including Nicolai and Carichner's Fundamentals of Aircraft and Airship Design and Raymer's Aircraft Design: A Fundamental Approach. Using this model as a guideline, the main cost groups are those involved in developing, testing,

evaluating, producing, and operating the aircraft. Maintenance (with the exception of maintenance of production tooling equipment) is considered an operating cost in this model and will be treated as such in all following discussions. The use of the Rand model entails several assumptions, most notably a decreased per unit production cost with increased total production quantity. This is attributed to the “learning curve” associated with commercial aircraft production.

12.2 Fly Away Cost of Each Member of Family

The flyaway cost of each aircraft is estimated at roughly \$192.6 million. Material, equipment, engine, avionics, sustainment engineering, tooling, manufacturing, and quality control costs are included in calculating the total production cost. The break down of this cost is shown in Figure 59.

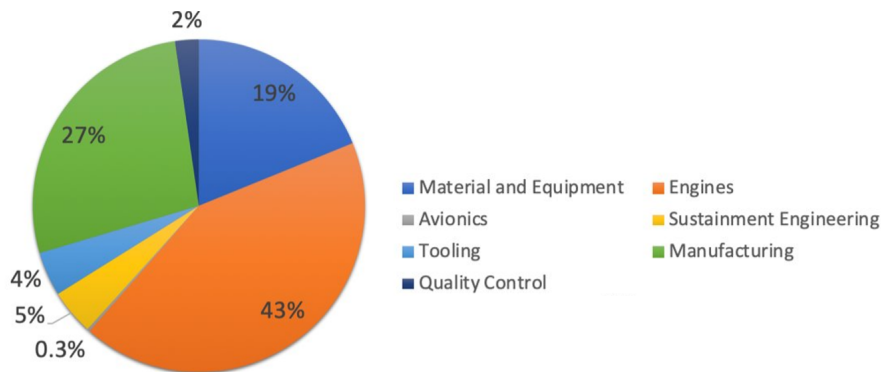


Figure 59: Production cost breakdown

This flyaway cost is based on an assumed production of 500 aircraft based on the production rate of 10 aircraft per month allowing a few years for production. With a greater overall number produced, this flyaway cost would be reduced due to the “learning curve” mentioned earlier. The main contributor to overall production costs is the cost of the engines, which is roughly 42% of the total production costs. The geared-turbofan engines used in the design are more expensive at time of purchase than more common turbofan engines, but their efficiency leads to lower operating cost. Minimizing operating cost was the prime goal regarding cost-considerations during the design phase, and therefore geared turbofan engines were chosen.

12.3 Estimate of Price

The aircraft will be sold at a unit price of \$221.5 million. This price is based on a 15% profit per aircraft. This selling price is a major upside to this aircraft. It is substantially less expensive than other commercial aircraft of similar passenger capacity, and less expensive than multiple single-aisle aircraft that would be required to transport 400 passengers.

The aircraft production rate is planned at 10 aircraft per month which was chosen based on a market analysis of similarly sized aircraft. This monthly production is also hugely beneficial because it represents a relatively fast path toward project profitability despite being a small percentage of the total aircraft orders in the short-range marketplace. With the total DTE and production costs calculated by the Rand model and the unit price of \$221.5 million, the overall project will reach its break-even point at 420 aircraft. At the planned rate of 10 aircraft per month, the project will begin generating an overall profit with every new aircraft produced at 42 months, or 3.5 years. After production runs smoothly and the monthly rate could be increased to 12, the overall project would reach a break-even point in less than 3 years as shown in 60.

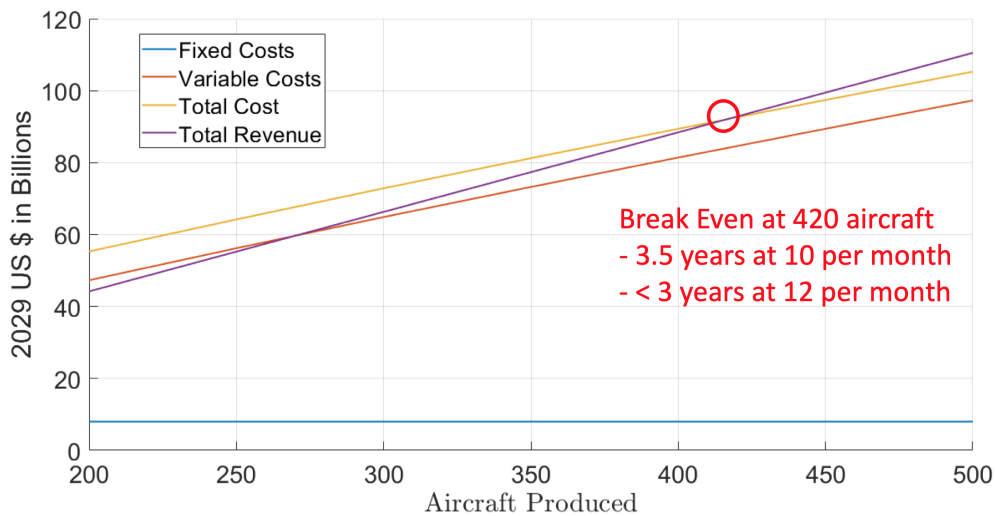


Figure 60: Break even analysis

12.4 Estimate Direct Operating Cost for 700 nm reference mission

Direct operating cost was calculated using Liebeck’s 1995 paper Advanced Subsonic Airplane Design and Economic Studies [38]. Oil, tires, brakes, and other consumable quantities are incorporated in the calculation of airframe material costs. When calculating the fuel costs, the \$3 per gallon carbon tax was included. All costs shown are for the 700 nautical mile reference mission.

Table 32: Direct operating costs

Direct Operating Cost of 700 nmi Reference Mission	
Fuel Cost	\$34,020
Pilot Cost	\$6,772
Cabin Crew Cost	\$2,498
Airframe Maintenance Labor	\$635
Airframe Material Cost	\$923
Engine Maintenance Labor	\$262
Engine Material Cost	\$388
Landing Fee	\$938
Total	\$46,437

12.5 Manufacturing Plan

There are several viable manufacturing locations such as Wichita, Kansas, Ann Arbor, Michigan and Atlanta, Georgia, but the best location for this project is Fort Worth, Texas. Fort Worth was chosen after careful consideration of factors such as available labor pool, supply chain logistics, and costs that are variable with location. Texas has a large current labor pool of employees in the aerospace and defense industry, and a large labor pool of manufacturing workers. The Dallas, Arlington, and Fort Worth areas are very densely populated, making it the easiest area to incorporate workers. Fort Worth also has the advantage of superior supply chain location. A significant number of part suppliers and manufactures have operations in Texas. American Airlines and Southwest Airlines are also headquartered in Texas. Texas also has the advantage of very favorable tax policies, including no corporate income tax.

Aerospace, Aviation & Defense Industry Workforce Concentration Map

Aerospace Product & Parts Manufacturing

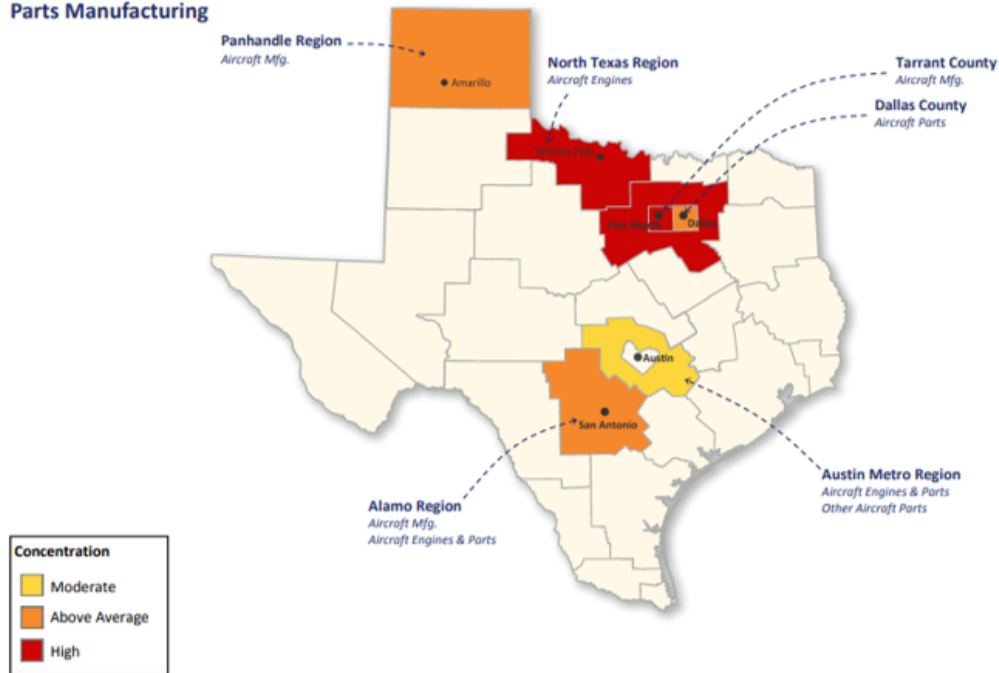


Figure 61: Texas aerospace industry workforce concentration map

13 Aircraft Emissions

13.1 CO₂ Emissions during Manufacturing

Approximately 2,346,000 lbs of CO₂ will be emitted per aircraft manufactured. This approximation was found using the following analysis. In 2017, Texas produced \$39,035,000,000 in value added AD products [39], which is 10.4% of \$374 billion in value added AD products produced in the entire country [40]. AD is responsible for more than 5% of manufacturing value-added in 15 U.S. states, respectively. Taken together, these states account for \$94 billion in manufacturing activity or 71% of total AD manufacturing value-added [40], thus there is \$132.39 billion in US manufacturing activity for the AD industry. 10.4% of this \$132.39 billion yields \$13.818 billion in Texas AD manufacturing activity. Further, of the \$374 billion in value added AD products, 27.8% is commercial aerospace products [40]. 27.8% of \$13.818 billion in Texas manufacturing activity yields \$3.84 billion in Texas commercial aerospace manufacturing

(a mere 1.027% of that original \$374 billion).

In 2018, Texas emitted 230,076 thousand metric tons of CO₂ as a state [41]. Also, as a state, the AD's GDP contribution was 2.3% of the total state GDP [39]. Assuming the AD GDP contribution matched the CO₂ emission contribution, Texas would have produced 5,291,748 metric tons of CO₂ for AD activity (1.16683*10¹⁰ lbs of CO₂ yearly). Next, recall that Texas commercial aerospace manufacturing was 1.027% of the total AD value added products produced. 1.027% of 1.16683*10¹⁰ lbs of CO₂ yearly is 148,630,861 lbs of CO₂ for Texas AD Commercial Aerospace Manufacturing per year or 12,385,905 lbs of CO₂ monthly.

Finally, Texas's share of the National AD workforce is 9.6% [39]. If approximately 55 commercial aircraft are produced per month, 9.6% of those 55, or 5.28 aircraft, would be produced in Texas.

13.2 CO₂ Emissions

13.2.1 In-service

Given a 3,500 nm (4027.72 miles) design mission, Exo will consume about 95,914 lbs of fuel while carrying 400 passengers, equating to 0.0595 lbs of fuel per passenger mile. Further, the US Energy Information Administration states approximately 21.1 lbs of CO₂ is emitted per gallon of Jet Fuel (1 gallon of jet fuel is approximately 6.8 lbs), thus resulting in 0.1847 lbs of CO₂ per passenger mile [31] [32]. At a cruise speed of Mach 0.82 at 35,000 ft (541.8 mph), Exo emits 100.08 lbs of CO₂ per hour per passenger [33].

Following the same procedure for the comparator aircraft, the A321neo and B777-300, Table 33 was constructed. Exo emits 117% less CO₂ per hour per passenger than the Boeing 777-300 and emits only 56% less CO₂ per hour per passenger than the required number of A321neo aircraft to complete the mission.

Table 33: Comparator CO₂ Emissions.

Aircraft	Passengers	Fuel Weight (lbs)	Range (nm)	Emissions (lbs of CO ₂ per hour per passenger)
Project Exo	400	95,914	3500	100.08
B777-300	398	325,652	5500	217.32
A321neo	206	32,940	3000	77.86

13.2.2 Lifecycle

The total amount of emissions produced by an aircraft from both its manufacturing and in-service performance is 482.3 million lbs of CO₂. For each flight with 400 passengers, Exo will produce 4,000 lbs of CO₂ per hour. Based on the lifecycle of the A320 family, Exo is expected to fly approximately 120,000 flight hours [42], which amounts to 480 million lbs of CO₂.

14 Aircraft Drawings

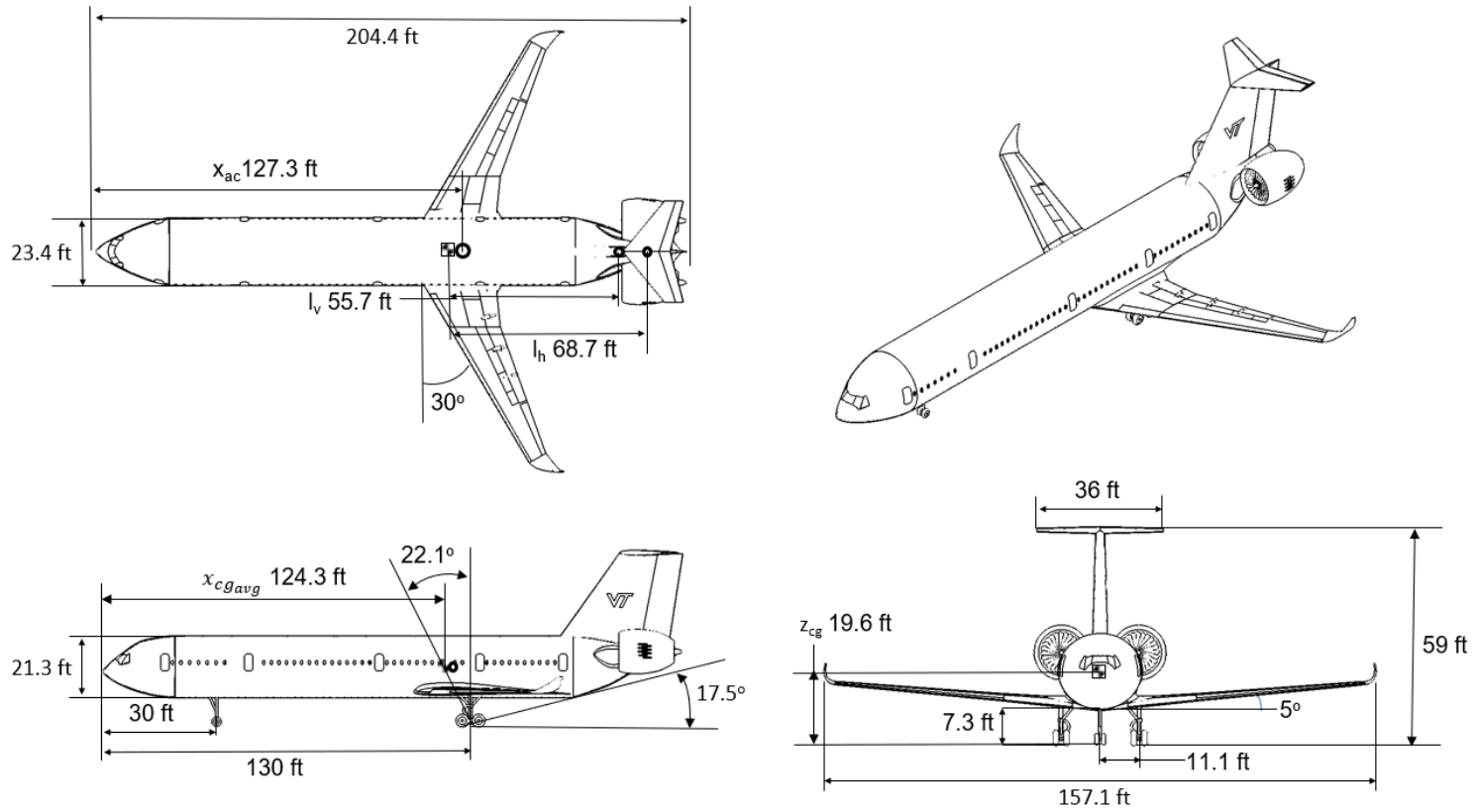


Figure 62: Dimensioned 3-view diagram of Exo

References

- [1] A. Dorsey, Request for Proposal, Reston: AIAA, 2019.
- [2] D. Casey, Busiest Routes in the World - The Top 100, Routesonline, 2019.
- [3] Busiest Routes 2019, London: Oag, 2019.
- [4] United States Department of Transportation, 2019.
- [5] Massachusetts Institute of Technology. "Performance of a Boundary Layer Ingesting (BLI) Propulsion System." Performance of a Boundary Layer Ingesting (BLI) Propulsion System | Aerospace Sciences Meetings, 18 June 2012, arc.aiaa.org/doi/10.2514/6.2007-450.
- [6] Sinnett, M., "787 No-Bleed Systems: Saving Fuel and Enhancing Operational Efficiencies," Aero, QTR4_07, 2007, pp. 06–11. www.boeing.com/commercial/aeromagazine/articles/qtr_4_07/article_02_1.html
- [7] "FAA Requiring Inspections For Aging Boeing 777s" Aviation Week, <https://aviationweek.com/mro/faa-requiring-inspections-aging-boeing-777s>.
- [8] Bishop, K. and Hansman, R. Assessment Of The Ability Of Existing Airport Gate Infrastructure To Accommodate Transport Category Aircraft With Increased Wingspan For Improved Fuel Efficiency. Report No. ICAT-2012-4. May 2012. https://dspace.mit.edu/bitstream/handle/1721.1/71120/MIT_Wingspan_Thesis_Bishop.pdf
- [9] Fundamentals of Aircraft and Airship Design, by Leland M. Nicolai and Grant E. Carichner, American Inst. of Aeronautics and Astronautics, 2013,
- [10] Mason, William H. "Software for Aerodynamics and Aircraft Design." http://www.dept.aoe.vt.edu/~mason/Mason_f/MRsoft.html
- [11] "Wing Design." Aircraft Design: a Systems Engineering Approach, by Mohammad H. Sadraey, Wiley, 2013
- [12] "Airfoil Tools." RAE(NPL) 5213 AIRFOIL (rae5213-II), airfoiltools.com/airfoil/details?airfoil=rae5213-il.

- [13] "U. S. Centennial of Flight Commission." Fowler Flap and Complex Slotted Flap, www.centennialofflight.net/essay/TheoriesofFlight/Devices/TH17G5.htm.
- [14] Dexmet Corporation. "Aircraft Lightning Strike Protection." <https://www.dexmet.com/applications/aerospace>
- [15] Aviation Week Space Technology. *Aircraft Recycling Gets Smart*. Pages 32-36. May 4, 2020.
- [16] Mason, William H. "Landing Gear Concept Selection." *Configuration Aerodynamics*, Jan. 2018, pp. 14–29., doi:http://www.dept.aoe.vt.edu/~mason/Mason_f/M96SC03.pdf.
- [17] J. Roskam, *Airplane Design*. DARcorporation, 1985.
- [18] J. C. Eppel, D. W. Riddle, and V. C. Stevens, "Flight Measured Downwash of the QSRA," Moffett, CA, tech., 1988.
- [19] "Rolls-Royce Trent." Wikipedia, Wikimedia Foundation, 10 Apr. 2020, en.wikipedia.org/wiki/Rolls-Royce_Trent#UltraFan.
- [20] Braunling, Willy J.G. *Flugzeugtriebwerke: Grundlagen, Aero-Thermodynamik, Ideale Und Reale Kriesprozesse, Thermische Turbomaschinen, Komponenten, Emissionen, Und Systeme*.
- [21] Smaha, Rachad, and Dragan Kozulovic. *Projekt Im Master: Identifizierung Der Wichtigsten Technologischen Entwicklungstrends Im Triebwerksbau*. Hamburg University of Applied Sciences, 2018.
- [22] "Future of Flight." Rolls-Royce, www.rolls-royce.com/media/our-stories/innovation/2016/advance-and-ultrafan.aspxchallenge.
- [23] "Rolls-Royce Studies More-Electric UltraFan." *Aviation Week*, 5 Nov. 2019, aviationweek.com/air-transport/aircraft-propulsion/rolls-royce-studies-more-electric-ultrafan.
- [24] "Type Certificate Data Sheet for Noise: Learjet Model 45." European Aviation Safety Agency, 8 Feb. 2017, www.easa.europa.eu/sites/default/files/dfu/TCDSN%20EASA.IM_.A.020%20Issue9.pdf.
- [25] "Type Certificate Data Sheet for Noise: Boeing 777." European Aviation Safety Agency, 12 April 2019, www.easa.europa.eu/sites/default/files/dfu/TCDSN%20EASA.IM_.A.003%20Issue22.pdf.
- [26] "Type Certificate Data Sheet for Noise: A321." European Aviation Safety Agency, 21 August 2019, www.easa.europa.eu/sites/default/files/dfu/TCDSN%20EASA.A.064.4%20Issue23.pdf.

- [27] "Type Certificate Data Sheet for Noise: Boeing 757." European Aviation Safety Agency, 7 August 2019, www.easa.europa.eu/sites/default/files/dfu/TCDSN%20EASA.IM_.A.205%20Issue10.pdf.
- [28] Bensel, Artur. Characteristics of the Specific Fuel Consumption for Jet Engines. 31 Aug. 2018, www.fzt.haw-hamburg.de/pers/Scholz/arbeiten/TextBensel.pdf.
- [29] Hall, David K., et al. "Boundary Layer Ingestion Propulsion Benefit for Transport Aircraft." *Journal of Propulsion and Power*, 13 Mar. 2017, arc.aiaa.org/doi/abs/10.2514/1.B36321.
- [30] Cousins, William T., et al. "Design of a Distortion-Tolerant Fan for a Boundary-Layer Ingesting Embedded Engine Application." 53rd AIAA/SAE/ASEE Joint Propulsion Conference. 2017.
- [31] "U.S. Energy Information Administration - EIA - Independent Statistics and Analysis." Environment - U.S. Energy Information Administration (EIA) - U.S. Energy Information Administration (EIA), www.eia.gov/environment/emissions/co2_vol_mass.php.
- [32] "Jet Fuel." Wikipedia, Wikimedia Foundation, 20 Apr. 2020, en.wikipedia.org/wiki/Jet_fuel.
- [33] Engineers Edge, LLC. "Speed of Sound Table Chart." Engineers Edge - Engineering, Design and Manufacturing Solutions, 3 Jan. 2015, www.engineersedge.com/physics/speed_of_sound_13241.htm.
- [34] P. D.-I. D. Scholz, "PreSTo1.0," HAW Hamburg, Hamburg, Germany, 2010.
- [35] Andreas Schiebert, Infrastructure Manager, Eurowings GmbH, Düsseldorf, Germany, 2020.
- [36] Xu, J., and Xu, L., *Integrated System Health Management Perspectives on Systems Engineering Techniques*, San Diego: Elsevier Science Technology, 2017.
- [37] Moir, Ian, et al. *Civil Avionics Systems*. 2nd ed., John Wiley Sons, Ltd, 2013. 4.2.2 Flight Safety Overview
- [38] Liebeck, Robert, et al. "Advanced Subsonic Airplane Design and Economic Studies." April 01, 1995, <https://ntrs.nasa.gov/search.jsp?R=19950017884>.
- [39] "State Data." Aerospace Industries Association, www.aia-aerospace.org/research-center/statistics/state-level-data/.
- [40] "Value Added." Aerospace Industries Association, www.aia-aerospace.org/research-center/statistics/industry-data/value-added/.

[41] "U.S. Energy Information Administration - EIA - Independent Statistics and Analysis." Emissions by Plant and by Region, 2018, www.eia.gov/electricity/data/emissions/.

[42] "New service package will extend A320's life." Internet: <https://www.airbus.com/newsroom/news/en/2008/03/new-service-package-will-extend-a320-039-s-life.html>, Mar. 06, 2008 [May. 14, 2020].

Appendix

Table 34: Example decision matrix for material selection.

Fuselage Skin	Weight (%)	7075 T761 + Epoxy Matrix/Aramid Fiber Layer			Epoxy/HS Carbon Fiber QI Layup			2024 T3 + Epoxy Matrix/Aramid Fiber layer			Epoxy/S Glass Fiber, QI Layup		
		Raw Value	Normalized	Weighted	Raw Value	Normalized	Weighted	Raw Value	Normalized	Weighted	Raw Value	Normalized	Weighted
Price(\$/ft ³)	20	24150	0.056935818	1.138716356	2470	0.556680162	11.13360324	24500	0.056122449	1.12244898	1375	1	20
Density(lb/in ³)	25	0.0849	0.670200236	16.75500589	0.0569	1	25	0.086	0.661627907	16.54069767	0.0689	0.825834543	20.64586357
Tensile Strength(ksi)	25	109	1	25	79.65	0.730733945	18.26834862	95.5	0.876146789	21.90366972	69.7	0.639449541	15.98623853
Young's Modulus (10 ⁶ Psi)	10	9.9	1	10	6.71	0.677777778	6.777777778	9.75	0.984848485	9.848484848	2.91	0.293939394	2.939393939
Fatigue at 10 ⁷ Cycles(ksi)	20	72.1	1	20	48.56	0.673509015	13.47018031	43.6	0.604715673	12.09431345	4.32	0.059916782	1.198335645
Total Score	100			72.89372225			74.64990995			61.50961468			60.76983169

Table 35: Engine Decision Matrix with Top Five Engines Considered.

Criteria	Weighting	UltraFan			GEnx-1B			GP7000			Trent 972			Trent 980		
		Raw Value	Normalized	Weighted	Raw	Normaliz	Weighted	Raw Value	Normaliz	Weighted	Raw Value	Normaliz	Weighted	Raw Value	Normaliz	Weighted
Unit	20	4.07E+07	0.97	1.95E+01	2.66E+07	0.47	9.39E+00	13500000	0.00	0.00E+00	26600000	0.47	9.39E+00	25000000	0.41	8.24E+00
Fan	10	11.67979	1.00	-1.00E+01	9.251969	0.03	-2.63E-01	9.7112861	0.21	-2.11E+00	9.2519685	0.03	-2.63E-01	9.6784777	0.20	-1.97E+00
Weight	25	18643.191	0.74	1.84E+01	13554.1	0.02	5.35E-01	14800	0.20	4.92E+00	13554.1	0.02	5.35E-01	13772.43	0.05	1.30E+00
Emissio	10	2.775	0.00	0.00E+00	2.78	0.00	6.01E-03	4.06	0.15	1.54E+00	5.62	0.34	3.42E+00	5.62	0.34	3.42E+00
SFC	35	0.3574527	0.00	0.00E+00	0.521694	0.62	2.18E+01	0.5507419	0.73	2.57E+01	0.5224987	0.63	2.19E+01	0.5224987	0.63	2.19E+01
total	100		6	35.8		3.0	31.8		5.0	33.3		1.0	28.6		2.0	30.4